I. ENTHALPY CHANGE UPON VAPORIZATION OF THE HYDROCARBONS n-PENTANE, CYCLOHEXANE AND 1-BUTENE

II. EVALUATIONS OF DIFFUSION COEFFICIENTS FOR THE METHANE-n-BUTANE SYSTEM BASED ON GRADIENTS IN THERMODYNAMIC STATE PROPERTIES

Thesis by

William Kozicki

In Partial Fulfillment of the Requirements

For the Degree of

Doctor of Philosophy

California Institute of Technology

Pasadena, California

1962

ACKNOWLEDGMENTS

I wish to express my appreciation and gratitude to Professor Bruce H. Sage, under whose direction this research was conducted, for the encouragement, helpful advice and assistance rendered throughout the course of the research.

Ernest R. Boller, Henry E. Smith and Robert F. Cuffel assisted in the measurements of the heat of vaporization for which I am most grateful. The cooperation and assistance received from H. Hollis Reamer is greatly appreciated. Lee T. Carmichael rendered invaluable assistance on several occasions in repair work on the calorimeter. The continued interest and helpful advice of Dr. R. A. McKay, who also kindly permitted the reproduction of his figures of the apparatus, is acknowledged with gratitude. The contributions of Y. L. Wang, who performed the chromatographic analysis on the 1-butene employed, and of Willard M. Dewitt, George A. Griffith, Paul B. Holmen, Raymond Reed, Virginia Berry, Larry Beaulieu, William Lockwood, Seiche Nakawatase and others are also gratefully acknowledged.

I wish to acknowledge with gratitude the financial support of the experimental work by the Standard Oil Company of California who also made me the recipient of a fellowship. Much of the apparatus available in this work was made available by the Jet Propulsion Laboratory of the California Institute of Technology.

ABSTRACT

I

An experimental investigation was made of the enthalpy change upon vaporization of three hydrocarbons in the pure state. The hydrocarbons studied were n-pentane, cyclohexane and 1-butene. Direct calorimetric determinations of the enthalpy change were carried out at 30° temperature intervals in the temperature range 100° F. up to 310° F. and at pressures in the range 3-250 lb. per sq. in. abs. The experimental data was smoothed and interpolated utilizing residual techniques. Critically chosen values of the enthalpy change upon vaporization of n-pentane, cyclohexane and 1-butene are presented at even temperature increments of 10° F. The data extrapolated to 77° F. is in excellent agreement with selected values at 77° F. reported by Rossini which were measured at the National Bureau of Standards.

II

Evaluations were made of the phenomenological coefficient and the diffusion coefficients based on gradients in the chemical potential and fugacity for methane diffusing in the liquid phase of the methane-n-butane system. Values of these coefficients are presented at six pressures evenly spaced in the pressure range 250-1500 lb. per sq. in. at each of the temperatures 100°, 160° and 220° F. The evaluated coefficients are marked functions of the state of the phase.

TABLE OF CONTENTS

LIST OF FIGURES

II

LIST OF TABLES

PART I

ENTHALPY CHANGE UPON VAPORIZATION OF THE HYDROCARBONS n-PENTANE, CYCLOHEXANE AND 1-BUTENE

INTRODUCTION

The enthalpy change upon vaporization is of importance in establishing the thermodynamic behavior of pure substances in the two phase region. Most of the available data relating to direct calorimetric evaluations of this quantity pertains to atmospheric pressure or lower (1). Calculated values obtained by application of the Clapeyron equation (2) to PVT data are available for a large number of hydrocarbons up to the critical states of the substances (3, 4, 5, 6). However, the accuracy of the enthalpy change upon vaporization, evaluated in this way, in general is not as good as that attainable by the direct measurement. In many cases, accurate enthalpy change measurements can be used to provide evaluations of the specific volume of the saturated gas under conditions when such data cannot be obtained conveniently by direct measurement. In addition, these measurements afford a desirable check upon the consistency of the thermodynamic data related to the saturated liquid and gas.

A review of the literature indicates that limited effort has been devoted to the direct calorimetric evaluation of the enthalpy change upon vaporization of n-pentane. Griffiths and Awbery (7) carried out measurements on a sample of commercial n-pentane at temperatures between -4° and 86° F. and reported their data in terms of linear functions of temperature. Young (3) studied the volumetric behavior of the saturated liquid and saturated gas of n-pentane, and from these measurements and measurements of the vapor pressure computed the enthalpy change

by the application of the Clapeyron equation. More recently Canjar et al. (5) repeated the analytical evaluation utilizing their more recent volumetric measurements. Calorimetric measurements of the enthalpy change had been made between 82° and 200° F. at this laboratory (8) with an earlier apparatus. Osborne and Ginnings (9) carried out direct measurements on a large number of hydrocarbons at 77° F. and have reported a value for n-pentane at the same temperature. Messerly (10) reported a determination by direct measurement at 77° F. There existed significant differences between all of the above data and a further investigation of the enthalpy change upon vaporization of n-pentane seemed desirable, particularly since relatively pure n-pentane is now readily available and the maximum previous temperature of measurement was 200° F. Rossini (1) has made a critical review of the thermodynamic properties of hydrocarbons including n-pentane and has reported values of the enthalpy change at 77° F. and at the normal boiling point.

Measurements of the enthalpy change upon vaporization of cyclohexane have been limited to only a few temperatures. Spitzer et al. (11) determined the enthalpy change at two temperatures from measurements conducted in a flow calorimeter system. Osborne and Ginnings (9) also obtained a value for cyclohexane at 77° F. Rossini (1) has reported values for the enthalpy change at 77° F. and at the normal boiling point.

Accurate information concerning the enthalpy change upon vaporization of 1-butene has been scarce. From available experimental PVT data, by means of the Clapeyron equation, Weber (4) computed the enthalpy change for a tabulation of the thermodynamic properties of

1-butene, Osborne and Ginnings (9) carried out a measurement at 77° F. Aston et al. (12) made measurements of the enthalpy change upon vaporization at six temperatures between -95.5° and 20.4° F. and represented this data by a quadratic function of temperature. Rossini (1) has also reported values for 1-butene at 77° F. and at the normal boiling point.

There is a great deal of information in the literature (6, 13, 14, 15, 16, 17, 18, 19) which pertains to the estimation of the enthalpy change upon vaporization. In general, such data is unsuitable for thermodynamic tabulations although it serves as a useful substitute in the practical situation where experimental data is lacking. Most of the methods described in the literature are based on utilization of the Clapeyron equation. Probably the most noteworthy of these is the technique of Pitzer et al. (13) which yields values appearing, in many instances, to agree quite well with the reliable experimentally determined data. In this method, PVT data required in the Clapeyron equation is supplied by the application of the law of corresponding states, with the inclusion of an additional variable, the "acentric factor," to account for the differences in geometry of the different molecular species. O'Hara (6) derived a relation for the enthalpy change, beginning with the Clapeyron equation, utilizing a relation derived by Haggenmacher (20) for the difference between the specific volumes of the saturated vapor and liquid and the Antoine equation (1) for the vapor pressure. He also calculated the enthalpy change of 88 organic compounds in the pressure range 1 mm to the critical pressure. A further discussion of the more approximate methods of evaluation as well as of correlations of the enthalpy change lies outside of the sphere of interest of this study.

METHOD AND APPARATUS

The method and general features of the apparatus used in the evaluation of the enthalpy change upon vaporization were essentially the same as developed by Osborne and co-workers (9, 21, 22).

The method consisted in vaporization of the material under investigation in an isochoric vessel, the material vaporized being withdrawn and collected in a cooled weighing bomb. A constant vaporization rate was maintained by means of an orifice, operating at sonic velocity, which maintained a steady discharge rate under isobaric conditions in the calorimeter. Energy required in the vaporization was provided by means of an electrical heater, at a rate necessary to maintain substantially steady state conditions within the calorimeter. By maintaining the surroundings at the same temperature as the bomb, energy transfers by conduction and radiation between the calorimeter bomb and the surroundings were essentially eliminated.

Figure 1 illustrates schematically the general features of the calorimeter and associated equipment. The calorimeter bomb, A, was situated within a vacuum jacket, B, which was enclosed by an oil bath, not shown in the figure. The pressure within the vacuum jacket was maintained below 10^{-8} inches of mercury by means of an oil diffusion pump, L, and a suitable mechanical forepump. To prevent the exchange of energy between the vacuum jacket and the calorimeter bomb, the temperature of the oil bath was controlled at the same temperature as the bomb. A small centrifugal agitator, C, provided circulation of the liquid

in the bomb. The liquid flowed past a heater, D, around and through ports in the shield, E, and past a thermometer well, F. The saturated gas was withdrawn from the top of the calorimeter through a small tube, H. The rate of withdrawal was controlled by the orifice, I, operated at an upstream to downstream pressure ratio greater than two to one in order to attain sonic flow conditions. At these conditions, the flow rate was insensitive to small variations in pressure downstream from the orifice and was dependent only upon the pressure within the calorimeter. The material withdrawn was condensed in either of two weighing bombs, J or K. Condensation in the withdrawal tube was prevented by maintaining the temperature of the walls of the tube slightly above that of the calorimeter. Provision was made for measurement of the pressure in the calorimeter bomb with a pressure balance, G, through a connection at the bottom of the calorimeter.

The enthalpy change upon vaporization, in the case of the idealized isothermal-isobaric process, is evaluated by means of the simple expression,

$$H_b - H_d = \frac{Q_{1,2}}{m_1 - m_2} \frac{V_d - V_b}{V_d} \quad .$$

However, the expression for the enthalpy change in an actual vaporization process involving minor perturbations from isothermal-isobaric conditions and a certain amount of superheating of the liquid phase and subcooling of the gas phase is lengthy and considerably more complicated. It involves several line integrals to be evaluated along the actual path of

the vaporization process. The net heat added during the process, $\underline{Q}_{1,\,2'}$ includes, in addition to the energy added electrically, small corrections due to the mechanical agitation of the material in the bomb and due to the existence of small temperature differences between the bomb and the adiabatic jacket.

THERMODYNAMIC ANALYSIS

A thermodynamic analysis of the vaporization process is available (23, 24) for a one-component system and a multi-component system with a single volatile component. The subsequent analysis of the one-component case does not differ materially from the previous treatments. An attempt has been made to present the derived relations in a form which clearly indicates the relative importance of the various experimental variables in the evaluation of the enthalpy change and the effect of the incorporation of certain refinements in the experimental procedure on the accuracy of the evaluation.

Thermodynamic System

The thermodynamic system under investigation is illustrated by the simple schematic diagram in fig. 2. Briefly, it is comprised of an isochoric vessel within which there is confined a one-component heterogeneous system consisting of a liquid phase and the coexisting gas phase. The vessel is provided with an electrical heater and an agitator and is enclosed within a jacket, as shown. The system undergoes a change in weight due to the withdrawal of material vaporized in the vessel. Energy is added by the heater during the process in the amount necessary to maintain steady conditions within the vessel, except for minor perturbations.

Analysis

The conservation of energy for the process may be conveniently written as,

$$d\underline{E} = \underline{q} - \underline{w} + E_a dm_a = \underline{q} + P_a V_a dm_a + E_a dm_a \qquad (1)$$

The second equality results since the vessel is isochoric and work involved in the process is limited to that associated with the withdrawal of material from the vessel.

Representing the state of the material being withdrawn by the state of the gas phase within the vessel, equation 1 may be rewritten

$$d\underline{E} = \underline{q} + PV_g dm_{g,a} + E_g dm_{g,a} \qquad (2)$$

It is convenient to consider that the electrical energy dissipated by the heater as well as the mechanical energy dissipated within the calorimeter by the agitator are transferred to the thermodynamic system as heat. The system also may exchange heat with the surroundings, by conduction and radiation, due to a temperature difference between the outer boundary of the system and the surroundings. In view of these considerations, the net heat gained by the system is given by

$$\underline{q} = \underline{q}_e + \underline{q}_s + \underline{q}_{c+r} \qquad (3)$$

It is assumed that each of the quantities on the right side of equation 3 can be determined as a function of the time elapsed during the vaporization process. The details pertaining to the actual evaluation of each of these terms do not properly belong in the thermodynamic analysis and are presented in another section. It should be realized that the net heat transferred to the system, $\underline{q}$, is comprised for the most part

of the energy transferred by the electrical heater, $\underline{q}_e$, the other energy terms being of smaller order of magnitude by comparison.

Utilizing the extensive character of internal energy, the change in the internal energy of the system may be related to the changes in the individual parts comprising the system as follows,

$$d\underline{E} = d\underline{E}_{\ell} + d\underline{E}_g + d\underline{E}_A[f(T)] \tag{4}$$

The assumption is made in equation 4 that the change in internal energy of the vessel, considered a part of the thermodynamic system, may be represented by a function of temperature alone.

The first law of thermodynamics may be utilized to obtain the changes in internal energy of the liquid and gas phases, $d\underline{E}_{\ell}$ and $d\underline{E}_g$ respectively, in equation 4. If this is done, then the expression obtained for the liquid phase is

$$d\underline{E}_{\ell} = m_{\ell}\left[c_P - P\left(\frac{\partial V}{\partial T}\right)_P\right]_{\ell} dT + m_{\ell}\left[\ell_P - P\left(\frac{\partial V}{\partial P}\right)_T\right]_{\ell} dP + E_{\ell} dm_{\ell,i}, \tag{5}$$

and for the gas phase,

$$d\underline{E}_g = m_g\left[c_P - P\left(\frac{\partial V}{\partial T}\right)_P\right]_g dT + m_g\left[\ell_P - P\left(\frac{\partial V}{\partial P}\right)_T\right]_g dP + E_g dm_g \quad . \tag{6}$$

Similarly, the change in the internal energy of the vessel can be established from

$$d\underline{E}_A[f(T)] = c_A dT . \tag{7}$$

In equation 5, the differential change in weight of the liquid phase is given by $dm_{\ell, i}$, representing material transferred across the interface. The differential change in weight of the gas phase in equation 6 involves, in addition to the material transferred across the interface $dm_{g, i}$, the weight of gas phase withdrawn from the vessel, $dm_{g, a}$. The following relationships involving these quantities may be written:

$$dm = dm_{g, a} = dm_{\ell} + dm_g \tag{8}$$

$$dm_{\ell} = dm_{\ell, i} \tag{9}$$

$$dm_g = dm_{g, i} + dm_{g, a} \tag{10}$$

It follows from these three relations that

$$dm_{\ell, i} = -dm_{g, i} \tag{11}$$

It is evident that the identity of dm and $dm_{g, a}$, in equation 8 is contingent upon the same assumption as was made in arriving at equation 2, viz., that the state of the material withdrawn is the same as that of the gas phase, which excludes liquid entrainment from the analysis.

The relationship between the weight of material withdrawn as gas and the amount of material vaporized is obtained from basic considerations utilizing the extensive property of volume and the basic assumption that the calorimeter is isochoric. It follows, therefore, from the relations

$$\underline{V} = m_g V_g + m_\ell V_\ell \tag{12}$$

and

$$d\underline{V} = 0 , \tag{13}$$

and the relationships given in equations 8, 9, 10, and 11 that

$$\frac{dm_{\ell, i}}{dm} = \frac{V_g + m_g \frac{dV_g}{dm} + m_\ell \frac{dV_\ell}{dm}}{V_g - V_\ell} \tag{14}$$

The superheating of the liquid phase and subcooling of the gas phase, which is encountered to various extents in vaporization processes, can be accounted for by means of the relation

$$H_g - H_\ell = (H_d + \Delta H_g) - (H_b + \Delta H_\ell) \tag{15}$$

where ΔH designates the change in the enthalpy of a phase resulting from superheating or subcooling. More specifically,

$$\Delta H_\ell = H_\ell - H_b = \int_{T_b}^{T_\ell} c_{P,\ell} dT$$

and (16)

$$\Delta H_g = H_g - H_d = \int_{T_d}^{T_g} c_{P,g} dT$$

Derivation of the General Enthalpy Change Relation

The general enthalpy change relation is readily derived by com-

bining the relations presented in the discussion of the previous section.

If the relations for $d\underline{E}_\ell$, $d\underline{E}_g$ and $d\underline{E}_A$ given by equations 5, 6 and 7 respectively, are substituted into equation 4, and the resulting expression is equated to the right side of equation 2, the following expression is obtained, after cancellation of the term $E_g dm_{g,a}$ from both sides of the equation,

$$\underline{q} + PV_g dm_{g,a} = \{m_\ell[c_{P,\ell} - P(\frac{\partial V}{\partial T})_P]_\ell + m_g[c_P - P(\frac{\partial V}{\partial T})_P]_g + c_A\}dT$$

$$+ \{m_\ell[\ell_P - P(\frac{\partial V}{\partial P})_T]_\ell + m_g[\ell_P - P(\frac{\partial V}{\partial P})_T]_g\}dP - (E_g - E_\ell)dm_{\ell,i} \quad (17)$$

Making the substitution,

$$E_g - E_\ell = (H_g - H_\ell) - (PV_g - PV_\ell) \quad (18)$$

in equation 17 and carrying out a simple rearrangement of the resulting expression yields

$$(H_g - H_\ell)dm_{\ell,i} = -\underline{q} + \{m_\ell[c_P - P(\frac{\partial V}{\partial T})_P]_\ell + m_g[c_P - P(\frac{\partial V}{\partial P})_P]_g + c_A\}dT$$

$$+ \{m_\ell[\ell_P - P(\frac{\partial V}{\partial P})_T]_\ell + m_g[\ell_P - P(\frac{\partial V}{\partial P})_T]_g\}dP - P(V_g dm_g + V_\ell dm_\ell) \quad (19)$$

A simple rearrangement of the expression obtained by combination of equations 12 and 13 results in

$$-(V_g dm_g + V_\ell dm_\ell) = (m_g dV_g + m_\ell dV_\ell), \tag{20}$$

which can be expanded to give

$$-(V_g dm_g + V_\ell dm_\ell) = m_g\left[\left(\frac{\partial V_g}{\partial T}\right)_P dT + \left(\frac{\partial V_g}{\partial P}\right)_T dP\right]$$

$$+ m_\ell\left[\left(\frac{\partial V_\ell}{\partial T}\right)_P dT + \left(\frac{\partial V_\ell}{\partial P}\right)_T dP\right] \tag{21}$$

Substituting the expression given in equation 21 for $-(V_g dm_g + V_\ell dm_\ell)$ into equation 19 and making the necessary cancellations results in the following relatively simple expression,

$$(H_g - H_\ell)dm_{\ell,i} = -\underline{q} + (m_\ell c_{P,\ell} + m_g c_{P,g} + c_A)dT$$

$$+ (m_\ell \ell_{P,\ell} + m_g \ell_{P,g})dP \tag{22}$$

Substitution of the relations given by equations 14 and 15 into equation 22 yields the following relation,

$$\frac{(H_d - H_b)(V_g + m_g \frac{dV_g}{dm} + m_\ell \frac{dV_\ell}{dm})}{V_g - V_\ell} dm = -\underline{q} + (m_\ell c_{P,\ell} + m_g c_{P,g} + c_A)dT$$

$$+ (m_\ell \ell_{P,\ell} + m_g \ell_{P,g})dP + \frac{(\Delta H_\ell - \Delta H_g)(V_g + m_g \frac{dV_g}{dm} + m_\ell \frac{dV_\ell}{dm})}{V_g - V_\ell} dm, \tag{23}$$

which can be integrated from the initial to the final conditions, along the path of the process, as follows,

$$\int_{m_1}^{m_2} \frac{(H_d - H_b)(V_g + m_g \frac{dV_g}{dm} + m_\ell \frac{dV_\ell}{dm})}{V_g - V_\ell} dm$$

$$= \int_1^2 -\underline{q} + \int_{m_1}^{m_2} (m_\ell c_{P,\ell} + m_g c_{P,g} + c_A) \frac{dT}{dm} dm$$

$$+ \int_{m_1}^{m_2} (m_\ell \ell_{P,\ell} + m_g \ell_{P,g}) \frac{dP}{dm} dm$$

$$+ \int_{m_1}^{m_2} \frac{(\Delta H_\ell - \Delta H_g)(V_g + m_g \frac{dV_g}{dm} + m_\ell \frac{dV_\ell}{dm})}{V_g - V_\ell} dm \qquad (24)$$

If an average value of $H_d - H_b$ is assumed, equation 24 reduces to the following expression for the enthalpy change upon vaporization,

$$(H_d - H_b)^* = \frac{1}{\int_{m_1}^{m_2} \frac{V_g + m_g \frac{dV_g}{dm} + m_\ell \frac{dV_\ell}{dm}}{V_g - V_\ell} dm} \left[\int_1^2 -\underline{q} \right.$$

$$+ \int_{m_1}^{m_2} (m_\ell c_{P,\ell} + m_g c_{P,g} + c_A) \frac{dT}{dm} dm + \int_{m_1}^{m_2} (m_\ell \ell_{P,\ell} + m_g \ell_{P,g}) \frac{dP}{dm} dm$$

$$\left. + \int_{m_1}^{m_1} \frac{(\Delta H_\ell - \Delta H_g)(V_g + m_g \frac{dV_g}{dm} + m_\ell \frac{dV_\ell}{dm})}{V_g - V_\ell} dm \right] \qquad (25)$$

The asterisk over the enthalpy difference term in equation 25 serves to indicate that the enthalpy change evaluated is an average value over the range of conditions encountered in the process. In the present work, however, the magnitudes of the perturbations were so small as to have substantially no effect on the enthalpy difference involved, within the precision of the measurement.

The analysis assumes that each of the phases involved in the vaporization process can be represented by a single state although in an actual process slight temperature gradients exist within each phase. Furthermore, in the derivation of equation 25, the assumption is made that the state of the material withdrawn from the vessel is the same as that of the gas phase, which precludes liquid entrainment in the gas phase withdrawn. The state of the vessel is represented by a function of temperature alone.

Simplified Enthalpy Change Relations

If average values of the subcooling and superheating terms are assumed, the general enthalpy change relation, equation 25, becomes

$$(H_d - H_b)^* = \frac{1}{\int_{m_1}^{m_2} \frac{V_g + m_g \frac{dV_g}{dm} + m_\ell \frac{dV_\ell}{dm}}{V_g - V_\ell}\, dm} \left[\int_1^2 -\underline{q} + \int_{m_1}^{m_2} \left[(m_\ell c_{P,\ell} + m_g c_{P,g} + c_A)\frac{dT}{dm} + (m_\ell \ell_{P,\ell} + m_g \ell_{P,g})\frac{dP}{dm} \right] dm \right] + \Delta H_\ell^* - \Delta H_g^* . \quad (26)$$

If the temperature variation in the process is sufficiently small and the temperature at condition 2 is made identically equal to the temperature at the initial condition, the second integral in the bracket equation 26, vanishes, the specification of averages becomes unnecessary and equation 26 reduces to the following simple form,

$$H_d - H_b = \frac{Q_{1,2}}{m_1 - m_2} \frac{V_g - V_\ell}{V_g} + \Delta H_\ell - \Delta H_g \qquad (27)$$

For the isothermal-isobaric process with no subcooling or superheating of the phases the following familiar simple expression results,

$$H_d - H_b = \frac{Q_{1,2}}{m_1 - m_2} \frac{V_d - V_b}{V_d} \quad . \qquad (28)$$

DESCRIPTION OF APPARATUS

The calorimeter used in this work was a modification of an earlier apparatus (25) used for the measurement of the heat capacity of liquids. As a consequence of the modification, the utility of the calorimeter was extended to include the measurement of the enthalpy change upon vaporization. A detailed description of the apparatus in substantially the present form is available (23, 25). In the following, an attempt has been made to present the main and important features of the apparatus. The reader interested in additional details is referred to the above references.

Calorimeter Assembly

Figure 3 shows the general arrangement of the calorimeter assembly, the principal part of the apparatus. The calorimeter bomb, A, in fig. 3, is comprised of two parts machined from type 302 stainless steel. These two parts are joined at the equator by means of a tapered Acme thread, which was sealed with pure tin. The vessel was designed originally to operate at pressures up to 1000 lbs. per sq. in., which corresponded to a maximum stress in the steel of 20, 000 lb. per sq. in. However a leak was developed in the tin seal of the bomb, (during a vaporization process with 1-butene at a temperature of 250° F. and a pressure of 385 lb. per sq. in.), after the calorimeter had been operating successfully for an extended period of time in which three systems had been investigated. The leak was repaired and the subsequent pressure test was conducted up to a pressure of 350 lb. per sq. in. This pressure

exceeded by more than a factor of 2 the maximum anticipated pressure of systems to be investigated. The calorimeter bomb is supported from the jacket J by means of three wires fastened to lugs in the upper part of the bomb.

Agitation of the liquid within the calorimeter was provided by means of a centrifugal agitator B, fig. 3. The liquid leaving the agitator through the ports C, in the shield D, flowed upward through the annular passage between the shield and the inner wall of the calorimeter, A, past a heater situated in this annular space which is not shown in the figure, down past the thermowell enclosing the resistance thermometer, E, returning to the agitator along the radial guide vanes, F. The calorimeter heater consists of a heating element enclosed within 1/8 inch diameter steel tubing turned into a helix of 7-1/2 turns on a diameter of 4-5/8 inches. The heater extends from just above the ports, C, in the shield, to slightly below the mid-point of the calorimeter. Additional ports in the shield D, not shown in fig. 3, permit circulation of liquid samples only slightly in excess of the amount required to cover the heater with no circulation. These additional ports and the heater arrangement permit a considerable variation in volume of the sample in the calorimeter. A small portion of the liquid leaving the agitator B, through the ports C in the shield D, flowed downward below the agitator then upward through openings located near the eye of the agitator.

The calorimeter agitator, supported by steel and bronze bearings, indicated in fig. 3, was driven by the shaft G. This shaft is enclosed

by the tube H, connected to the lowest point of the calorimeter bomb and leaving the vacuum jacket through the seal I, located in the sleeve U. The sleeve U, which is an extension of the vacuum jacket, serves to lengthen the path of direct contact between the calorimeter and its surroundings at the lower end of the calorimeter, thereby reducing the temperature gradient along the path. The tube H is thin-walled along this path. The annular space between the shaft, G, and the interior of the tube, H, is connected to the interior of the bomb through two small ports, located at the lowest point of the bomb. These passages were used in the loading and unloading operations of the bomb. The shaft G, the tube H, and all of the parts within the bomb, excluding the bronze bearings, are of stainless steel.

Oil Bath

The vacuum jacket, J, is enclosed by the oil bath, K, in fig. 3. Circulation within the oil bath was provided by the impeller L, which pumps oil through the ports M, up and along the circulation shield N, past two heaters arranged helically and parallel to one another in the annular region between the shield N and the outer wall of the oil bath K. The brackets supporting the posts on which the oil bath heaters are wound may be seen in the photograph, fig. 4. The oil then flowed downward, through the opening O at the top of the circulation shield, fig. 3, past a resistance thermometer, not shown, and along the wall of the vacuum jacket, J. The flow continued, past the radial guide vanes P, through the ports S, downward past the circulation shield T turning

with the impeller, then inward toward tube H and upward, past sleeve U back into the impeller. A detailed description of the impeller drive assembly and associated bearings, packing glands, etc. is available (23). The main features are readily discerned from fig. 3 and the accompanying legend.

Calorimeter Agitator Drive

The tube H, which encloses the drive shaft for the agitator B, is sealed to the steel shell E' just below the nut F'. The armature housing G' is suspended by means of the drive shaft G and rotates between small steel and bronze bearings, located at I' and J'. The bearing at I' is a combination journal and thrust bearing, although in the assembly of the apparatus the parts had been proportioned so as to leave a small gap at the thrust bearing I', so that the bearing supporting the agitator also supported the armature. This arrangement insured that the shaft G was under tension, thereby minimizing whip.

Torque for turning the agitator was transmitted to the armature H' by means of rotating electromagnets K', energized through the slip rings L' and M', in fig. 3. The electromagnetic assembly is supported by bearings at O' and N' and was driven by the pulley P'.

Calorimeter Agitator Motor Assembly

The calorimeter agitator motor assembly consisting of a motor and speed reducer is a replacement of the motor previously in use (23). The motor is the synchronous type with a power rating of 1/8 horsepower operating at a speed of 1800 revolutions per minute. The speed reducer

output rating is 85 in. lb. of torque and a speed of 75 revolutions per minute corresponding to the reduction ratio 24:1.

Arrangement for Pressure Measurement

The tube H, which encloses the agitator drive shaft is connected at the lower end to the steel shell E'. This tube and a tube leaving the bottom of the shell are connected to the free space within the shell through small ports, not shown in fig. 3, which bypass the bearings at I' and J'. Provision was made for measurement of the pressure in the shell with a pressure balance (26). A steel diaphragm transmits the pressure and prevents mixing of the oil in the pressure balance system with the material in the calorimeter.

Adiabatic Jacket

The oil bath, K, in fig. 3, which encloses the vacuum jacket and calorimeter bomb, is enclosed by an adiabatic jacket, not shown in the figure. Air is confined in the annular space between the oil bath and the adiabatic jacket. The adiabatic jacket is equipped with heaters and manual controls for maintaining the jacket temperature close to the temperature of the oil bath. In this way, small additions of energy were required to maintain a constant oil bath temperature, a necessary condition for the fine temperature control needed in this work.

Calorimeter Bomb Heater Details

The calorimeter heater is constructed of No. 24 AWG Chromel-A wire, approximately nine feet in length, installed within a stainless steel

tube 0. 055 inch in diameter. No. 24 AWG copper wire leads, extending five inches within the calorimeter, are connected to the heater. Electrical energy was supplied by two 6 volt batteries in series and was controlled by means of a suitable resistor in series with the heater. Potential leads, of No. 36 AWG copper wire for establishing the voltage drop are connected to the heater circuit leads one inch from the external surface of the calorimeter bomb.

Calorimeter Thermometer Well

The calorimeter bomb resistance thermometer is enclosed within a thermometer well E, fig. 3. An atmosphere of helium gas, supplied from a helium reservoir by the same tube carrying the thermometer leads, was maintained within the well to improve the response of the thermometer to variations in the temperature of the bomb. The reservoir for the helium is situated outside of the calorimeter assembly where it is in contact with surroundings at room temperature. The volume of the reservoir is sufficient for the pressure of the helium not to be affected appreciably by the temperature excursions of the calorimeter.

Tube for Calorimeter Thermometer Leads

The calorimeter bomb resistance thermometer leads are enclosed within a thin-walled stainless steel tube (outside diameter 0.093 inch). This tube extends from a fitting at the top of the calorimeter bomb to a small chamber situated just outside of the calorimeter assembly, serving as the reservoir for the helium in the thermowell. The tube leaves the vacuum jacket and the vacuum system via the vacuum line. It

is soldered to a copper junction block at the junction of the vacuum line and the vacuum jacket to eliminate temperature gradients and thermal losses along the tube. A heating element is also wound around the tube one inch from the junction block on the vacuum jacket side. It was controlled manually to maintain nearly zero temperature difference between a point on the tube near the bomb and another near the heater. A differential two-junction thermocouple measures the temperature difference between the two points.

The resistance thermometer leads emerge from the helium reservoir through a wax seal on top of the chamber. The chamber is equipped with a pressure gauge which indicates the pressure of the helium.

Tube for Vapor Withdrawal

The vapor phase was withdrawn from the top of the calorimeter bomb through a withdrawal tube, of stainless steel (outside diameter 0. 072 inch), which passes through the vacuum chamber and the vacuum line in the same manner as the tube carrying the thermometer leads. The withdrawal tube is connected at the top of the calorimeter bomb to the same fitting to which the tube carrying the thermometer leads is fastened. The fitting and the paths of the two tubes from the top of the calorimeter to the vacuum line are shown in the photograph fig. 4. The withdrawal tube emerges from the vacuum line through a suitable fitting and terminates in a valve block, located near the fitting.

The section of withdrawal tube between the bomb and the junction block is provided with a guard heater and differential thermocouple in

the same manner as the tube with the thermometer leads. The sections of withdrawal tube in the vacuum line and between the vacuum fitting and the valve block are each clad with close fitting copper tubing (outside diameter 1/8 inch). Two separate heaters are wound around the length of copper tubing in the vacuum line and one heater is situated along the length of tubing between the vacuum fitting and the valve block. One heater is also wound around the vacuum fitting. Each heater is provided with an autotransformer in series with an isolation transformer for manual control of the vapor line temperature.

A comparison of the temperature of the vapor tube at the two heated sections with the temperature of the vacuum jacket, at a point remote from the vacuum line, is afforded by means of differential two-junction thermocouples. Differential thermocouples are also provided for comparison of the temperatures of the vacuum fitting and the section of vapor line between the fitting and the valve block with the temperature inside the tube enclosing the thermometer leads, at a point about one inch from the calorimeter bomb.

Orifice Block

The vapor withdrawal rate was controlled by three orifices, used individually or in combination, which were situated in the orifice block. Eight orifice sizes in the range from 0. 0014 to 0. 0198 inch in diameter at the throat were available for use.

The orifice block also is provided with a heater for manual control of the temperature of the block. A differential two-junction thermo-

couple, used in the measurement of the temperature of the block, utilizes the same reference junction as the thermocouples associated with the vacuum fitting and the adjacent downstream section of tubing.

Withdrawal Manifold

The material withdrawn was collected in one of two weighing bombs connected to the withdrawal manifold and serving as condensers. No heaters are installed on the withdrawal manifold or along the section of copper tubing (outside diameter 3/16 inch) which connects the orifice block to the manifold.

Calorimeter Thermocouple Locations

Three differential two-junction thermocouples are available for comparison of the temperature at three locations on the exterior surface of the calorimeter bomb with the temperature of the vacuum jacket J, fig. 3. The locations of the thermocouple junctions situated on the bomb, with respect to the vertical position, corresponded approximately to the 1/3, 1/2, and 2/3 volume levels in the bomb. A differential two-junction thermocouple is installed within the thermometer well with one junction situated near the top and the other approximately 3.1 inches lower.

Temperature Measurement

The temperature of the oil bath K, in fig. 3, was determined by means of a strain-free platinum resistance thermometer of the coiled filament type. The thermometer was calibrated relative to the International Platinum Scale with an instrument calibrated by the National

Bureau of Standards. The temperature within the calorimeter bomb was measured in the same manner.

The resistances of the resistance thermometers were measured with Mueller bridges using the conventional four-lead connections. Temperatures evaluated by this method could be determined to within 0.02° F. in relation to the International Platinum Scale. Changes in temperature could be measured with an uncertainty of not more than 0.003° F.

Calorimeter Heater Circuit Details

Figure 5 is a circuit diagram showing the calorimeter heater circuit and the arrangement of the equipment used in establishing the voltage drop and current through the heater. The nomenclature and circuit values accompanying the figure are presented on the two pages following the figure.

In the figure, A represents the calorimeter heater and includes the portion of the leads situated within the heater tube. F is an auxiliary heater situated outside of the calorimeter assembly of approximately the same resistance as heater A. It serves the purpose of permitting a current flow, required for the stabilization of the heater circuit in advance of actual operation. Two high capacity 6-volt storage batteries arranged in series provide the electrical energy supply, C.

Adjustments to the current in the circuit were made by means of the variable resistors E and M. Both of these resistors are decade boxes, M having a smaller current capacity than the similar resistor E. The finer adjustments to the heater current were made by means of the variable resistor M. A shunt resistor P of fixed resistance serves

the double purpose of decreasing the current requirement through the control resistor M and reducing any effects due to unstable contact resistance (23).

The current in the circuit was determined from the voltage drop across the series resistor D. The voltage drop across the heater A was established by means of the high resistance voltage divider JK, in parallel with the heater. The voltage divider is connected to the current leads B, with the potential leads ℓ, at points one inch from the calorimeter. The potential drop across the heater A was determined from the voltage drop across the resistor K of the voltage divider. On account of the fact that the resistors D and K were measured with the same potentiometer G, these resistances have been selected so that the voltage values measured with the potentiometer fell in the same region of the slidewire scale for convenience in measurement.

Voltage Measurement

A White double potentiometer was used in the measurement of the electromotive force of the thermocouples with both junctions in the vacuum jacket. These included the thermocouples measuring the temperature difference between the calorimeter bomb and jacket, thermocouples measuring temperature gradients along the tubes leaving the top of the bomb and along one heater lead, and the thermocouple within the thermometer well. The uncertainty involved in the voltage measurements was about 0.1 microvolts.

A Leeds and Northrup "student potentiometer" was used in the measurement of the electromotive force of those thermocouples having

a single junction in the vacuum jacket. These thermocouples play a prominent part in the control of the temperature along the path followed by the vapor leaving the calorimeter. The uncertainty in the voltage measurements obtained with this instrument was approximately 2 microvolts.

Voltage measurements for evaluation of the electrical power input to the calorimeter bomb heater were made with a K-2 model Leeds and Northrup potentiometer with an estimated uncertainty of not more than 0.02 per cent.

General Layout

The general arrangement of the calorimeter and some of the associated equipment is shown schematically in fig. 6 and in a perspective view in fig. 7. The calorimeter and associated equipment is enclosed in a housing unit comprising two small rooms. The structure of the housing unit is steel. The inner and outer walls of the room containing the calorimeter have been constructed of transite sheeting as a safety measure against failure of the calorimeter during previous studies conducted with corrosive materials.

The calorimeter assembly in fig. 3 is located in the calorimeter room B, fig. 7. The drive mechanisms for the calorimeter agitator and oil bath impeller are situated on the floor, below the bench E. The adiabatic jacket D and other barriers to thermal transfer surrounding the calorimeter are supported above the bench, E, by a supporting structure mounted on the bench. The location of the orifice block and condensers may be seen in fig. 6.

Auxiliary Equipment

Most of the auxiliary equipment is housed in the second small room in fig. 7. A mechanical vacuum pump G in series with a three-stage jet pump H was used to evacuate the vacuum jacket between the calorimeter bomb and oil bath. A second vacuum system consisting of a mechanical forepump and mercury diffusion pump and auxiliary equipment used in the evacuation of the lines up to the orifice block is situated in the space below G, near W. The potentiometer I, a Leeds and Northrup student model, was used in the measurement of the temperature differences along the vapor path, in conjunction with the light source M and galvanometer J. Galvanometer deflections were observed on the ground glass scale, O, which receives the light beam originating at the light source M, after deflection by the galvanometer mirror, the mirror N and another mirror not shown. The controls for potentiometer I are located on panel Q.

The Leeds and Northrup type K-2 potentiometer used in establishing the calorimeter heater voltage drop and current is shown as R in fig. 7. Controls for the heater circuit are located above the galvanometer J on the panel S. Controls for the K-2 are located on the panels Q and S. Galvanometer deflections were observed on the ground glass scale T, receiving a light beam from the light source U after reflection by the galvanometer mirror V and another mirror not shown in the figure. Variacs used in the control of immersion and external heaters associated with the oil bath are located on panel X. The heaters controlled from this panel were used only for heating the oil bath to the desired operating

temperature. The control panels of fig. 7 are shown in the photograph, fig. 8. Additional controls mounted below the bench in fig. 8 are shown in the photograph, fig. 9. The upper variac in this photograph controls the electrical input to a transformer providing power for heating the adiabatic jacket. The other variacs control the input to transformers providing the electrical supply to various heaters situated along the vapor line to the orifice block.

Additional Equipment

Additional instruments and control equipment used in conjunction with the calorimeter are located in another room and may be seen in the photograph, fig. 10. These include the two Mueller bridges used in the measurement of the calorimeter bomb and oil bath temperatures, a K-2 model potentiometer for measurement of the temperature difference between the adiabatic jacket and oil bath and the White double potentiometer used in evaluating temperature differences inside the vacuum jacket. These have been enumerated earlier in this section. The electronic modulating circuit used in conjunction with one of the Mueller bridges to control the temperature of the oil bath is not shown, although the associated controls may be seen on the panel above the bridges, fig. 10.

Two operators located at the two control stations, shown in figs. 8 and 10, were required for the successful operation of the equipment and to take readings during the run. Communication between the operators was carried on through an inter-communication system with components located at the two consoles.

MATERIALS

The n-pentane employed in this investigation was obtained as research grade from the Phillips Petroleum Company, which reported it to contain not more than 0. 0002 mole fraction of impurities from determinations of the melting point. The sample yielded an index of refraction of 1. 3549 relative to the D-lines of sodium at 77° F., as compared to a value of 1. 35472 reported by Rossini (1) for an air-saturated sample at the same temperature. From these indications, it is believed that the effect of impurities in the n-pentane employed on the evaluation of the enthalpy change was negligible. Before use, the n-pentane was dried with freshly extruded metallic sodium and then deaerated. The dissolved air was removed by freezing the material, using liquid nitrogen as the refrigerant, and subsequent evacuation. This operation was repeated until a constant pressure was observed above the frozen material in two successive operations.

The cyclohexane involved in this investigation was also obtained from the Phillips Petroleum Company, as research grade, and was reported to contain not more than 0. 0006 mole fraction of impurities from determinations of the melting point. The sample showed an index of refraction of 1. 42353 relative to the D-lines of sodium at 77° F., which compares favorably with a value of 1. 42354 reported by Rossini (1) for an air-saturated sample at the same temperature. On the basis of this information, it is believed that the uncertainty involved in the measurements by the presence of the impurities is negligible. The cyclohexane

sample was dried and deaerated before use in the same manner as the n-pentane.

The research grade 1-butene used in this work was also obtained from the Phillips Petroleum Company and was reported to contain 0.0030 mole fraction of impurities. The most probable impurities were listed as 1, 3-butadiene, isobutylene and trans 2-butene. An independent purity check, obtained by chromatographic analysis, indicated the presence of propylene, n-butane and 1, 3-butadiene in the amount 0.00024, 0.00126 and 0.00147 mole fraction, respectively. The total impurity level agrees with that reported by the Phillips Petroleum Company. The 1-butene was deaerated before use in the same manner as the n-pentane.

PROCEDURES

Material Transfer into Calorimeter

A material transfer was first preceded by an evacuation of the calorimeter bomb to remove the remaining traces of the previous material under investigation. The transfer was carried out by distillation of the material from the transfer cylinder to the calorimeter bomb, the transfer cylinder being fastened to a loading block and submerged in boiling water. The quantity of material transferred was sufficient to insure that the calorimeter heater was well below the surface of the liquid phase and that at least 20 per cent of the volume of the bomb was occupied by the gas phase. The latter requirement was necessary to prevent the carry-over of liquid entrainment with the gas phase withdrawn in a vaporization process. Since material was continually removed from the calorimeter, a record was kept of the amount of material remaining in the bomb and subsequent additions were made when necessary.

Preliminary Operations

The operations described subsequently were carried out in preparation for a vaporization process. The calorimeter bomb and oil bath first were heated to the selected vaporization temperature. At this temperature, the oil bath temperature was set on automatic control by means of the thyratron control circuit. The temperature gradient along each of the two tubes leading from the top of the bomb was reduced to nearly zero by adjustment of the appropriate guard heaters. The temperature

of the section of withdrawal tube between the vacuum jacket and orifice block was adjusted to approximately 3-5° F. above the temperature of the bomb by means of four guard heaters situated along this length of tube. The temperature of the orifice block was similarly adjusted by means of a separate guard heater.

At this stage, two weighing bombs were attached to the vapor receiving manifold and cooled with liquid nitrogen. The appropriate lines were evacuated to the weighing bombs and the orifice block. In addition, the vacuum in the vacuum jacket, maintained by a separate vacuum system, was checked.

The agitator was then started and electrical energy introduced to the heater within the calorimeter bomb. A valve to one of the weighing bombs and one or more of the orifice valves were opened, starting a vapor flow. The rate of energy addition to the heater was then adjusted until the temperature of the calorimeter bomb was nearly constant and close to that of the jacket. A withdrawal rate in the range 0.2 to 0.6 grams per minute was usually selected which required a heater current between 0.25 and 0.50 amperes.

Vaporization Test Run

When the various operating variables as described above were adjusted to the desired conditions, the vaporization test run was started by diverting the vapor flow into the second tared weighing bomb. The timer switch, strategically situated near the weighing bombs, was tripped simultaneously. During the run, readings were taken to determine the

following:

(1) Voltage drop and current through the calorimeter heater, taken at one or two minute intervals.

(2) Temperature inside calorimeter bomb.

(3) Temperature of the oil bath.

(4) Temperature difference between the calorimeter bomb and the jacket.

(5) Temperature difference between liquid phase and outgoing gas within calorimeter bomb.

(6) Differences in temperature between the withdrawal line and the calorimeter bomb, determined at four points along the withdrawal line and at the orifice block.

(7) Temperature gradients along the two tubes leaving the top of the calorimeter bomb.

(8) Temperature gradient along one of the calorimeter heater leads situated between the calorimeter bomb and the jacket.

Manual adjustments of the heaters along the withdrawal line and on the orifice block were made, as required, to maintain the temperatures within acceptable limits during the test (3-5° F. above the temperature of the calorimeter bomb). The minor adjustments to the current through the calorimeter heater were made at specified integral times noted on the timer.

The run was usually stopped after a minimum of 10 grams of sample was withdrawn by diverting the flow of vapor back to the original

weighing bomb and stopping the timer. The weight of sample collected during the run was determined from the initial and final weights of the second weighing bomb.

Control of Operating Conditions

The temperature of the oil bath and vacuum jacket could be maintained constant to within approximately 0.01° F. during the vaporization tests. The maximum variation in the temperature of the calorimeter bomb experienced in the tests was 0.05° F. and the average of the maxima for all of the determinations was about 0.025° F. In all of the tests, the temperature of the bomb at the end of a test was identical to the temperature at the start of the test, as a result of corrective adjustments to the calorimeter heater current before the end of each test. This practice of matching the initial and final temperatures eliminated an energy correction term in the calculations as a result of the heat capacity of the calorimeter bomb and contents.

A typical figure illustrating the variation in the temperature of the bomb with elapsed time during a test is shown in fig. 11. The power input to the calorimeter heater is also shown over the same time interval.

The difference between the temperature of the liquid phase and outgoing gas, associated with the thermal transport process, varied between approximately 0.04 and 0.31° F. depending upon the rate of vaporization and other factors affecting it. However, the temperature difference was substantially constant over the duration of an individual test.

Calorimeter Bomb Agitator Calibration

In the calibration of the agitator, the calorimeter bomb and oil bath were heated to the desired temperature region for the calibration. With the calorimeter agitator in operation, the temperature of the oil bath was then adjusted by approximate adjustments of the thyratron control circuit temperature control setting, as indicated on the Mueller bridge, until it was the same as the temperature of the bomb. Since the calorimeter temperature increased with time, as a result of the operation of the agitator, it was necessary to continually reset the temperature control setting to maintain the condition of zero temperature difference between the oil bath and the bomb. The two differential thermocouples measuring the temperature difference between the calorimeter bomb and adiabatic jacket in the upper and lower regions of the calorimeter were used in establishing the condition of zero temperature difference.

When this condition was reached, readings of the temperature of the calorimeter as a function of time were started. The oil bath temperature control point was adjusted upwards as required during these readings to maintain the zero temperature difference between the calorimeter bomb and adiabatic jacket. After a sufficient number of readings were taken to determine the rate of rise of temperature of the bomb due to the operation of the agitator, electrical energy was introduced in the heater at about the same rate as added by the agitator. The readings of temperature versus time were continued and a zero temperature difference between the bomb and jacket maintained in the same

manner as earlier. In addition, readings were taken to establish the voltage drop and current through the heater as a function of time. Approximately the same number of readings, taken over an equal temperature increment of the bomb, were taken with the heater in operation as in the previous case with just the agitator in operation. The evaluation of the rate of energy addition by the agitator, described in the subsequent section, consisted in comparing the rate of temperature rise of the bomb due to the operation of the agitator and heater with the rate due to the operation of the agitator alone. The actual calibration was usually started at a temperature slightly lower than that of interest so that the temperature of the bomb at the instant of the electrical energy addition was the same as the desired temperature of calibration.

EVALUATION OF ENTHALPY CHANGE UPON VAPORIZATION FROM EXPERIMENTAL DATA

The general relation for evaluation of the enthalpy change from experimental data is given by equation 25. In the present case however the perturbations from isothermal-isobaric conditions were sufficiently small to permit the use of the simpler expression presented as equation 27. The maximum perturbation in temperature, experienced in this work, was 0.04° F. The uncertainty introduced by the use of equation 27 in place of equation 25 was determined to be less than 0.01%.

Rewriting equation 27 here for convenience the enthalpy change is given by

$$H_d - H_b = \frac{\underline{Q}_{1,2}}{m_1 - m_2} \frac{V_g - V_\ell}{V_g} + \Delta H_\ell - \Delta H_g \qquad (27)$$

The net heat added during the vaporization process, $\underline{Q}_{1,2}$, is comprised of three parts, each of which is evaluated separately. As discussed in the thermodynamic analysis, these quantities are related as follows,

$$\underline{Q}_{1,2} = \int_1^2 \underline{q} = \int_1^2 \underline{q}_e + \int_1^2 \underline{q}_s + \int_1^2 \underline{q}_{c+r} \qquad (28)$$

The remainder of this section is devoted to a presentation and discussion of the methods employed in the evaluation of the terms appearing in equations 27 and 28.

Energy Added Electrically

The energy added electrically was established from the voltage readings taken during the vaporization process in order to yield the voltage drop and current through the heater as a function of the elapsed time. The following expression involving the voltage drop and current was used to evaluate the energy dissipated electrically in the heater:

$$\underline{Q}_e = \int_1^2 \underline{q}_e = \int_1^2 i_A v_A d\theta \,. \tag{29}$$

The actual integration of equation 29 was performed graphically utilizing the evaluations which were made of the current and voltage as a function of time.

The calorimeter heater circuit and the arrangement of the associated equipment used to obtain the measurements for use in the evaluation of the current and voltage are described in detail in the Description of Apparatus section. For present purposes, the circuit diagram presented as fig. 5 is sufficient to illustrate the method which was used in obtaining the current and voltage. Additional information pertinent to the diagram is to be found on the two pages which follow the figure. The relations by means of which the current and voltage were calculated from the voltage readings and a knowledge of the resistances of the standard resistors, as well as of the leads, are given by

$$i_A = \frac{v_D}{r_D} - \frac{v_k}{r_k} \tag{30}$$

and

$$v_A = v_k \left(\frac{r_J + r_K + r_{\ell_1} + r_{\ell_2}}{r_K} \right) - 2i_A r_A \qquad (31)$$

These relations have also been presented with the circuit diagram.

The second term in equation 31 represents the correction for the voltage drop across the portion of the heater leads situated outside of the calorimeter bomb but within the part of the calorimeter heater circuit which is within the voltage divider loop. The resistance of this section of the leads was calculated from the resistivity of copper, taken from the literature (27), and the dimensions of the leads. A plot of the resistance of the leads as a function of temperature is shown in fig. 12. The resistance values r_D and r_K and the combined values $r_J + r_K$ and $r_{\ell_1} + r_{\ell_2}$ were obtained by calibration against standard resistors.

The extent of uncertainty in the resistances of the standard resistors was less than 0. 02 per cent. The uncertainty involved in the evaluation of the power input to the heater was estimated to be less than 0. 04 per cent. The time readings could be obtained with a maximum uncertainty of 0. 2 second. From this, it was estimated that the maximum uncertainty involved in the evaluation of the energy added electrically was less than 0. 05 per cent. Since the net heat added, $\underline{Q}_{1,2}$, is comprised for the most part of the energy added electrically, the same uncertainty was introduced into the net heat added.

Energy Added Mechanically

The energy transferred mechanically by the agitation of the calorimeter contents is given by

$$\underline{Q}_s = \int_1^2 \underline{q}_s = \int_{\theta_1}^{\theta_2} \dot{\underline{q}}_s \, d\theta , \tag{32}$$

which reduces to the following under the conditions of the vaporization process

$$\underline{Q}_s = \dot{\underline{q}}_s(\theta_2 - \theta_1) \tag{33}$$

The rate of energy addition by the agitation, $\dot{\underline{q}}_s$, was determined at each temperature of measurement by calibration against a known rate of electrical energy input. The calibration procedure consisted in comparing the rate of rise of temperature of the calorimeter bomb, resulting from the operation of the agitator, with the rate of rise due to the operation of the agitator and the simultaneous addition of energy electrically with the heater. The electrical energy addition rate was about the same as that with the agitator. A representative plot of temperature versus time obtained in such an agitator calibration is shown in fig. 13. The rate of the energy addition by the agitator was determined from the slopes of the two lines, in such a plot, and a knowledge of the power input to the electrical heater by means of the relation

$$\dot{\underline{q}}_s = \frac{S_1}{S_2 - S_1} P_E \tag{34}$$

where S_1 is the slope corresponding to the operation of the agitator, S_2 the slope due to the operation of both the agitator and the heater and P_E is the electrical power input to the heater.

The rate of the energy addition by agitation is a function of a number of variables including the speed of rotation of the agitator and the viscosity, specific weight and quantity of the fluid in the calorimeter. For this reason a constant speed motor was employed to drive the agitator and the agitator calibrations were carried out at each temperature investigated. In addition, a separate set of agitator calibrations were carried out for each new system investigated. The amount of variation in the quantity of fluid in the calorimeter was small and the effect of this variation on the agitator calibration was less than the uncertainty involved in the evaluation of the rate of energy addition by the agitator and hence was neglected.

It is estimated that the uncertainties in the rate values for the energy addition by the agitator were not greater than 10 per cent. Since the energy contributed by the agitator amounted to as much as 2 per cent of the net energy added in the vaporization process, the uncertainty introduced into the net energy term, $\underline{Q}_{1,2}$, amounted to as much as 0.2 per cent.

Energy Transferred by Conduction and Radiation

The rate of energy transfer by conduction and radiation was assumed to be directly proportional to the temperature difference existing between the calorimeter and the surrounding jacket. It can be shown (23)

that this assumption, which is not in general agreement with Stefan's law for energy transfer by radiation, is reasonable in the present case involving a small temperature difference. Hence, the energy transferred by conduction and radiation is given by

$$\underline{Q}_{c+r} = \int_{1}^{2} \underline{q}_{c+r} = \int_{\theta_1}^{\theta_2} k(T_J - T_A)d\theta \,, \tag{35}$$

which reduces to the following under the conditions of the process:

$$\underline{Q}_{c+r} = k \int_{\theta_1}^{\theta_2} (T_J - T_A)\, d\theta \tag{36}$$

The integration of equation 36 for the energy transferred by conduction and radiation was performed graphically. In the calculations, the temperature difference $(T_J - T_A)$ was represented by the difference in temperature between the calorimeter and the oil bath. It was convenient in the calculations to express the temperature difference and proportionality constant in terms of resistance units read directly off the Mueller bridges which were used in the measurement of the thermometer resistances.

The proportionality constant, k, was determined by applying equation 36 to an actual case in which a known amount of energy was exchanged, under conditions approximating those of the vaporization process. The procedure consisted in adding a measured amount, $\underline{Q}_e$, of energy electrically to the calorimeter and recording the temperature difference between the calorimeter and surrounding jacket, $(T_J - T_A)$,

as a function of the time, θ, over the time interval required for the calorimeter to return to its initial temperature. The temperature of the jacket T_J, was maintained at a constant value throughout the determination. The proportionality constant was solved for directly utilizing the above data and equation 36. The proportionality constant determinations were carried out at two temperatures, 130° F. and 310° F., and values at the other temperatures of interest were obtained by linear interpolation and extrapolation of these values. The values of the proportionality constant are presented in Table 1.

The values of the proportionality constant actually measured are probably known to within 4 per cent and it is believed that the interpolated values are uncertain by not more than 10 per cent. This uncertainty introduced less than 0. 006 per cent uncertainty in the evaluation of the net energy associated with the vaporization process. In this work, the energy transferred by conduction and radiation amounted to less than 0. 06 per cent of the net energy involved in the vaporization process.

Weight of Material Withdrawn

The weight of material withdrawn, which established the change in the weight of the calorimeter contents, $m_1 - m_2$ in equation 27, was obtained from the initial and final weights of the weighing bomb used to collect the material. It is estimated that the uncertainty involved in the weight measurement did not exceed 0. 02 per cent.

Volumetric Factor

The volumetric factor, $\frac{V_g - V_\ell}{V_g}$, was evaluated from published experimental data which were available for the n-pentane and 1-butene systems (28, 29, 30). In the case of cyclohexane, however, such data was available only for the saturated liquid (31). The specific volume of the saturated gas was obtained by the simultaneous solution of equation 27 and the Clapeyron equation,

$$H_d - H_b = T \frac{dP''}{dT} (V_d - V_b), \qquad (37)$$

using unpublished vapor pressure data of cyclohexane available in this laboratory. Residual techniques were employed in the evaluation of the slope of the vapor pressure curve, $\frac{dP''}{dT}$, utilizing a theoretical logarithmic relationship similar to the Antoine equation (1) for the reference vapor pressure as a function of temperature. It was established that volumetric data for the saturated gas, obtained in this way, is in excellent agreement with reliable experimentally measured values (32, 33, 34).

The effect of uncertainties in the volumetric data on the volumetric factor, and hence, the enthalpy change, depends upon the location of the region of measurement relative to the critical state. An analysis of the uncertainty involved indicates that the uncertainty in the volumetric factor, and the enthalpy change, is inversely proportional to the value of the volumetric factor, which approaches zero as the critical state is approached. In this work, the enthalpy change measurements were

terminated at a temperature sufficiently remote from the critical region that the uncertainty involved as a result of the uncertainties in the volumetric data was not significant.

On the basis of the reported accuracy of the volumetric data, the maximum uncertainty in the enthalpy change introduced through the volumetric factor was calculated to be less than 0. 03%. The lowest value of the volumetric factor involved in the calculations was 0. 88491 calculated for n-pentane at 310° F.

Superheat and Subcooling Corrections

The evaluation of the superheat and subcooling correction terms, ΔH_l and ΔH_g respectively, in equations 16 and 27, requires a knowledge of the actual temperature of the vaporization. This temperature could not be determined exclusively from a knowledge of the temperature of the liquid and the temperature difference between the liquid and the gas phase withdrawn, which were measured. It has been shown (23) however that for the purposes of the evaluation of the temperature-enthalpy change relationship, the relationship obtained is the same regardless of the temperature of vaporization that is selected in the calculation, in the range extending from the temperature of the liquid to the temperature of the gas phase. In view of this, the temperature of vaporization assumed in the calculations was the same as that of the liquid phase since this temperature was actually measured and therefore could be determined accurately. Hence, the superheat involved in the calculations was zero and the measured temperature difference between

the liquid and the gas phase withdrawn represented subcooling of the gas phase.

The correction to the enthalpy change due to subcooling was evaluated by means of the following relation, obtained from equation 16,

$$\Delta H_g = \int_{T_d}^{T_g} c_{p_g} dT = c_{p_g} (T_g - T_\ell) \qquad (38)$$

The last equality in this relation follows from the last sentence in the previous paragraph.

The heat capacity of the dew-point gas used in the calculations was obtained from published experimental data (35, 36) and the data of Rossini for the ideal gas state (1). It was also calculated from published data of other thermodynamic properties (28, 37) by means of the following rigorous thermodynamic expression,

$$c_{p_d} - c_{p_b} = \frac{d(H_d - H_b)}{dT} \left[\left(\frac{\partial H}{\partial P} \right)_{T_\ell} - \left(\frac{\partial H}{\partial P} \right)_{T_g} \right] \frac{dP''}{dT} \qquad (39)$$

The maximum contribution to the enthalpy change by the correction for subcooling of the gas phase amounted to less than 0.10 per cent of the enthalpy change upon vaporization. The uncertainty introduced in the enthalpy change as a result of the uncertainty in the evaluation of the subcooling correction is believed to be less than 0.03 per cent.

Evaluation of Internal Energy Change upon Vaporization

The internal energy change was evaluated from the enthalpy change and PVT data by means of the familiar relation

$$E_d - E_b = (H_d - H_b) - P(V_d - V_b) \qquad (40)$$

The same volumetric data was used in this evaluation as in the evaluation of the volumetric factor. The vapor pressure data required in the calculation was available in published (28, 29, 30, 31) and unpublished form from measurements conducted in this laboratory.

With reference to equation 40, it may appear that uncertainties in the volumetric data would have a more pronounced influence on the accuracy of the internal energy change evaluation than in the case of the enthalpy change. However, an analysis of the error involved indicates this is not the case over the region of measurement covered by this investigation. This can be explained by the fact that the PV term in equation 40 amounts to less than 15 per cent of the enthalpy term and there is a partial cancellation of errors involved due to the fact that the uncertainty introduced in each of the terms on the right side of equation 40 is of opposite sign. On the basis of the reported accuracy of the volumetric data, it has been estimated that the uncertainty in the internal energy change values introduced by the volumetric data is less than 0.04% over the region of measurement.

RESULTS

The individual experimental measurements for n-pentane are recorded in Table II. Recorded for each determination are the electrical energy added, the energy added mechanically by the agitator, the small correction for conduction and radiation, the weight of material withdrawn, the measured temperature difference between the liquid phase and the gas phase withdrawn, the volumetric correction factor and the evaluation of the enthalpy change. The values of the enthalpy change set forth in Table II are shown plotted versus the temperature in fig. 15. This diagram illustrates the density of experimental measurement and the general behavior of the enthalpy change as a function of temperature. To indicate the deviations between the measurements for n-pentane more clearly, a residual method has been employed. The following relatively simple analytical expression was used to calculate the residual enthalpy change from the enthalpy change and the temperature of vaporization:

$$(H_d - H_b)_{res.} = (H_d - H_b) - (31694.45 - 82.127\,T)^{1/2}$$

where T represents the temperature in degrees Fahrenheit. A comparison of the measurements of this work with the determinations of several investigators (1, 3, 8) can be seen in the plot of the residual enthalpy change versus temperature shown in fig. 16. The full line in this figure represents the critically chosen values of the enthalpy change obtained from a consideration of the experimental values of this work only. The average deviation, with and without regard to sign, and the

standard deviations of the data of each investigator, calculated with reference to the current critically chosen values are presented in Table III. The temperature range over which the comparison was made is also included. The critically chosen values of the enthalpy and internal energy change upon vaporization, based on the smooth curve in fig. 16 as depicting the experimental data, are recorded in Table IV at ten degree intervals in the temperature range 100° F. to the critical temperature 385.9° F. The variation of the volumetric factor for n-pentane with temperature is shown in fig. 17. It is seen that the volumetric factor decreases rapidly above 310° F. towards the value of zero at the critical temperature. Enthalpy change measurements were not made above this temperature for this reason. The energy addition rates of the agitator, obtained by calibration and used in the evaluation of the energy added by the agitator, are presented for each temperature of measurement in Table V.

The experimental results obtained with cyclohexane are presented in Table III in the same manner as for n-pentane. In addition, the specific volumes of the saturated liquid and the saturated gas are also included for each temperature of measurement. Since volumetric data pertaining to the saturated gas was not available in the literature, it was computed as described previously. The values of the enthalpy change upon vaporization of cyclohexane recorded in Table VI are plotted versus the temperature of vaporization in fig. 18. Critically chosen values reported by Rossini (1) at two temperatures have been included. The standard error

of estimate of the experimental points from the smooth curve is 0.35 Btu per lb. Residual methods were also employed in the smoothing of the data for cyclohexane. The residual enthalpy change upon vaporization in this case was evaluated from

$$(H_d - H_b)_{res.} = (H_d - H_b) + 0.18T - 181 .$$

A plot of the residual enthalpy change as established from the current experimental data and the two values of Rossini (1) is shown in fig. 19. In locating the curve in the figure, the measurements at 190° F. identified in Table VI as number 289 were not considered since the vaporization rate involved was lower than in the other measurements and therefore probably involved larger uncertainty. The energy addition rates of the agitator obtained by calibration for cyclohexane are presented in Table VII for each temperature of measurement. As can be seen from fig. 19, the agreement of the current measurements with the point of Rossini (1) at 77° F. measured at the Bureau of Standards (9) is excellent. However, the deviation at 177° F. is approximately 1.3 Btu per lb. The smoothed values of the enthalpy change and internal energy change are reported in Table VIII at 10° increments over the temperature range 100° - 310° F. involved in the measurement. In addition, the specific volumes at dew-point and bubble-point have been included.

The experimental results for 1-butene are presented in Table IX in the same form as in the case of the two previous systems. These measurements were stopped at 220° F. because of the approach to the critical state where the volumetric behavior exerts a pronounced

influence upon the values obtained from the calorimetric measurements. The variation of the volumetric correction factor of 1-butene with temperature, computed from experimental volumetric data (29), is illustrated graphically in fig. 20. In Table X, the results of the agitator calibration conducted on 1-butene are recorded for each vaporization temperature. The following relation was used in the calculation of the residual enthalpy change upon vaporization of 1-butene:

$$(H_d - H_b)_{res.} = (H_d - H_b) - (29,584 - 90.78T)^{1/2}$$

The experimental data for 1-butene obtained in this work and the two values reported by Rossini (1) are shown in fig. 21 in the plot of the residual enthalpy change versus temperature.

It is seen that the extrapolation of the smooth curve drawn through the currently reported data is consistent with the values reported by Rossini (1). A value obtained by the National Bureau of Standards was not available in Rossini and hence a comparison could not be made for the case of 1-butene. Table XI records the critically chosen values of the enthalpy change upon vaporization of 1-butene as well as the internal energy change based on the curve in fig. 21.

DISCUSSION

An estimate of the uncertainty involved in an evaluation of the enthalpy change upon vaporization can be obtained by considering the uncertainties in the individual quantities by means of which the enthalpy change is evaluated. These quantities, which appear in equations 27 and 28, include the energy added electrically, the energy added by the agitator, and by conduction and radiation, the weight of material withdrawn, the volumetric correction factor and the subcooling of the gas phase. The uncertainty introduced by the individual energy terms in equation 28 into the net energy added $\underline{Q}_{1,2}$, has been discussed in the respective sections dealing with the evaluation of these terms. The maximum uncertainty in $\underline{Q}_{1,2}$ is the sum of the uncertainties introduced individually by these terms. The maximum uncertainty associated with the evaluation of the volumetric correction factor and the weight of material withdrawn, respectively, has also been discussed previously in the sections dealing with the evaluation of the particular quantities. It can be shown from an error analysis that the maximum uncertainty introduced in the enthalpy change by the uncertainties in the evaluations of the net energy added $\underline{Q}_{1,2}$, the weight of material withdrawn, and the volumetric correction factor is the sum of the uncertainties involved in each of these quantities. The amount of the uncertainty associated with the evaluation of the subcooling correction term, which is added to this sum, is small and has also been discussed previously.

Two additional sources of uncertainty must be considered which

arise as a result of the limitations in the precision and the accuracy of the temperature measurement associated with the calorimeter bomb. Referring to the "Thermodynamic Analysis" section and equations 26 and 27 in this section, equation 27 follows from equation 26 if the perturbations from isothermal-isobaric conditions are small, a good assumption in the present case, and in addition, if the initial and final temperatures are identical. The validity of the latter assumption is determined by the precision of the temperature measurement. It is estimated that the uncertainty involved in matching the initial and final temperatures because of limitations in the precision of temperature measurement introduced an uncertainty of 0.08% in the enthalpy change evaluated. It should be emphasized that this uncertainty arises from practical limitations alone and is not due to the use of equation 27 in place of equation 25 in the evaluation of the enthalpy change. As discussed earlier, the use of equation 27 introduced an uncertainty amounting to less than 0.01%. The uncertainty introduced into the enthalpy change as a result of limitations in the accuracy of temperature measurement is given by

$$\delta(H_d - H_b) = \frac{d(H_d - H_b)}{dT}\,\delta T + O(\delta T)^2$$

where the δ is used to denote the uncertainty involved in the temperature and enthalpy change. It is evident that for the same uncertainty in temperature, the uncertainty in the enthalpy change depends upon the region of the measurement and increases with an increase in temperature. In the present case, a liberal estimate of the uncertainty, representing

most of the region investigated, is 0. 01 per cent of the enthalpy change.

The aforementioned uncertainties associated with the evaluation of the enthalpy change are listed below.

Source of Uncertainty	Max. resultant uncertainty in $H_d - H_b$, %
Evaluation of:	
electrical energy	0. 05
agitator energy	0. 20
energy exchange by conduction and radiation	0. 006
weight of material withdrawn	0. 02
volumetric correction factor	0. 03
subcooling of vapor	0. 03
Limitations in:	
precision of temperature measurement	0. 08
accuracy of temperature measurement	0. 01
use of equation 27	0. 01
TOTAL	0. 436

It is seen that the maximum possible uncertainty in an evaluation of the enthalpy change is 0. 436%. It is reasonable to expect however, that the actual uncertainty involved is much lower since this figure represents an extreme case. This is supported by the excellent reproducibility in the values of the enthalpy change upon vaporization for n-pentane, observed in Table II.

All of the uncertainties in the individual quantities and in the final evaluation of the enthalpy change discussed above were evaluated by considering the limitations in the instruments involved in the measurements. Obviously, an additional uncertainty attributable to limitations in the operator carrying out the measurements might be considered. This would depend upon such factors as experience, aptitude, interest and desire of the operator, and others. The uncertainty introduced by the operator cannot be easily predicted beforehand although an approximate evaluation can be made from a consideration of the reproducibility of the final results obtained. In this connection, it may be worthwhile to mention that the author was assisted by a different operator in carrying out the measurements of each different system.

With reference to the above table, the agitator constitutes the greatest source of error in the evaluation of the enthalpy change. This error can be reduced by reducing the fraction of the total energy contributed by the agitator, which can be accomplished by a reduction in the speed of rotation of the agitator. However, the resultant mixing obtained may not be sufficient to maintain a relatively uniform system with respect to temperature gradients. It is felt that the present speed represents a reasonable compromise between a high speed resulting in a more uniform temperature within the calorimeter and a low speed desired for reasons of calibration.

The enthalpy change evaluation is based on the absence of liquid entrainment in the gas phase withdrawn and the existence of a uniform temperature throughout the individual phases (no temperature gradients).

These assumptions are involved in the thermodynamic analysis. Measures taken to ensure against entrainment consisted in operation at reasonable vaporization rates and maintenance of a vapor space of at least 20% within the calorimeter bomb. The problem of temperature gradients has been discussed in the previous paragraph.

REFERENCES

1. Rossini, F. D., others, "Selected Values of Physical and Thermodynamic Properties of Hydrocarbons and Related Compounds," Carnegie Press, Pittsburgh, Pa., 1953.

2. Lacey, W. N., Sage, B. H., "Thermodynamics of One-Component Systems," Academic Press, New York 3, N. Y., 1951.

3. Young, Sidney, Sci. Proc. Roy. Dublin Soc., 12, 374 (1910).

4. Weber, J. H., J. Am. Inst. Chem. Engr., 1, 210 (1955).

5. Brydon, J. W., Walen, N., Canjar, L. N., Chem. Eng. Prog. Symp. Series No. 7, 49, 147 (1953).

6. O'Hara, J. B., Fahien, R. W., Ind. Eng. Chem., 43, 2924 (1951); Am. Doc. Inst., Doc. 3327.

7. Griffiths, Ezer, Awbery, J. H., Proc. Phys. Soc. (London), 44, 121 (1932).

8. Sage, B. H., Evans, H. D., Lacey, W. N., Ind. Eng. Chem., 31, 763 (1939).

9. Osborne, N. S., Ginnings, D. C., J. Res. Natl. Bur. Stds,, 39, 453 (1947).

10. Messerly, G. H., Kennedy, R. M., J. Am. Chem. Soc., 62, 2988 (1940).

11. McCullough, J. P., Person, W. B., Spitzer, R., J. Am. Chem. Soc., 73, 4069 (1951).

12. Ason, J. G., Fink, H. L., Bestul, A. B., Pace, E. L., Szaz, G. J., J. Am. Chem. Soc., 68, 52 (1946).

13. Pitzer, K. S., Lippmann, D. Z., Curl, R. F., Jr., Uggins, C. M., Petersen, D. E., J. Am. Chem. Soc., 77, 3433 (1955).

14. Watson, K. M., Ind. Eng. Chem., 23, 360 (1931).

15. Othmer, D. F., Ind. Eng. Chem., 32, 841 (1940).

16. Othmer, D. F., Ind. Eng. Chem., 34, 1072 (1942).

17. Gordon, D. H., Ind. Eng. Chem., 35, 851 (1943).

18. Haggenmacher, J. E., Ind. Eng. Chem., 40, 436 (1948)

19. Weber, J. H., Inbody, G. W., Hobson, M., Petrol. Ref., 36, No. 3, 221 (1957).

20. Haggenmacher, J. E., J. Am. Chem. Soc., 68, 1123 (1946).

21. Osborne, N. S., Stimson, H. F., Fiock, E. F., J. Res. Natl. Bur. Stds., 5, 411 (1930).

22. Osborne, N. S., Stimson, H. F., Ginnings, D. C., J. Res. Natl. Bur. Stds., 23, 197 (1939).

23. McKay, R. A., Ph. D. Thesis, Dept. Chem. Eng., Calif. Inst. Tech., Pasadena, Calif. (1959).

24. McKay, R. A., Sage, B. H., Am. Doc. Inst., Washington, D. C., Doc. No. 6072 (1959).

25. Sage, B. H., Hough, E. W., "A Calorimeter for Corrosive Liquids," Jet Propulsion Laboratory Progress Report No. 1 - 52, Calif. Inst. of Tech., Pasadena, Calif. (1947).

26. Sage, B. H., Lacey, W. N., Trans. Am. Inst. Mining and Met. Engrs., 136, 136 (1940).

27. Hodgman, C. D., "Handbook of Chemistry and Physics," Chemical Rubber Publishing Co., 35th Ed., P. 2361.

28. Sage, B. H., Lacey, W. N., Ind. Eng. Chem., 34, 730 (1942).

29. Olds, R. H., Sage, B. H., Lacey, W. N., Ind. Eng. Chem., 38, 301 (1946).

30. Sage, B. H., Lacey, W. N., "Thermodynamic Properties of the Lighter Paraffin Hydrocarbons and Nitrogen," American Petroleum Institute, New York 20, N. Y. (1950).

31. Reamer, H. H., Sage, B. H., Chem. Eng., Data Series, 2, No. 1, 9 (1957).

32. Derived Data Book # 1520, Department of Chemical Engineering, California Institute of Technology, Pasadena, California.

33. Derived Data Book # 1536, Department of Chemical Engineering, California Institute of Technology, Pasadena, California.

34. Derived Data Book # 1563, Department of Chemical Engineering, California Institute of Technology, Pasadena, California.

35. Edmister, W. C., Petrol. Ref., 27, No. 11, 129 (1948).

36. Kobe, K. A., Long, E. G., Petrol.Ref., 28, No. 3, 125 (1949).

37. Sage, B. H., Backus, H. S., Vermeulen, T., Ind. Eng. Chem., 28, 489 (1936).

NOMENCLATURE

c	heat capacity
c_p	heat capacity at constant pressure
d	differential operator
E	specific internal energy
$\underline{E}$	total internal energy
f	function of
H	specific enthalpy
k	heat transfer coefficient
ℓ_p	latent heat of pressure change
m	weight of material within calorimeter
O	order
P	pressure
P''	pressure in two-phase region
$\underline{q}$	infinitesimal amount of energy transferred to calorimeter
$\underline{Q}_{1,2}$	net energy added to calorimeter
$\dot{\underline{Q}}$	energy flux
T	temperature
V	specific volume
$\underline{V}$	total volume
w	infinitesimal amount of work performed by the system
θ	time
ΔH	finite increment in enthalpy associated with superheating or subcooling

Subscripts

A	calorimeter
a	pertaining to the material leaving the calorimeter
b	bubble-point liquid
c	by conduction
d	dew-point gas
e	electrical
g	gas
i	interface
J	vacuum jacket
ℓ	liquid
r	by radiation
s	agitator
1	initial condition
2	final condition

Superscript

*	average value

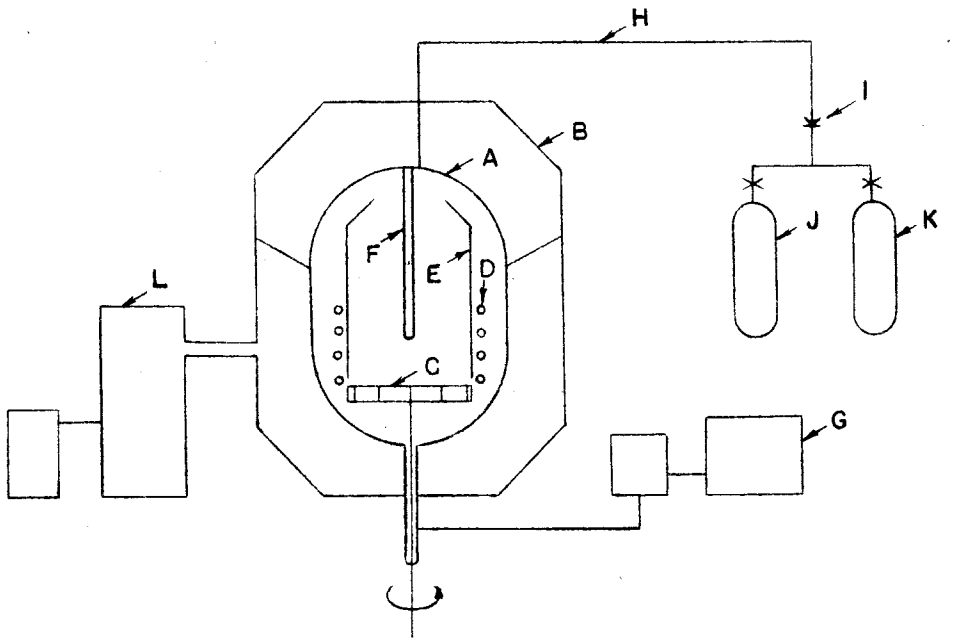

Figure 1. Schematic Arrangement of Equipment

Legend - Figure 1

A	calorimeter bomb
B	vacuum jacket
C	agitator
D	heater
E	circulation shield
F	thermometer well
G	pressure balance
H	vapor withdrawal tube
I	orifice
J	condenser weighing bomb
K	condenser weighing bomb
L	oil diffusion pump

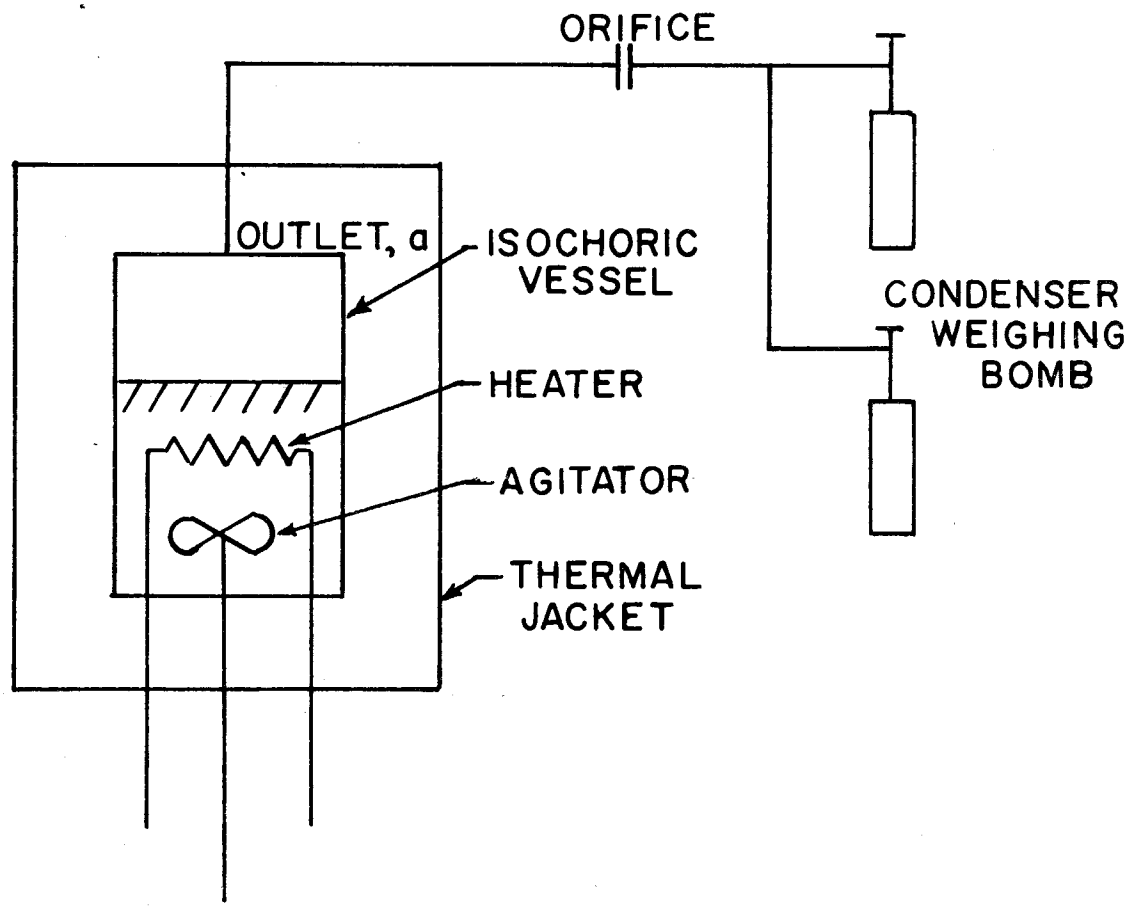

FIGURE 2 - SCHEMATIC DIAGRAM OF THERMODYNAMIC SYSTEM

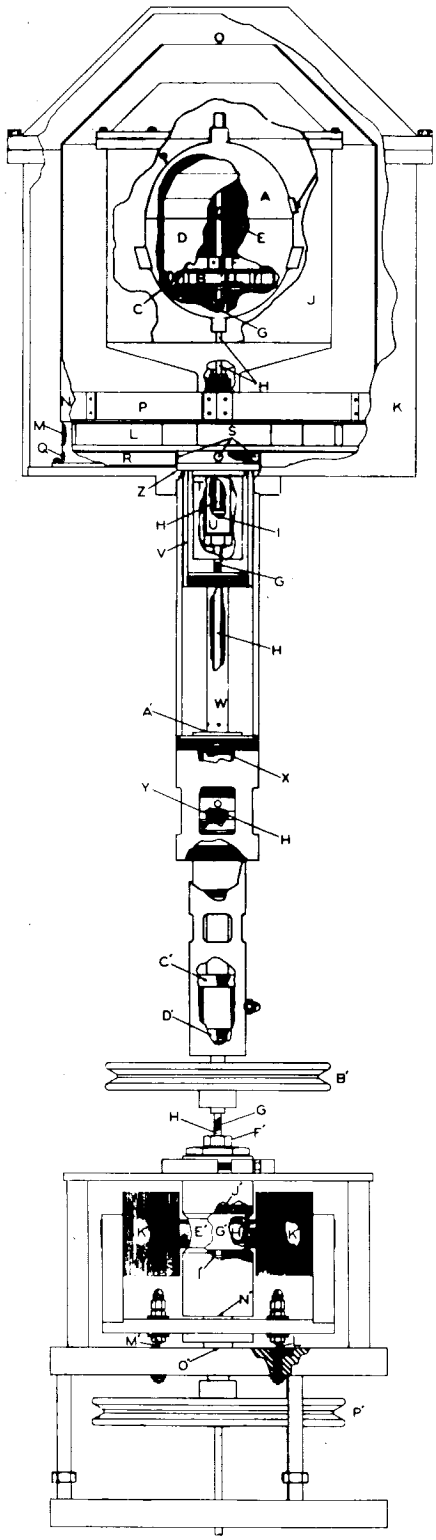

Figure 3 General Arrangement of Equipment

Legend - Figure 3

A	calorimeter bomb
B	agitator
C	ports in circulation shield D
D	circulation shield
E	resistance thermometer
F	radial guide vanes
G	drive shaft for the agitator B
H	tube
I	seal between tube H and sleeve U
J	vacuum jacket
K	oil bath
L	impeller
M	ports in circulation shield N
N	circulation shield
O	opening in circulation shield
P	radial guide vanes
Q	ports in path Q-R-S-T
R	guide vanes
S	ports
T	circulation shield
U	sleeve--part of vacuum jacket
V, W	sleeve--part of drive for the impeller L
X	packing gland through which the sleeve W leaves the oil bath

Legend - Figure 3 (cont.)

Y	packing gland through which the tube H leaves the oil bath
A'	bearing
B'	pulley
C', D'	support bearings for the pulley B'
E'	steel shell
F'	sealing nut between tube H and shell E'
G'	armature housing
I', J'	steel--bronze bearings in which the armature housing rotates
K'	electromagnets
L', M'	slip rings through which the electromagnets are energized
N', O'	support bearings for the electromagnet assembly
P'	pulley to drive the electromagnetic assembly

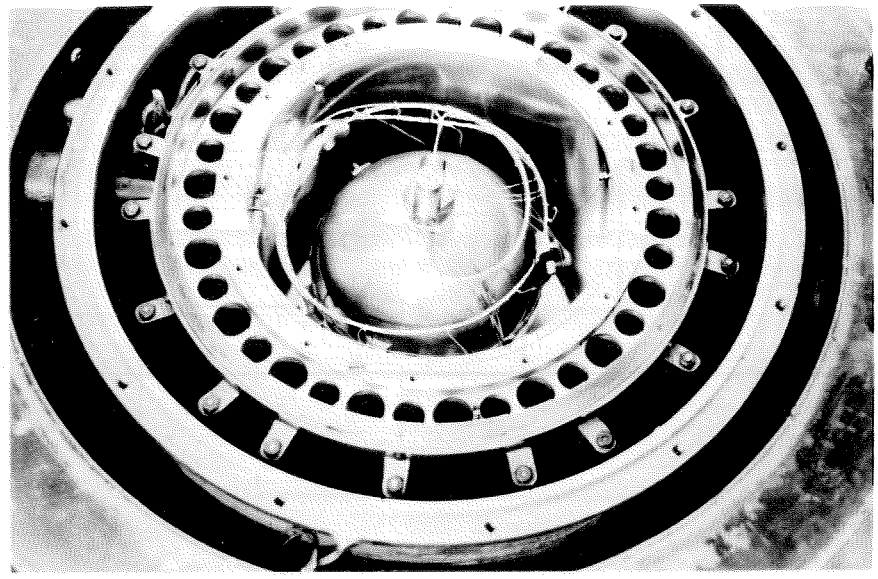

Figure 4. View Showing Paths of Tubes from Top of Calorimeter

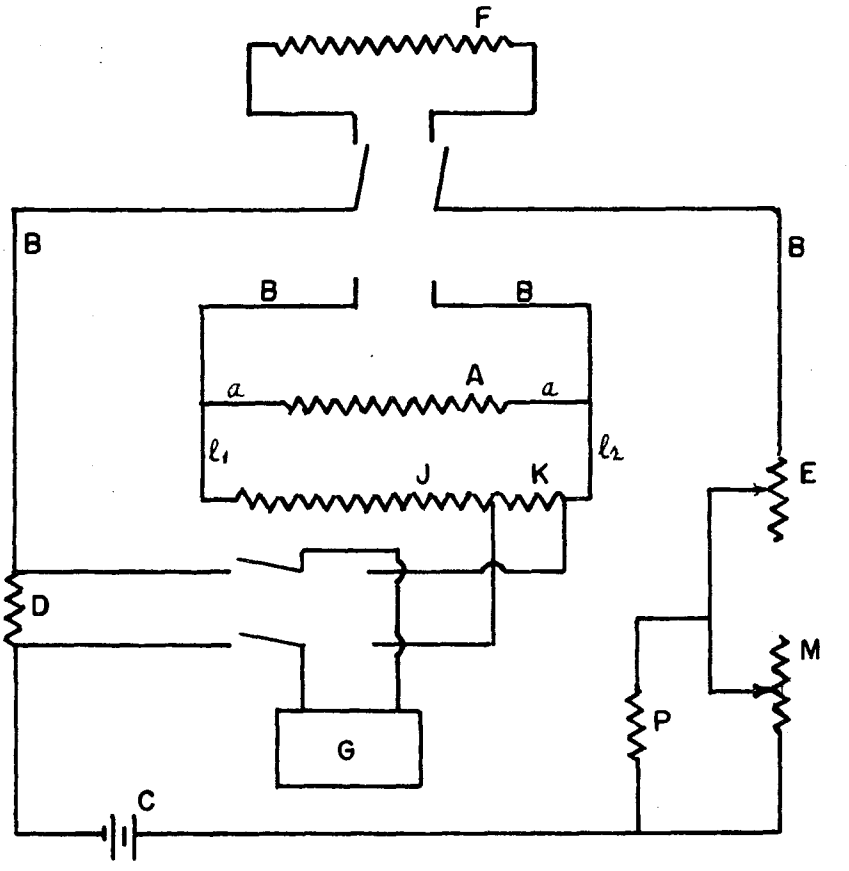

$$i_A = \frac{v_D}{r_D} - \frac{v_K}{r_K}$$

$$v_A = v_K\left(\frac{r_J + r_K + r_{\ell_1} + r_{\ell_2}}{r_K}\right) - 2i_A r_A$$

$$Q_e = \int_{\theta_1}^{\theta_2} i_A v_A \, d\theta$$

Figure 5 - Circuit Diagram, Calorimeter Heater

Nomenclature - Figure 5

A	calorimeter heater
a	part of current leads
B	current leads
C	batteries
D	resistor for measuring current in circuit
E	variable resistor for coarse control
F	auxiliary heater
G	potentiometer
i	current
JK	voltage divider
ℓ	leads in voltage divider loop
M	variable resistor for fine control
P	shunt resistor
$\underline{Q}_e$	energy (electrical)
r	resistance
v	voltage

Circuit Values - Figure 5

v_c	12 volts
r_o	0. 01001376 abs. ohm
r_e	0, 1, 2, ... 19, 20, or 240 ohms
$r_J + r_K$	10, 344 abs. ohms
r_K	679. 07 abs. ohms
$r_{\ell_1} + r_{\ell_2}$	1. 41 ohms
r_M	40, 41, 42, ... 48, 49 ohms
r_P	10 ohms
$2r_a$	See figure 2A

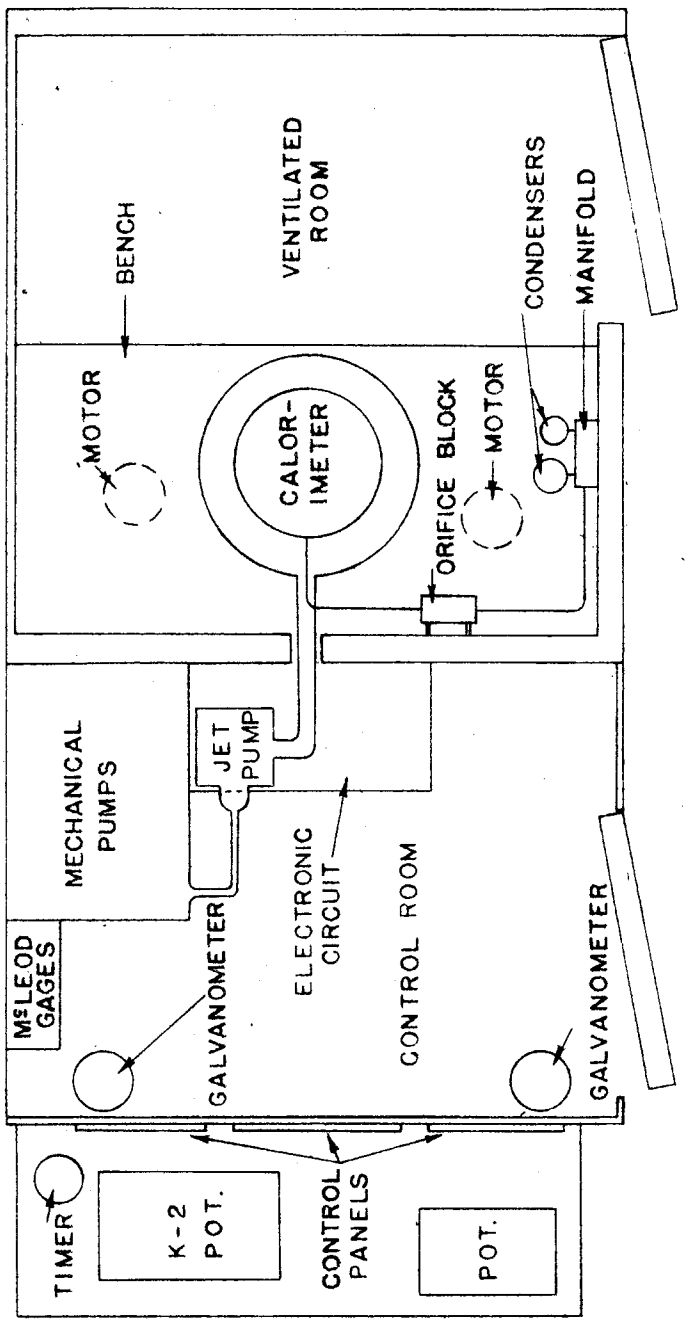

Figure 6. General Arrangement of Calorimeter and Control Equipment

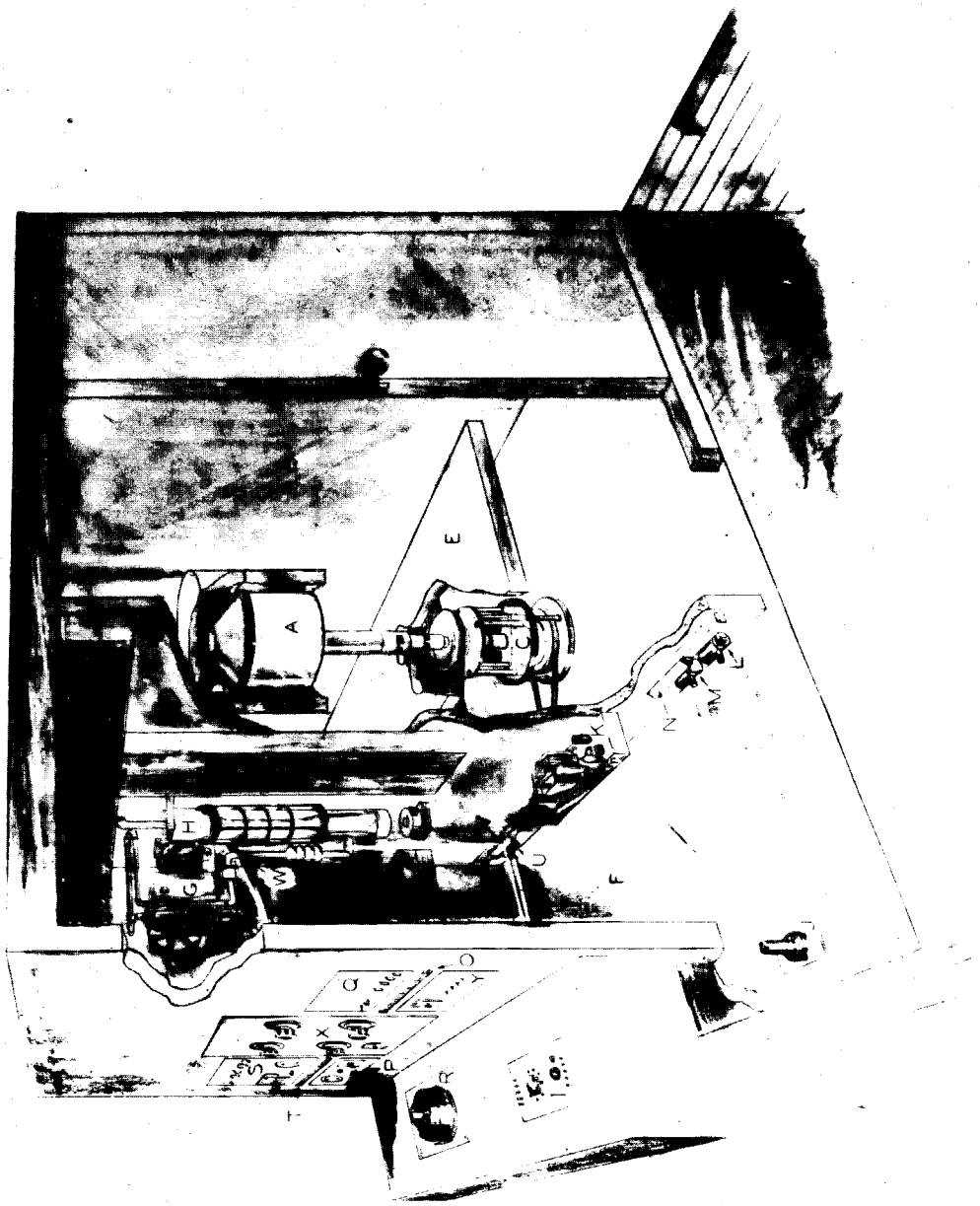

Figure 7. Calorimeter Housing Unit

Legend - Figure 7

A	oil bath
B	calorimeter room
C	drive mechanisms for agitator and impeller
D	adiabatic jacket
E	shelf
F	equipment room
G	mechanical vacuum pump
H	three-stage jet pump
I	L & N student potentiometer
J	galvanometer
K	photoelectric circuit
L	light source
M	light source
N	mirror in light path from M to O
O	ground glass scale
P	control panel for circuit K
Q	control panel for potentiometer I
R	L & N type K-2 potentiometer
S	controls for calorimeter heater
T	ground glass scale
U	light source
V	mirror in light path from U to T
W	location of vacuum pumps
X	control panel for oil bath heaters

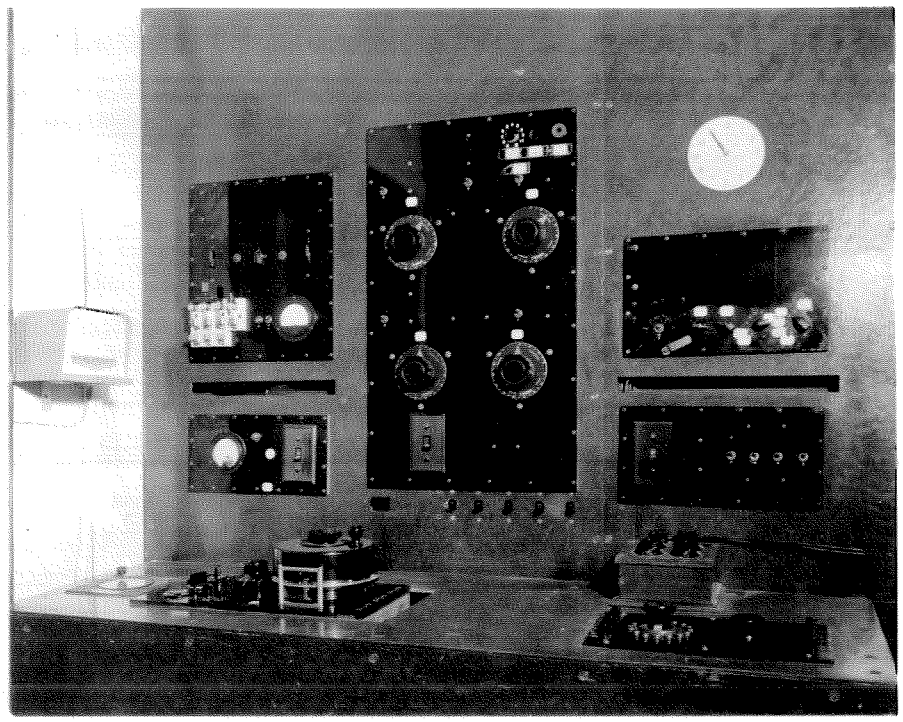

Figure 8. Control Panels of Figure 7

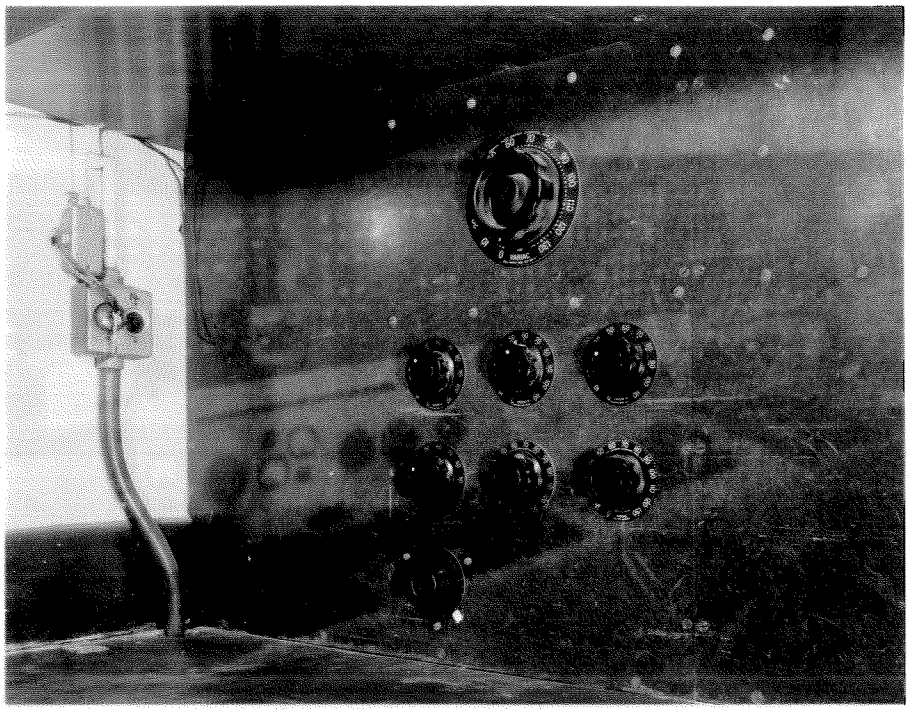

Figure 9. Control Panel

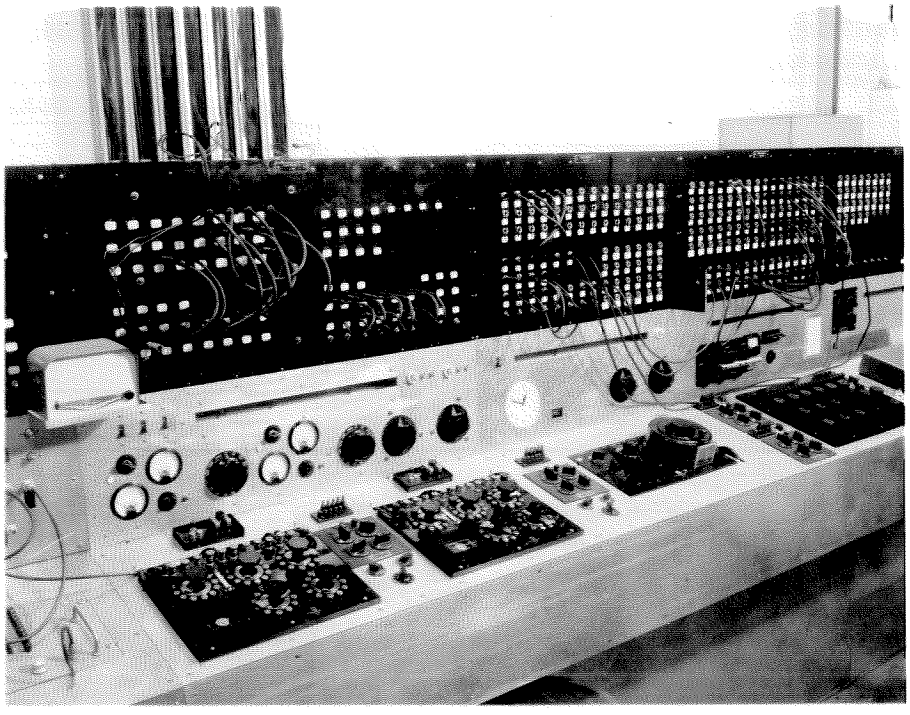

Figure 10. Controls and Instruments

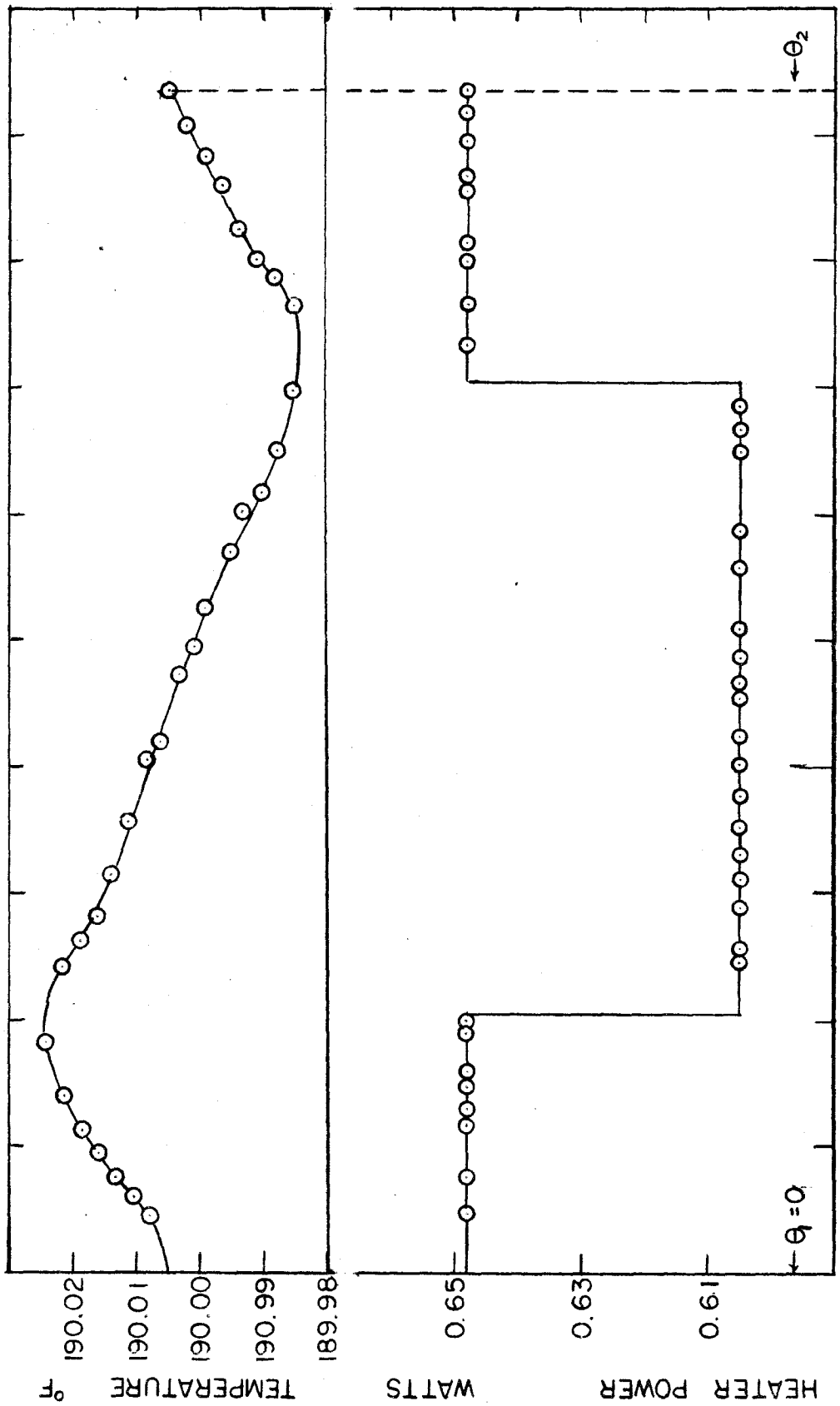

Figure 11. Temperature of Calorimeter and Calorimeter Heater Power as a Function of Time in a Representative Vaporization Process.

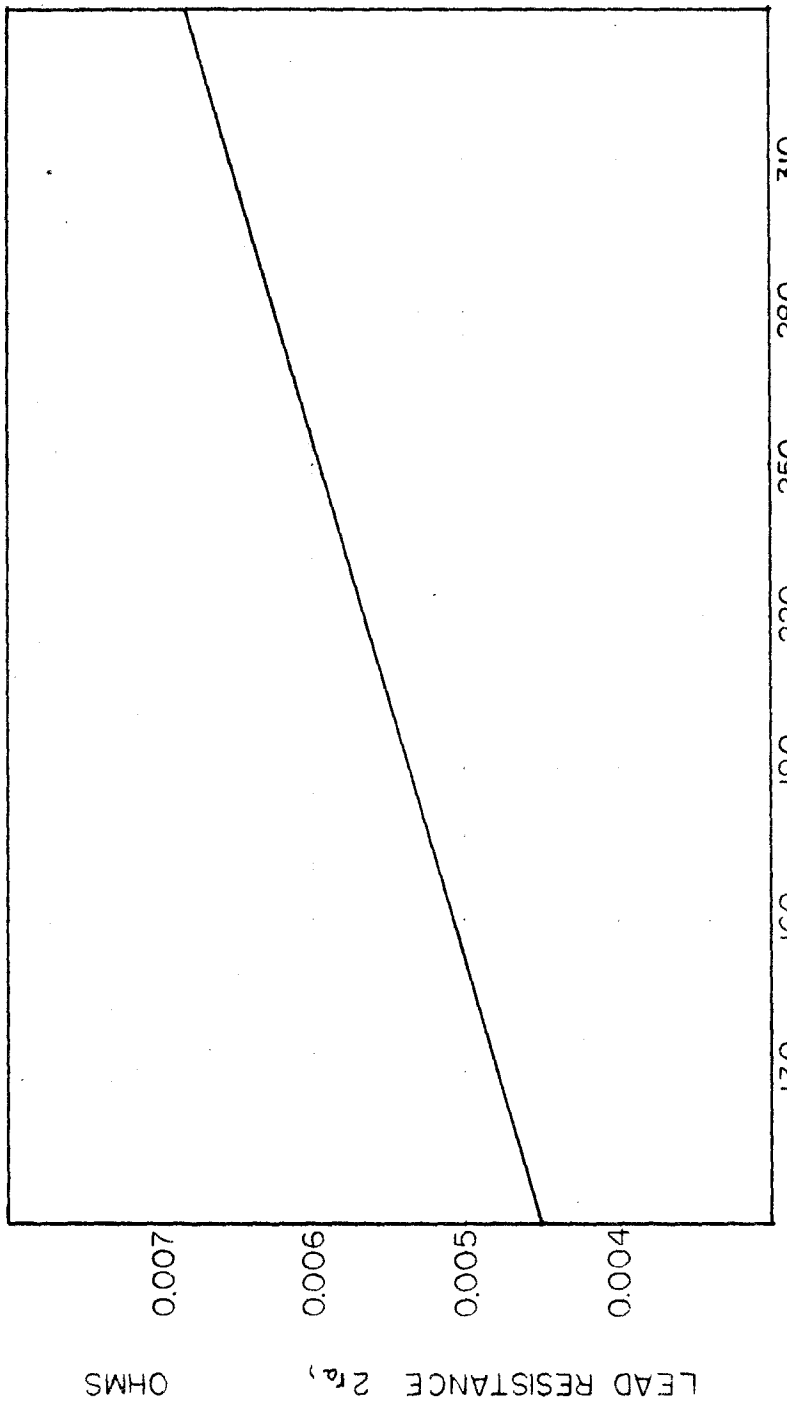

Figure 12. Lead Resistance $2r_a$ Versus Temperature

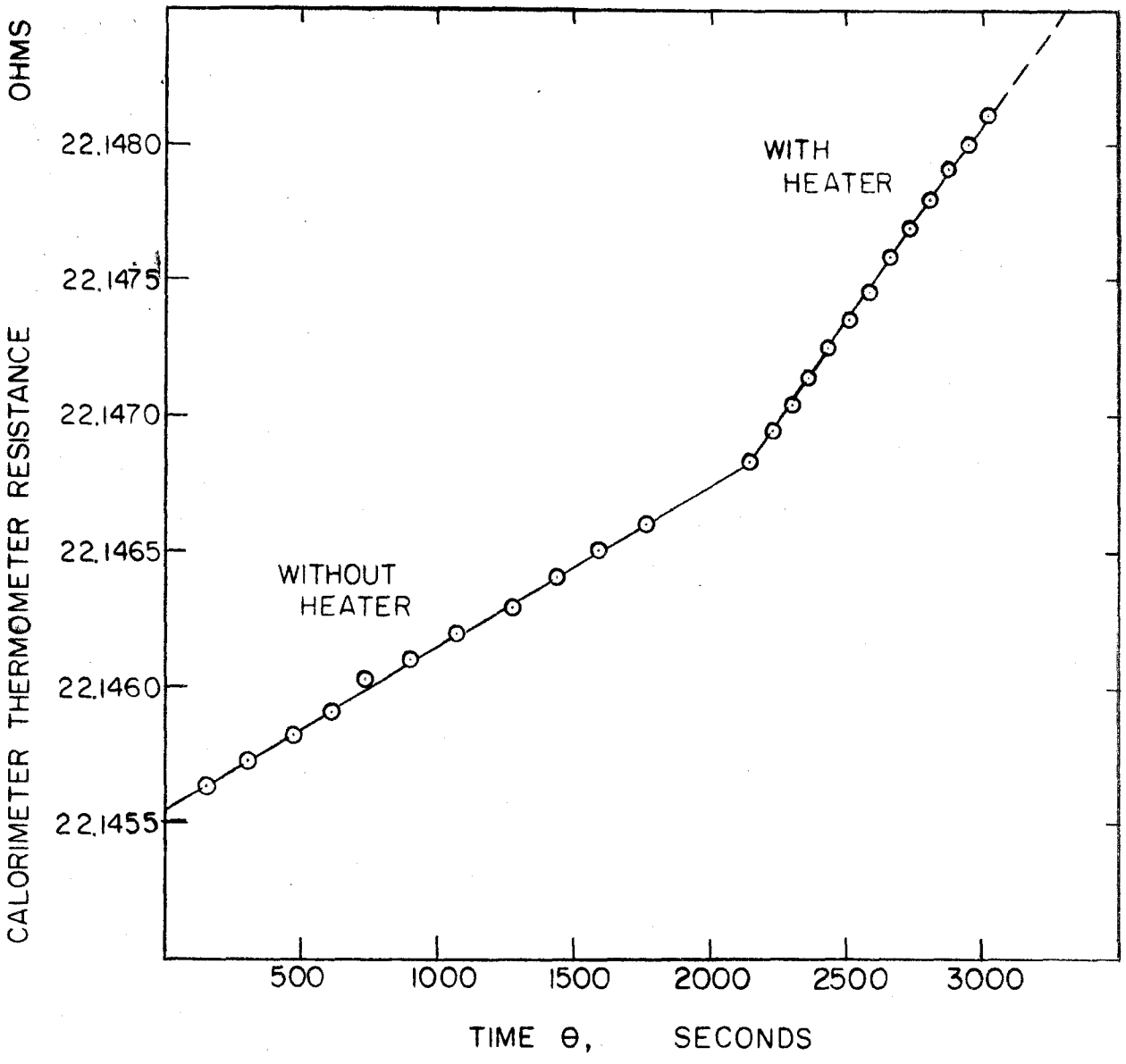

Figure 13. Calorimeter Temperature Versus Time Relationship During an Agitator Calibration.

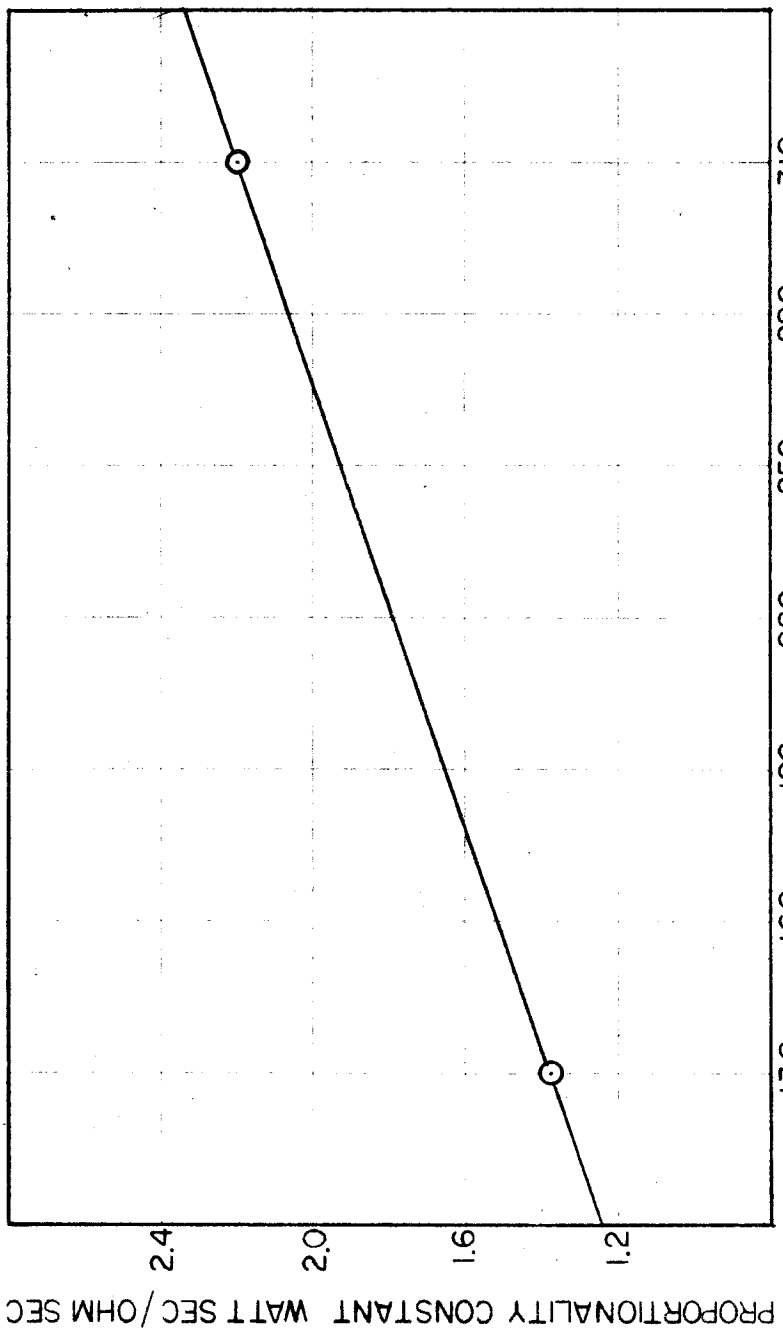

Figure 14. Proportionality Constant k Versus Temperature.

Table I

Results of Heat Transfer Calibration

Temperature, °F.	Proportionality Constant k, watt sec./ohm sec.
100	1.229
130	1.369
160	1.505
190	1.642
220	1.781
250	1.918
280	2.057
310	2.197
340	2.335

Table II

Experimental Results for n-Pentane

Identification	Temp., °F.	Energy Added, Btu: Electrically	Energy Added, Btu: By agitation	Energy Added, Btu: By conduction and radiation	Material Withdrawn, lb.	Superheat of Liquid, °F.	Vol. Corr. Factor	Enthalpy change upon Vaporization, Btu/lb.
249	100.000	4.7748	0.0780	0.0000	0.031502	0.30	0.99480	153.37
241	100.887	6.8270	0.0000	-0.0080	0.044377	0.30	0.99480	152.99
239	130.000	3.6519	0.1026	0.0000	0.025358	0.12	0.99144	146.84
259	130.042	3.7889	0.1022	0.0000	0.026276	0.12	0.99144	146.87
243	160.000	4.5944	0.0767	0.0000	0.032906	0.13	0.98574	139.99
244	190.044	5.9814	0.0606	0.0000	0.044511	0.14	0.97805	132.83
245	220.000	4.9357	0.0313	0.0000	0.038574	0.17	0.96614	124.49
246	249.978	7.6785	0.0407	-0.0023	0.063545	0.17	0.94922	115.26
248	280.011	5.6325	0.0206	0.0000	0.050028	0.14	0.92383	104.46
247	280.121	7.2765	0.0266	-0.0016	0.064656	0.14	0.92383	104.40
251	310.000	4.2330	0.0377	0.0047	0.041551	0.04	0.88491	91.07

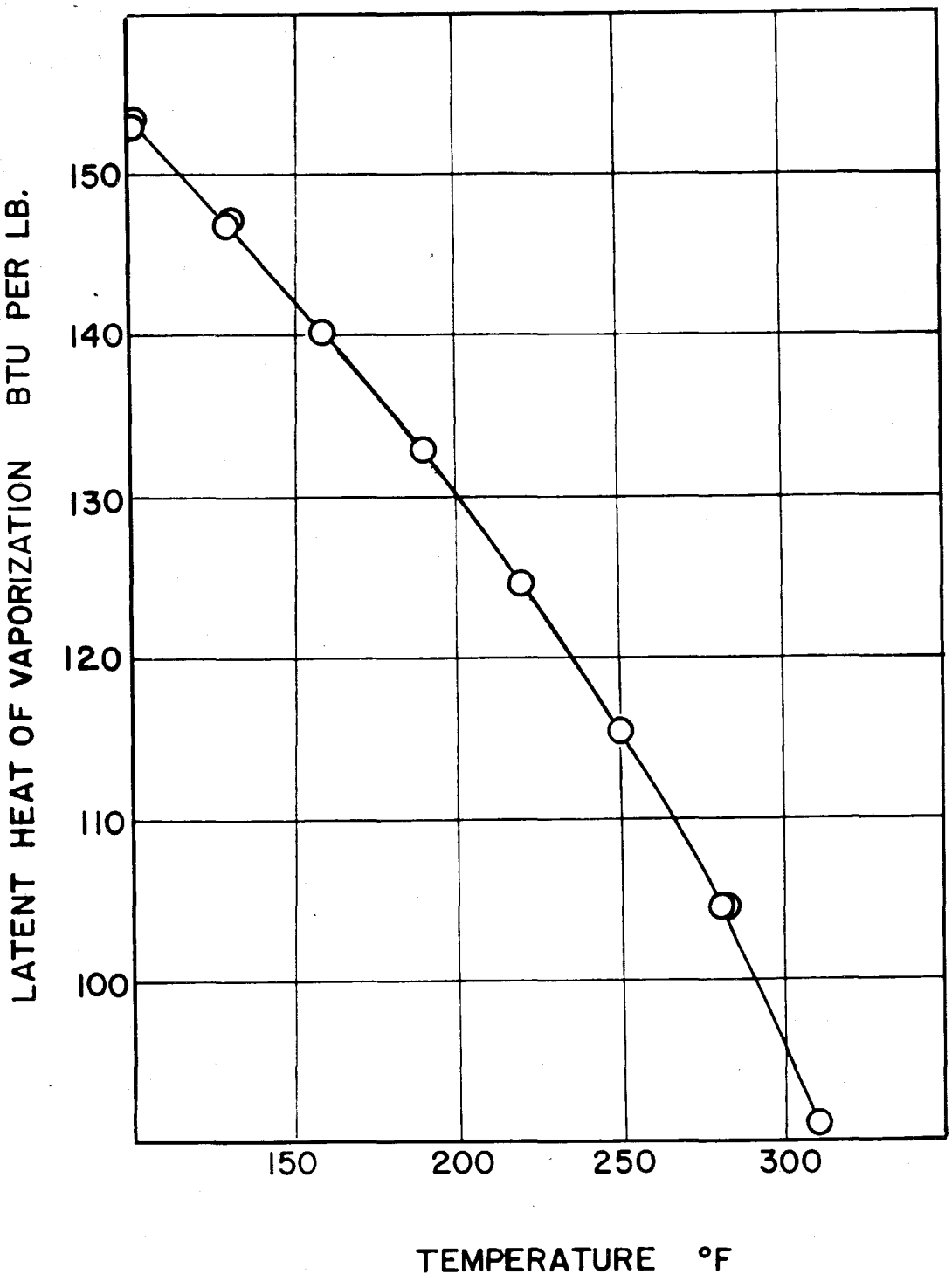

Fig. 15. Effect of Temperature on Heat of Vaporization for n-Pentane

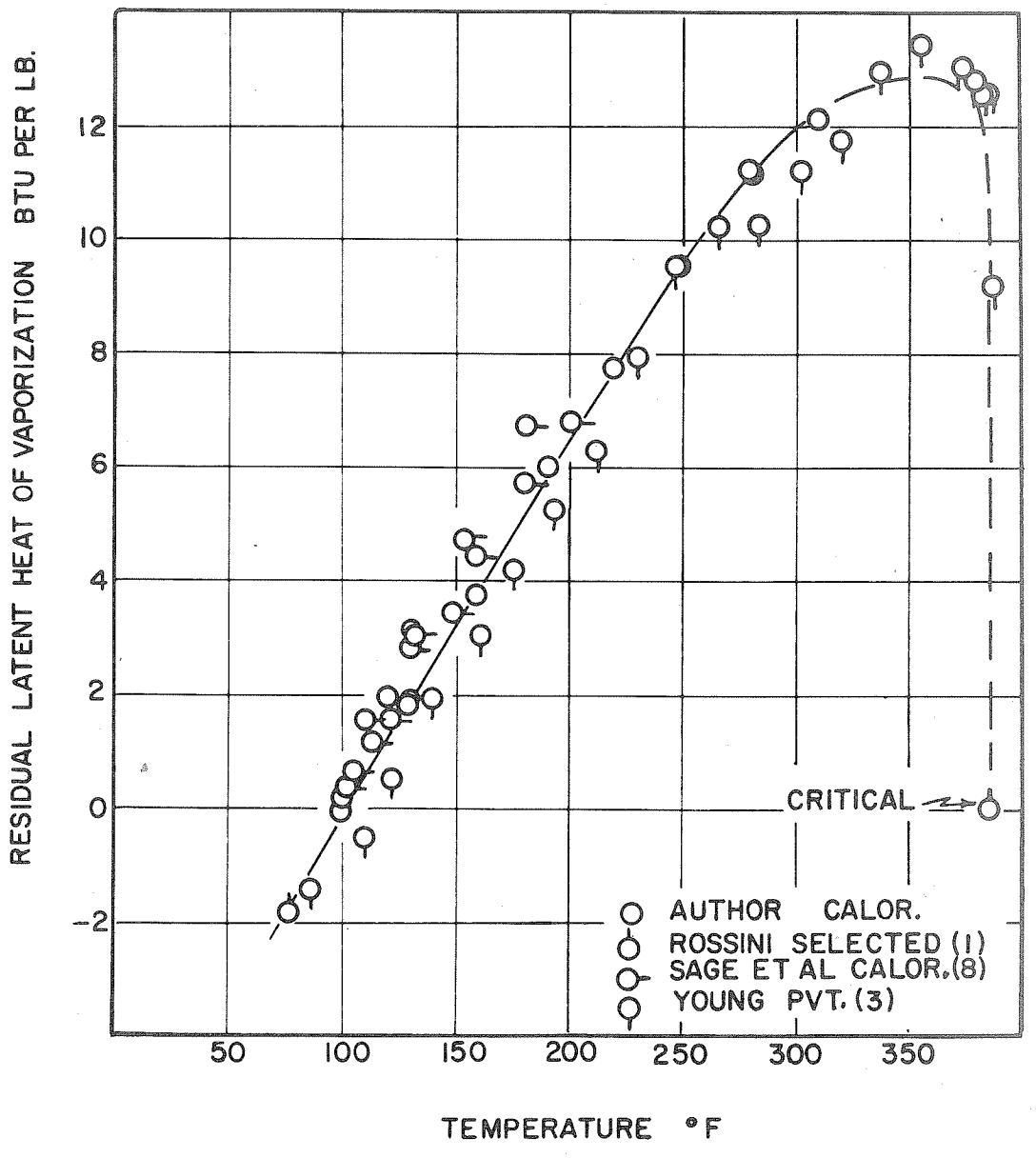

Fig. 16. Comparison of Heat of Vaporization for n-Pentane from Several Sources

Table III

Comparison of Experimental Results for n-pentane from Different Investigators

Source	Temp.[a], °F.	Av. Deviation		Standard Error Est.[d], Btu/lb.
		With sign[b], Btu/lb.	Without sign[c], Btu/lb.	
Rossini (1)	77[e]	-	-	-
Sage, others (8)	100-200	0.72	0.72	0.84
Young (3)	104-302	-0.68	0.68	0.73

[a] Range of temperature within which comparison with present measurements was possible.

[b] $\left[\sum (\ell_S - \ell_A)\right]^f /N$

[c] $\left[\sum |(\ell_S - \ell_A)|\right] /N$

[d] $\left\{\left[\sum (\ell_S - \ell_A)^2\right] /N\right\}^{1/2}$

[e] Single value.

[f] ℓ represents the enthalpy change upon vaporization; the subscripts S and A denoting smoothed and actual values, respectively.

Table IV

Critically Chosen Values of Internal Energy and Enthalpy Change upon Vaporization for n-pentane

Temperature °F	Internal Energy Change on Vaporization Btu/lb.	Enthalpy Change on Vaporization Btu/lb.
100	138.75	153.12
110	136.63	151.09
120	134.41	149.00
130	132.14	146.94
140	129.90	144.62
150	127.66	142.35
160	125.33	140.01
170	123.00	137.63
180	120.55	135.18
190	118.19	132.63
200	115.63	130.04
210	112.98	128.34
220	110.42	124.49
230	107.55	121.54
240	104.65	118.46
250	101.73	115.26
260	98.68	111.86
270	95.55	108.28
280	92.35	104.47
290	88.60	100.36
300	84.62	95.95
310	80.32	91.16
320	75.51	86.05[a]
330	70.39	80.42
340	65.13	74.21
350	59.95	67.20
360	54.96	59.06
370	48.94	49.21
380	34.41	38.45
385.9[b]	0	0

[a] Values at this and higher temperatures extrapolated from the data at lower temperatures.

[b] Critical (1).

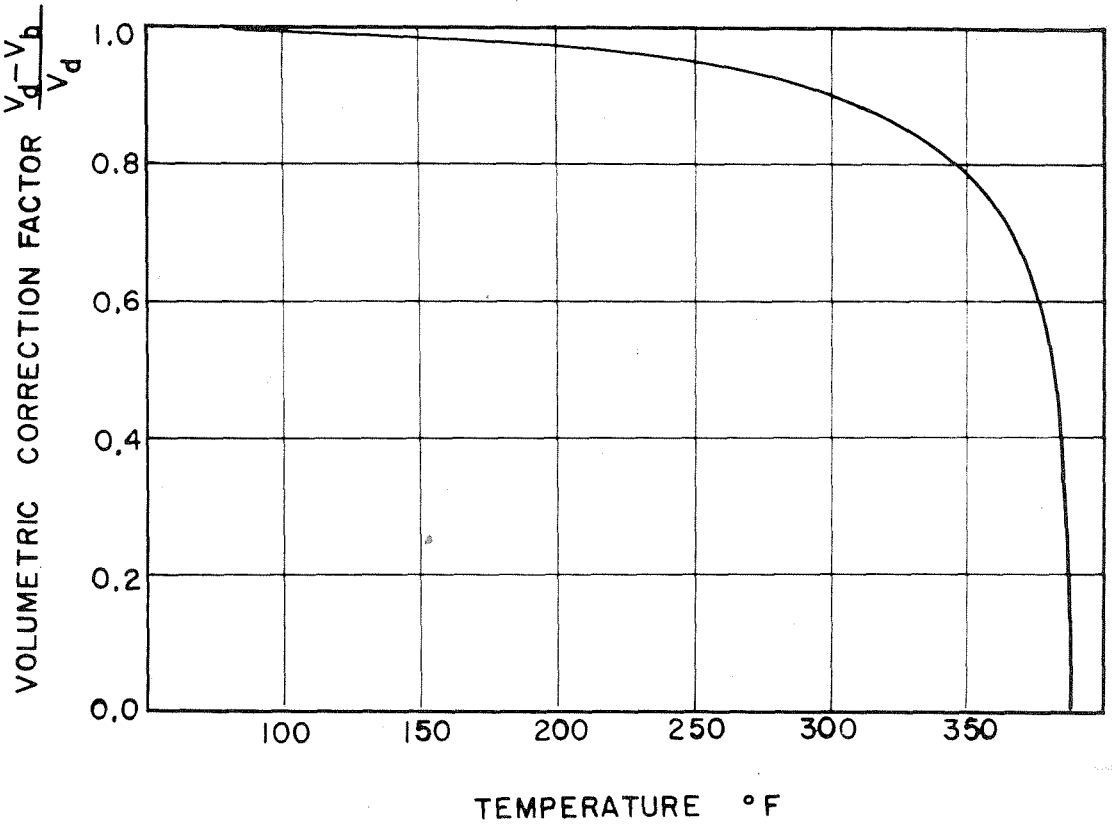

Fig. 17. Volumetric Correction Factor as a Function of Temperature for n-Pentane

Table V

Agitator Calibration Data for n-pentane

Temperature, °F.	Agitator Energy Addition Rate, watts
100	0.0284
130	0.0250
160	0.0219
190	0.0195
220	0.0172
250	0.0152
280	0.0134
310	0.0119

Table VI

Experimental Results for Cyclohexane

Identification	Temp., °F.	Energy Added, Btu: Electrically	Energy Added, Btu: By agitation	Energy Added, Btu: By conduction and radiation	Material Withdrawn, lb.	Superheat of Liquid, °F.	Specific Volume cu. ft./lb.: Dew Point	Specific Volume cu. ft./lb.: Bubble Point	Vol. Corr. Factor	Enthalpy change upon Vaporization Btu/lb.
273	100.00	1.6907	0.0748	0.0019	0.010745	0.16	21.55	0.02109	0.99902	164.36
261	130.00	1.8832	0.0403	0.0000	0.012010	0.29	11.85	0.02147	0.99819	159.97
262	130.00	3.9617	0.0846	0.0000	0.025262	0.29	11.85	0.02147	0.99819	159.98
272	130.00	4.1218	0.0882	0.0000	0.026244	0.29	11.85	0.02147	0.99819	160.22
291	160.00	3.9629	0.1090	0.0021	0.026148	0.21	6.995	0.02200	0.99685	155.38
289[a]	190.00	2.4077	0.0813	-0.0023	0.016550	0.15	4.369	0.02252	0.99485	149.54
275	220.00	3.1524	0.0660	0.0014	0.022017	0.21	2.854	0.02311	0.99190	145.15
292	220.00	3.4658	0.0782	0.0030	0.024271	0.20	2.854	0.02311	0.99190	145.04
290	250.00	2.8309	0.0431	0.0022	0.020409	0.26	1.931	0.02376	0.98771	139.28
293	280.00	5.3099	0.0584	-0.0092	0.039359	0.31	1.345	0.02442	0.98185	133.84
294	310.05	1.8120	0.0592	0.0096	0.014450	0.09	0.9559	0.02523	0.97361	126.82

[a] The period of time associated with obtaining these calorimetric measurements was nearly twice that required for the other measurements.

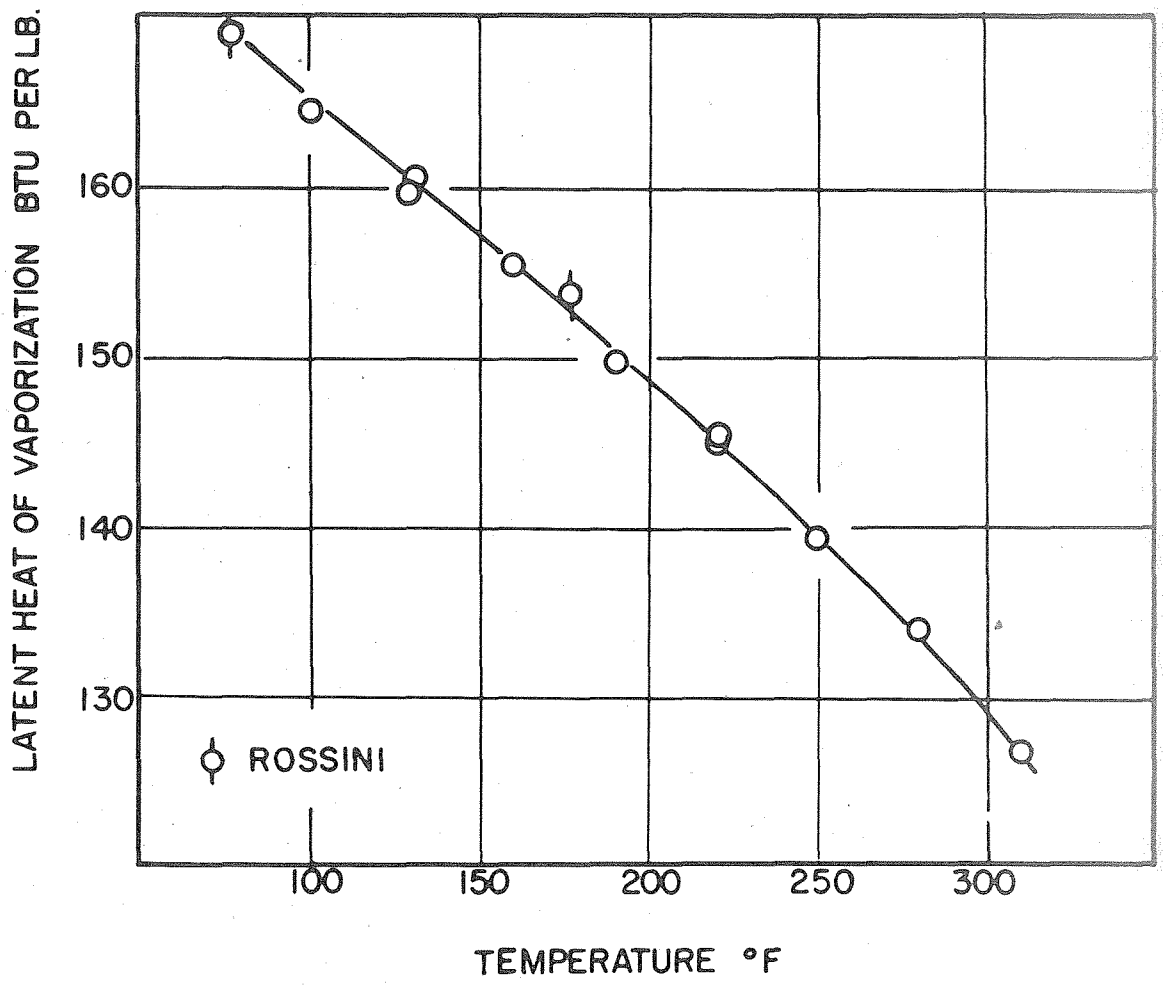

Fig. 18. Effect of Temperature on Latent Heat of Vaporization for Cyclohexane

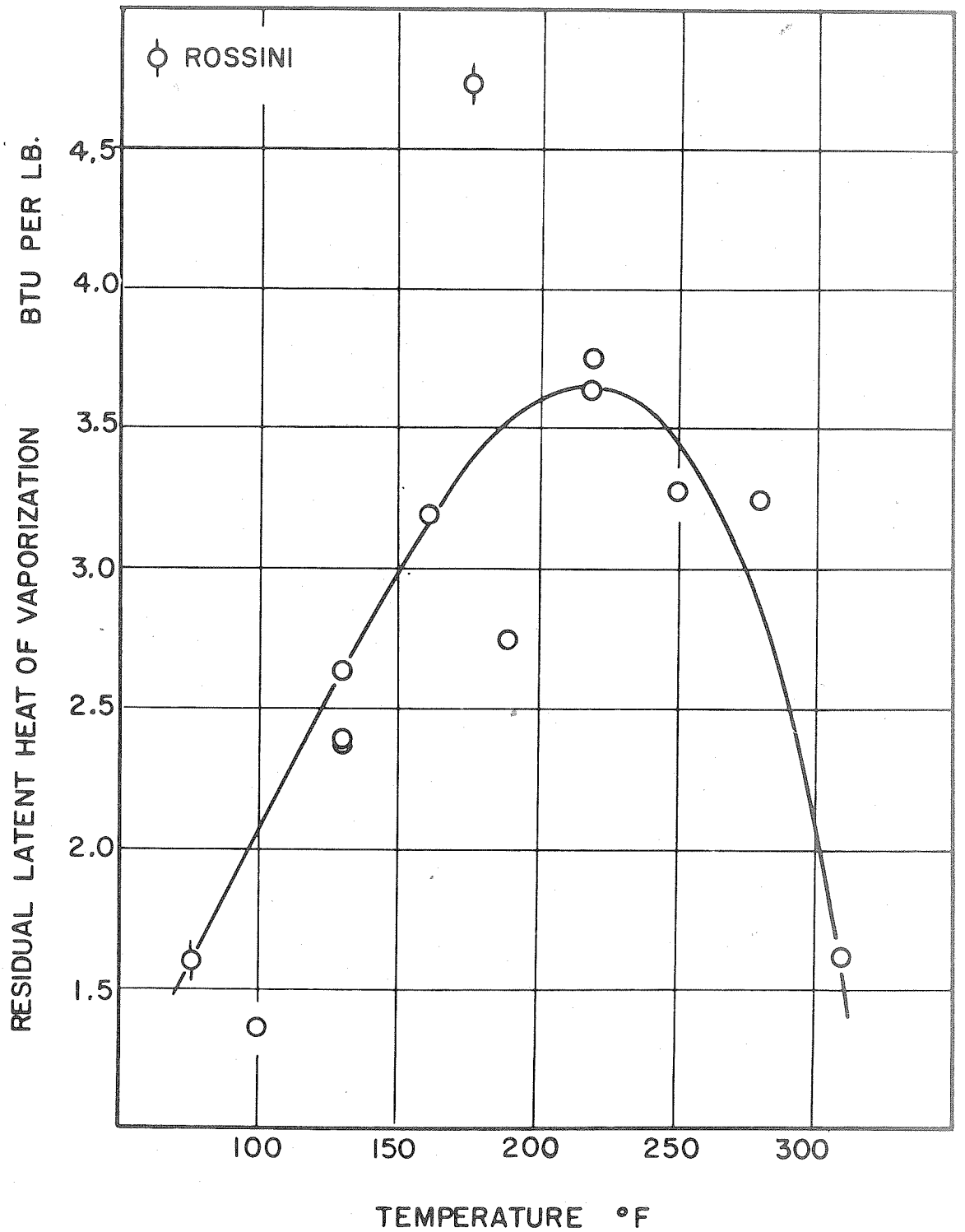

Fig. 19. Residual Latent Heat of Vaporization for Cyclohexane

Table VII

Agitator Calibration Data for Cyclohexane

Temperature, °F.	Agitator Energy Addition Rate, watts
100	0.0205
130	0.0202
160	0.0199
190	0.0196
220	0.0194
250	0.0191
280	0.0188
310	0.0185

Table VIII

Critically Chosen Values of Internal Energy and Enthalpy Change upon Vaporization for Cyclohexane

Temperature °F	Internal Energy change upon Vaporization Btu/lb.	Enthalpy change upon Vaporization Btu/lb.	Specific Volume, cu. ft. /lb.	
			Dew Point	Bubble Point
100	152.10	165.05	21.55	0.02109
110	150.30	163.45	17.49	0.02121
120	148.48	161.84	14.31	0.02134
130	146.67	160.22	11.85	0.02147
140	144.88	158.61	9.893	0.02165
150	143.08	156.99	8.283	0.02180
160	141.29	155.37	6.995	0.02200
170	139.47	153.71	5.941	0.02216
180	137.64	152.03	5.085	0.02234
190	135.79	150.32	4.369	0.02252
200	133.92	148.58	3.769	0.02271
210	131.04	146.82	3.305	0.02291
220	130.15	145.04	2.854	0.02311
230	128.22	143.20	2.515	0.02333
240	126.30	141.35	2.197	0.02355
250	124.34	139.46	1.931	0.02377
260	122.38	137.54	1.710	0.02397
270	120.38	135.56	1.522	0.02418
280	117.32	133.50	1.345	0.02442
290	116.20	131.36	1.195	0.02466
300	114.00	129.13	1.066	0.02494
310	111.69	126.77	0.9559	0.02523

Table IX

Experimental Restults for 1-Butene

Identification	Temp., °F.	Energy Added, Btu: Electrically	Energy Added, Btu: By agitation	Energy Added, Btu: By conduction and radiation	Material Withdrawn, lb.	Superheat of Liquid, °F.	Vol. Corr. Factor	Enthalpy change upon Vaporization Btu/lb.
304	99.997	2.8169	0.0494	0.0018	0.018918	0.11	0.98150	148.85
310	99.996	4.3082	0.0514	0.0000	0.028690	0.15	0.98150	149.21
301	130.005	2.4472	0.0634	0.0075	0.017488	0.06	0.97047	139.77
312	130.000	5.7300	0.0412	0.0006	0.040020	0.19	0.97047	140.05
308	160.002	4.3784	0.0223	-0.0033	0.032298	0.21	0.95423	130.03
303	190.002	3.8457	0.0421	0.0021	0.030786	0.07	0.92985	117.53
314	219.996	6.3695	0.0372	-0.0030	0.055237	0.09	0.89218	103.49
315	220.025	4.9761	0.0290	-0.0053	0.043269	0.09	0.89218	103.15

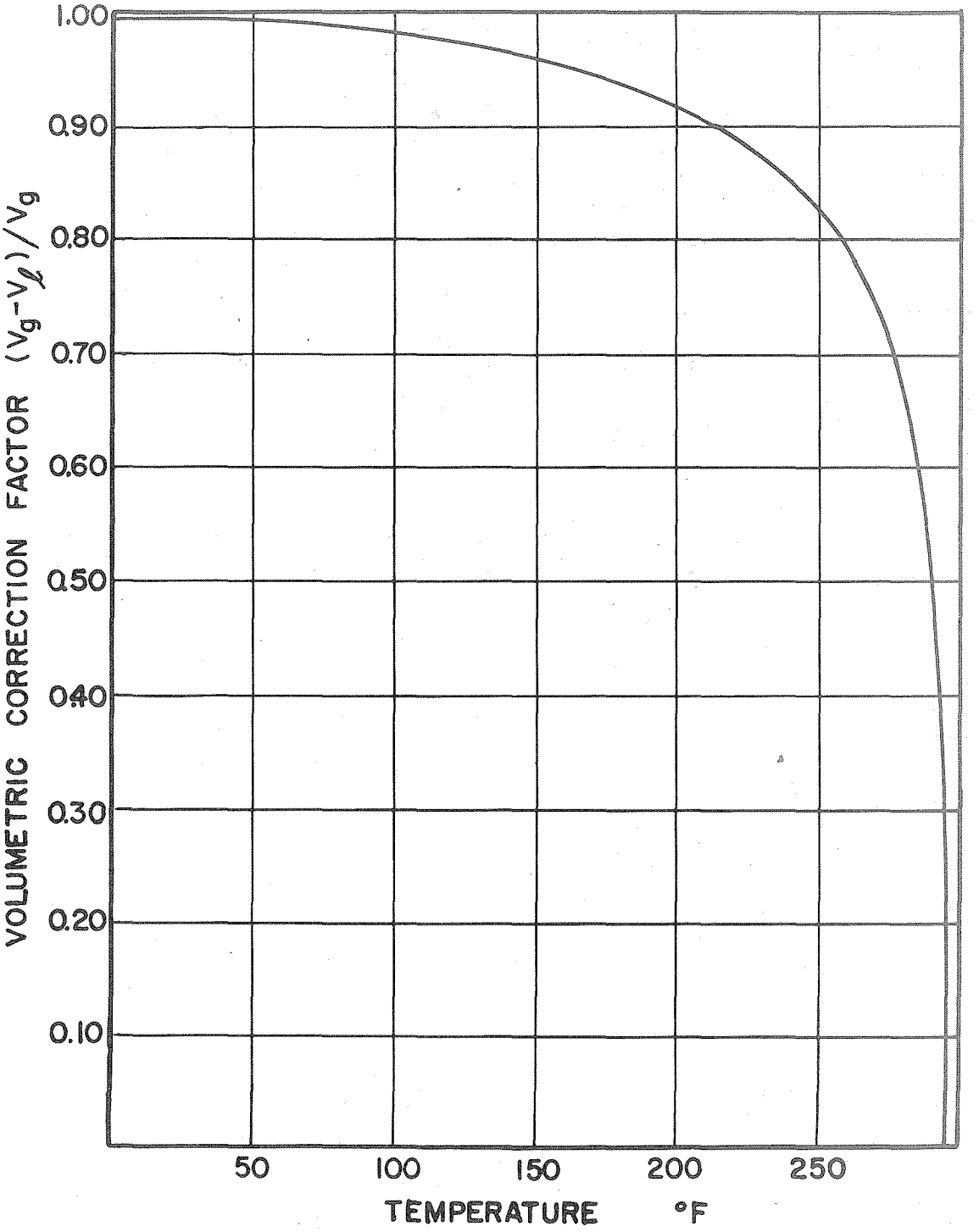

Fig. 20. Volumetric Correction Factor for 1-Butene

Table X

Agitator Calibration Data for 1-Butene

Temperature, °F.	Agitator Energy Addition Rate, watts
100	0.0186
130	0.0172
160	0.0157
190	0.0143
220	0.0129

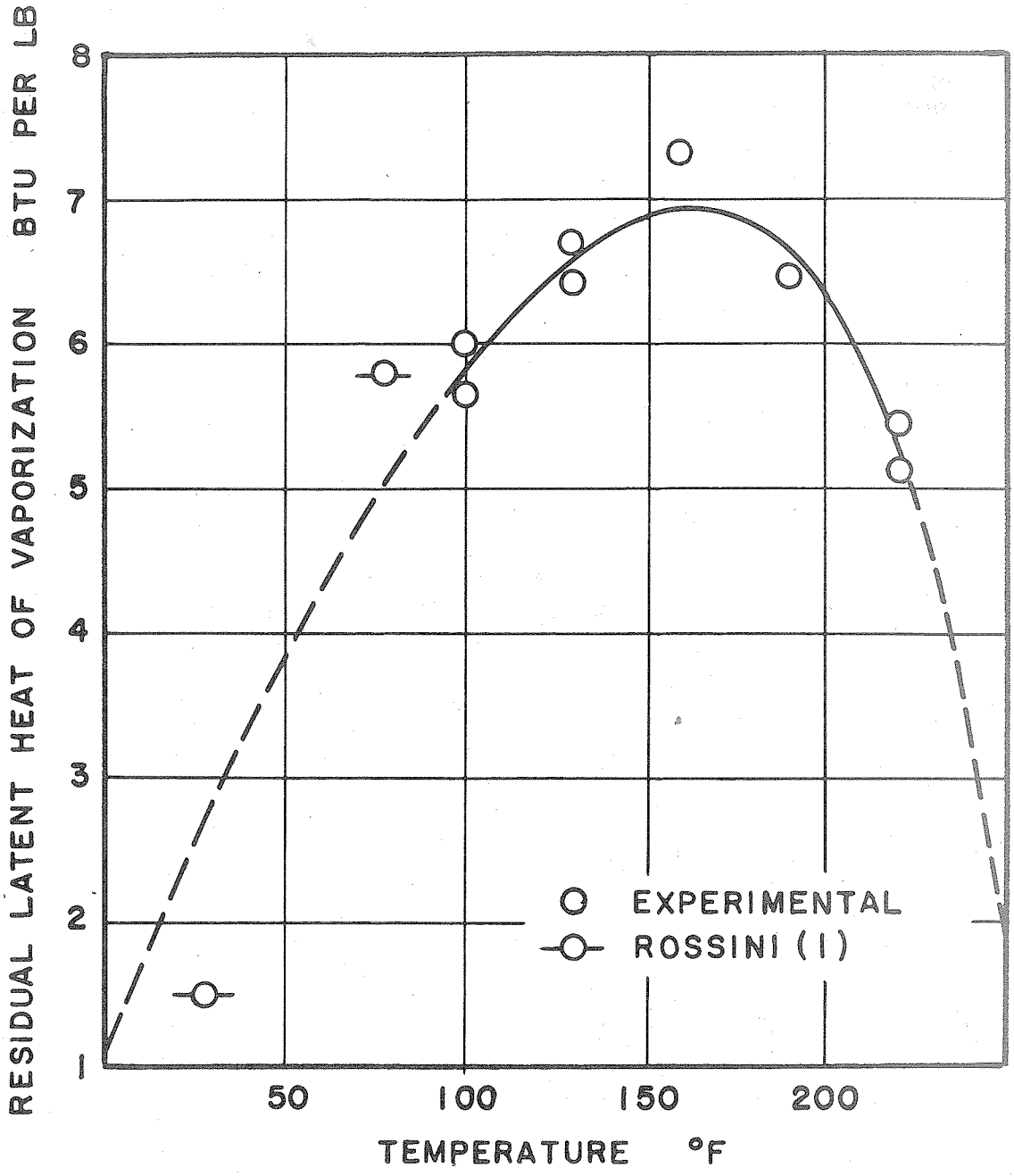

Fig. 21. Residual Latent Heat of Vaporization

Table XI

Critically Chosen Values of Internal Energy and Enthalpy Change upon Vaporization of 1-Butene

Temperature °F.	Internal Energy Change on Vaporization Btu/lb.	Enthalpy Change on Vaporization Btu/lb.
10	155.01	171.03
20	152.72	168.96
30	150.33	166.78
40	147.87	164.49
50	145.33	162.12
60	142.73	159.67
70	140.08	157.15
80	137.36	154.53
90	134.58	151.83[a]
100	131.75	149.03
110	128.94	146.10
120	125.88	143.07
130	122.63	139.92
140	119.33	136.64
150	116.00	133.22
160	112.61	129.65
170	109.02	125.88
180	105.29	121.91
190	101.40	117.72
200	97.25	113.25
210	92.87	108.45
220	88.31	103.34
230	83.35	97.77[b]
240	78.06	91.68
250	72.19	84.93

[a] Values at this and lower temperatures extrapolated from data of higher temperatures, also utilizing data of Rossini (1) in this range.

[b] Values at this and higher temperatures extrapolated from data at lower temperatures.

PART II

EVALUATIONS OF DIFFUSION COEFFICIENTS FOR THE METHANE-n-BUTANE SYSTEM BASED ON GRADIENTS IN THERMODYNAMIC STATE PROPERTIES

INTRODUCTION

The available relations in material transport (1) involve diffusion coefficients which are marked functions of the properties used to describe the state of the system. In general, when these relations are applied to problems involving diffusional processes they do not yield solutions readily, except for a few simple cases. Reliable information concerning the behaviour of the diffusion coefficient as a function of the state of the system is usually relatively scarce because such information must be determined experimentally. In many cases, correlations (2) for estimation of diffusion coefficients must be used.

These considerations point to the advantages and desirability of a diffusion coefficient which is constant with respect to variations in the state properties of the system. The discovery of such a coefficient would undoubtedly also lead to a better understanding of the diffusion process. The possibility of either of the coefficients based on the gradient in chemical potential or on the gradient in fugacity of the diffusing species satisfying the requirement has been proposed (1). A dependence of diffusion on the chemical potential or fugacity gradient is suggested from thermodynamic considerations.

The purpose of this study was to evaluate these coefficients for methane diffusing in the liquid phase of the methane-n-butane system, for which data was available, and to investigate the suitability of these coefficients in regard to the aforementioned requirement.

Evaluations also were made of the phenomenological coefficient (3, 4, 5, 6) of irreversible thermodynamics since little additional calculation work was involved and this represented an additional possibility.

ANALYSIS

Chemical Potential Gradient Diffusion Coefficient

The ordinary Fick diffusion coefficient is defined by the relation*

$$\dot{m}_k = u_k \sigma_k = u\sigma_k - D_{F,k} \text{grad } \sigma_k \quad (k = 1, 2, \ldots, n) \tag{1}$$

The hydrodynamic velocity u is related to the individual component velocities u_k as follows (1)

$$u = \frac{\sum_{k=1}^{n} u_k \sigma_k}{\sigma} \tag{2}$$

In view of equations 1 and 2 the following expression can be written

$$\sum_{k=1}^{n} D_{F,k} \text{grad } \sigma_k = 0 \tag{3}$$

By analogy with the above definition of the Fick diffusion coefficient, a diffusion coefficient based on the chemical potential gradient can be defined as follows

$$\dot{m}_k = u\sigma_k - D_{\mu,k} \text{grad } \mu_k \tag{4}$$

The following expression, analogous to equation 3, can also be written

---

*Isotropy is assumed throughout this analysis.

No special effort was made in the nomenclature to distinguish the vector quantities since these quantities are readily discernible from the context.

$$\sum_{k=1}^{n} D_{\mu, k} \text{ grad } \mu_k = 0 \tag{5}$$

Combination of equations 1 and 4 results in the following equality

$$D_{\mu, k} \text{ grad } \mu_k = D_{F, k} \text{ grad } \sigma_k \tag{6}$$

If the concept of local equilibrium is utilized,

$$\mu_k = \phi_k(T, P, \sigma_1, \sigma_2, \ldots \sigma_{n-1}) , \tag{7}$$

the chemical potential gradient can be related to the gradients in temperature, pressure and partial specific weights of n-1 components as follows

$$\text{grad } \mu_k = \frac{\partial \mu_k}{\partial T} \text{ grad } T + \frac{\partial \mu_k}{\partial P} \text{ grad } P + \sum_{m=1}^{n-1} \frac{\partial \mu_k}{\partial \sigma_m} \text{ grad } \sigma_m \tag{8}$$

For the case of binary diffusion in a system at uniform temperature and pressure, equation 8 reduces to the following simple expression relating the chemical potential and concentration gradients of the diffusing species

$$\text{grad } \mu_k = \frac{\partial \mu_k}{\partial \sigma_k} \text{ grad } \sigma_k \tag{9}$$

Consideration of the expression which results from a combination of equations 9 and 6 yields the following relationship between the ordinary Fick diffusion coefficient and the coefficient based on chemical potential gradient

$$D_{\mu,k} = \frac{D_{F,k}}{\left(\frac{\partial \mu_k}{\partial \sigma_k}\right)_{T,P}} \tag{10}$$

Equation 10 can be rewritten in terms of the fugacity, related to the chemical potential as follows

$$\mu_k = \beta_k(T) + b_k T \ln f_k \tag{11}$$

If this is done, equation 10 becomes

$$D_{\mu,k} = \frac{D_{F,k}}{b_k T \left(\frac{\partial \ln f_k}{\partial \sigma_k}\right)_{T,P}} = \frac{f_k D_{F,k}}{b_k T \left(\frac{\partial f_k}{\partial \sigma_k}\right)_{T,P}} \tag{12}$$

Either of the equations 10 or 12 enables the evaluation of the chemical potential diffusion coefficient in a binary system from a knowledge of the Fick diffusion coefficient and data pertaining to the thermodynamic behaviour of the system.

In the same manner as in the foregoing, a diffusion coefficient based on the fugacity gradient can be defined

$$\dot{m}_k = u\sigma_k - D_{f,k} \operatorname{grad} f_k , \tag{13}$$

bearing the following relationship to the ordinary Fick coefficient

$$D_{f,k} = \frac{D_{F,k}}{\left(\frac{\partial f_k}{\partial \sigma_k}\right)_{T,P}} \tag{14}$$

Irreversible Thermodynamic Considerations

The phenomenological relations of irreversible thermodynamics (3, 4, 5, 6) for diffusion in a system at uniform temperature and pressure may be written

$$-j_k = \sum_{\ell=1}^{n} L_{k\ell} \operatorname{grad} \mu_\ell \quad (k = 1, 2, \ldots, n) \tag{15}$$

where the "forces" are represented by chemical potential gradients. The "fluxes," j_k in equation 15, are defined as follows

$$j_k = \sigma_k(u_k - u) \tag{16}$$

In the present case of barycentric diffusion, u is the hydrodynamic velocity whose relationship to the individual component velocities is given by the same expression as in the previous section

$$u = \frac{\sum_{k=1}^{n} u_k \sigma_k}{\sigma} \tag{2}$$

It follows from the latter relations, equations 2 and 16, that

$$\sum_k j_k = 0 \tag{17}$$

The entropy production as a result of the diffusion process σ_d is given by the following expression (3, 4, 5, 6) involving the fluxes and chemical potential gradients of the diffusing species

$$\sigma_d = \frac{\left(\sum_{k=1}^{n} -j_k \cdot \text{grad } \mu_k \right)}{T} \tag{18}$$

As a consequence of Onsager's theory (3, 4, 5, 6), the phenomenological coefficients $L_{k\ell}$ in equation 15 satisfy the reciprocal relationship

$$L_{k\ell} = L_{\ell k} \tag{19}$$

A number of additional relations between the n^2 coefficients in equation 15 exist as a result of the relationship existing between the fluxes, expressed by equation 17. In view of equation 17, the entropy production given by equation 18 can be rewritten

$$\sigma_d = \frac{\sum_{k=1}^{n-1} -j_k \cdot (\text{grad } \mu_k - \text{grad } \mu_n)}{T} \tag{20}$$

At the condition

$$\text{grad } \mu_1 = \text{grad } \mu_2 = \ldots = \text{grad } \mu_n,$$

the entropy production is zero, no diffusion flows exist, and hence

$$\sum_{\ell=1}^{n} L_{k\ell} = 0 \qquad (k = 1, 2, \ldots, n) \tag{21}$$

Another relationship between the coefficients is obtained when equation 15 is inserted in equation 17 resulting in an identity between arbitrary values of the gradients in chemical potential and the require-

ment that

$$\sum_{k=1}^{n} L_{k\ell} = 0 \qquad (\ell = 1, 2, \ldots, n) \tag{22}$$

Utilization of equation 21 in elimination of the phenomenological coefficients L_{kn} in equation 15 yields the n-1 independent relations

$$-j_k = \sum_{\ell=1}^{n-1} L_{k\ell} \operatorname{grad} (\mu_\ell - \mu_n) \qquad (k = 1, 2, \ldots, n-1) \tag{23}$$

which could be expected from the form of equation 20.

The coefficients $L_{n\ell}$ $(\ell = 1, 2, \ldots, n)$ in the nth relation of equation 15 can be eliminated by the utilization of equation 22 resulting in the relation

$$-j_n = \sum_{k=1}^{n-1} j_k \ ,$$

expressing the already familiar fact that the fluxes are not independent.

In the foregoing, the original phenomenological relations of equation 15 were reduced, with the help of the relations 21 and 22, to the n-1 independent relations presented in the expression 23. In view of this and the restrictions imposed on the coefficients by the Onsager relations $L_{k\ell} = L_{\ell k}$, it is seen that the number of independent phenomenological coefficients is given by

$$(n-1)^2 - \frac{1}{2}(n-1)(n-2) = \frac{1}{2} n(n-1) \ .$$

Generalization of Fick's First Law of Diffusion

If the relation for the chemical potential gradient given by equation 8, at the condition

$$\text{grad } T = \text{grad } P = 0,$$

is substituted in equation 15, the expression obtained is

$$-j_k = \sum_{m=1}^{n-1} \sum_{\ell=1}^{n} L_{k\ell} \frac{\partial \mu_\ell}{\partial \sigma_m} \text{grad } \sigma_m \tag{24}$$

which, upon making the substitution

$$D_{km} = \sum_{\ell=1}^{n} L_{k\ell} \frac{\partial \mu_\ell}{\partial \sigma_m} \tag{25}$$

becomes

$$-j_k = \sum_{m=1}^{n-1} D_{km} \text{grad } \sigma_m \tag{26}$$

Combination of this equation with equation 16 yields

$$\dot{m}_k = u_k \sigma_k = u\sigma_k - \sum_{m=1}^{n-1} D_{km} \text{grad } \sigma_m \quad (k = 1, 2, \ldots, n) \tag{27}$$

which is a generalization of Fick's first law for diffusion. Although this relationship was deduced directly from the phenomenological relations of equation 15, the diffusion coefficients D_{km} defined by equation 21 do not obey the Onsager reciprocal relations. It is interesting to observe that for a binary system equation 27 reduces to the ordinary Fick diffusion expression in equation 1.

Application to Binary Diffusion

For the case of diffusion in a binary system, the phenomenological relations 15 become

$$-j_1 = L_{11} \text{ grad } \mu_1 + L_{12} \text{ grad } \mu_2$$

$$-j_2 = L_{21} \text{ grad } \mu_1 + L_{22} \text{ grad } \mu_2 \qquad (28)$$

In accordance with equations 21 and 22, the coefficients are related as follows:

$$L_{11} + L_{12} = 0, \quad L_{21} + L_{22} = 0 \qquad (29)$$

and

$$L_{11} + L_{21} = 0, \quad L_{12} + L_{22} = 0 \qquad (30)$$

Combination of the relations 28, 29 and 30 yields the following relations, analogous to the relations 23,

$$-j_1 = j_2 = L_{11} \text{ grad } (\mu_1 - \mu_2) = -L_{12} \text{ grad } (\mu_1 - \mu_2) \qquad (31)$$

Utilization of the local equilibrium concept enables the following relationship involving the gradients in chemical potential and concentration to be written

$$\text{grad } (\mu_1 - \mu_2) = \left[\frac{\partial(\mu_1 - \mu_2)}{\partial \sigma_1} \right]_{T, P} \text{grad } \sigma_1 \qquad (32)$$

Combination of this equation with equation 31 yields

$$-j_1 = L_{11}\left[\frac{\partial(\mu_1-\mu_2)}{\partial\sigma_1}\right]_{T,\,P} \text{grad}\ \sigma_1 \tag{33}$$

which can be combined with the following relation, derived from equations 1 and 16,

$$-j_1 = D_{F1}\ \text{grad}\ \sigma_1 \tag{34}$$

to yield a relation between the phenomenological coefficient and the ordinary Fick diffusion coefficient

$$D_{F1} = L_{11}\left[\frac{\partial(\mu_1-\mu_2)}{\partial\sigma_1}\right]_{T,\,P} . \tag{35}$$

It is seen that this relation is identical to the expression for the generalized Fick diffusion coefficient obtained simply with equation 25, which is to be expected since equation 27 reduces to the ordinary Fick diffusion relation 1 in the binary diffusion case.

With the help of the Gibbs-Duhem relation

$$\sigma_1 d\mu_1 + \sigma_2 d\mu_2 = 0 \quad \text{(at constant T and P)}, \tag{36}$$

equation 35 can be rearranged to give the following simple relation between the phenomenological coefficient and the ordinary Fick diffusion coefficient

$$L_{11} = \frac{N_2 D_{F1}}{\left(\frac{\partial\mu_1}{\partial\sigma_1}\right)_{T,\,P}} . \tag{37}$$

The various relations existing between the diffusion coefficients, presented in the foregoing, have been summarized in the following expression relating the diffusion coefficients

$$L_{11} = \frac{N_2 D_{F1}}{\left(\frac{\partial \mu_1}{\partial \sigma_1}\right)_{T,P}} = \frac{N_2 D_{11}}{\left(\frac{\partial \mu_1}{\partial \varpi_1}\right)_{T,P}} = N_2 D_{\mu_1} = \frac{N_2 f_1}{b_1 T} D_{f1} \qquad (38)$$

EVALUATION OF COEFFICIENTS

The chemical potential and fugacity gradient diffusion coefficients were evaluated using the relations given by equations 12 and 14 respectively. The phenomenological coefficient was derived from the chemical potential gradient diffusion coefficient by the simple relationship given in equation 38.

The Fick diffusion coefficient data required in the evaluations was taken from the published work of Reamer and Sage (7). Values of the Fick diffusion coefficient for methane were available for the bubble-point states of the methane-n-butane system at six pressures equally spaced in the pressure interval 250-1500 lb. per sq. in. and at the temperatures 100°, 160° and 220° F. The diffusion coefficient evaluations presented subsequently are for the same conditions of state.

The relationship between the fugacity and the partial specific weight of methane, σ_{CH_4}, required in the solution of equations 12 and 14, was established from the experimental data of Sage et al. (8, 9) relating to the volumetric and phase behaviour in the liquid and two-phase regions. The fugacities for methane in the liquid phase at bubble-point conditions were available (8) and the fugacities at pressures greater than the bubble-point pressure were calculated by means of the familiar equation

$$\ln \frac{f_k}{f_{k,b}} = - \frac{1}{b_k T} \int_{P_b}^{P} \overline{V}_k \, dP$$

The integration indicated by this relation was performed at the condition of constant temperature and weight fraction of methane. The partial specific weight of methane at each state was determined from the weight fraction of methane and the specific weight of the phase by means of the relation

$$\sigma_k = N_k \sigma$$

The evaluation of the derivative of the fugacity of methane with respect to the partial specific weight of methane was performed graphically utilizing plots similar to those illustrated in figs. 1, 2 and 3.

RESULTS

The behaviour of the fugacity of methane as a function of the temperature, pressure and partial specific weight of methane is shown graphically in figs. 1, 2 and 3. The derivative $\partial f_{CH_4}/\partial \sigma_{CH_4}$, in equations 12 and 14, was obtained from the slope of the tangent to an isobar, at the point of intersection of the isobar with the bubble-point curve. In fig. 4, the evaluations of the derivative are plotted versus the fugacity of methane for 100°, 160° and 220° F. values of the temperature parameter. It is seen that the derivative decreases continuously, with an increase in the fugacity of methane, to the value of zero at the fugacity corresponding to the critical state. An estimate of the uncertainty involved in an evaluation of the fugacity-partial specific weight derivative, as well as in an evaluation of the resultant coefficient, can be obtained from fig. 4. The fugacity values used in the subsequent calculations are tabulated in Table I as a function of the state of the methane-n-butane system. The partial specific weight of methane at each individual state is also included in the table. The evaluations of the various diffusion coefficients are summarized in Table II. Included in this table are the diffusion coefficients based on the gradients in chemical potential, fugacity and partial specific weight (ordinary Fick coefficient) of the diffusing species as well as the phenomenological coefficient. In addition to the temperature and pressure of the bubble-point states represented in the evaluations, the table presents the weight fraction, partial specific weight and fugacity of methane at each state.

The various diffusion coefficients listed in Table II are shown plotted in the figs. 5, 6, 7 and 8 as a function of the fugacity of methane at the values 100°, 160° and 220° F. of the temperature parameter. The curves in the figs. 6, 7 and 8 correspond to smooth values of the fugacity-partial specific weight derivative represented by the curves in fig. 4. The dashed vertical lines in the figures, which are approached asymptotically by the curves in the figs. 6, 7 and 8, represent the fugacity of methane at the critical state for the temperature in question.

DISCUSSION

In figs. 6, 7 and 8, each of the vertical dashed lines passing through the critical state fugacity is asymptotic to the diffusion coefficient curve representing the same temperature. The infinite value of the diffusion coefficients at the critical state arises from the fact that the fugacity-partial specific weight derivative is zero at the critical state, if it is also supposed that the Fick diffusion coefficient at the critical state is not zero. Referring to fig. 5, it is seen that this is not an unreasonable assumption.

It should be emphasized that the relations used were derived for the case of a system at uniform pressure, the pressure gradient associated with a gravitational field being neglected. It can be shown that if the effect of this pressure gradient is considered, the value of the diffusion coefficient evaluated at the critical state will not be infinite. The effect of the gravitational field was neglected in this study because of the unavailability of the additional experimental information that would have been required in the evaluations. It is suggested, however, that it be considered for future work.

From irreversible thermodynamic considerations, the phenomenological coefficients should be evaluated at conditions approaching equilibrium, that is, where the gradients involved are small. The applicability of the Fick diffusion coefficient data to this condition could not be ascertained from the available information (7). Furthermore, it was not possible to determine the probable error involved in the

evaluation of the phenomenological coefficient because of the lack of information.

The uncertainty involved in the Fick diffusion coefficient data was reported (7) to be about 5 per cent for the conditions of measurement. On the basis of the reported accuracy of the volumetric data (8, 9) and in view of the procedure by means of which the fugacity is evaluated, it is estimated that an uncertainty of up to 5 per cent was involved in the fugacity values. It is difficult to specify a representative value for the uncertainty associated with the evaluation of $\partial f_{CH_4}/\partial \sigma_{CH_4}$ since it varies for each state of the phase. From consideration of the curvature of the curve in the vicinity of the point where the derivative is determined and the magnitude of the slope of the tangent at the point, it is probable that the values for the states in close proximity to the critical state involve the greatest uncertainty. An estimate of the uncertainty might be obtained from the deviations of the individual values from the curves in fig. 4.

CONCLUSIONS

Evaluations of diffusion coefficients based on gradients in the chemical potential and the fugacity, as well as the phenomenological diffusion coefficient, have been presented for methane diffusing in the liquid phase of the methane-n-butane system. The diffusion coefficients evaluated are marked functions of the state of the phase. In the case of the chemical potential and the phenomenological diffusion coefficients, the values vary from zero to infinity, the latter value obtaining at the critical state. The values for the coefficient based on the fugacity gradient vary from a finite value to infinity at the critical state.

REFERENCES

1. Opfell, J. B., Sage, B. H., Ind. Eng. Chem., 47, 918 (1955).

2. Wilke, C. R., Chem. Eng. Prog., 45, No. 3, 219 (1949).

3. De Groot, S. R., "Thermodynamics of Irreversible Processes," North-Holland Publishing Co., Amsterdam (1958).

4. Prigogine, I., "Thermodynamics of Irreversible Processes," Charles C. Thomas - Publisher, Springfield, Ill., U. S. A. (1955).

5. Denbigh, K. G., "The Thermodynamics of the Steady State," John Wiley and Sons Inc., N. Y., (1951).

6. Fitts, D. D., "The Thermodynamics of Irreversible Processes," Department of Chemistry, University of Pennsylvania, Philadelphia 4, Pa., (1960).

7. Reamer, H. H., Sage, B. H., Chem. Eng. Data Series, 1, No. 1, 71, (1956).

8. Sage, B. H., Hicks, B. L., Lacey, W. N., Ind. Eng. Chem., 32, 1085, (1940).

9. Sage, B. H., Budenholzer, R. A., Lacey, W. N., Ind. Eng. Chem., 32, 1262, (1940).

10. Derived Data Book #1541, Department of Chemical Engineering, California Institute of Technology, Pasadena, California.

NOMENCLATURE

b_k	gas constant given by $\frac{\text{Universal gas constant}}{\text{molecular weight of k}}$
D	generalized Fick diffusion coefficient, sq. ft./sec.
$D_{f,k}$	diffusion coefficient of k used in conjunction with the fugacity gradient, ft/sec.
$D_{F,k}$	ordinary Fick diffusion coefficient, sq. ft./sec.
$D_{\mu,k}$	diffusion coefficient of k used in conjunction with the chemical potential gradient, lb./(sq. ft.)(sec.)
f_k	fugacity of component k, lb./sq. in.
j_k	flux of component k, $j_k = \sigma_k(u_k - u)$, lb./(sq. ft.)(sec.)
ln	natural logarithm
L	phenomenological coefficient, lb./(sq. ft.)(sec.)
$\dot{m}_k$	transport rate of component k, lb./(sq. ft.)(sec.)
N_k	weight fraction of component k
P	pressure, lb./sq. in.
T	temperature, ^{o}F.
u	hydrodynamic velocity, related to the momentum per unit volume m by $u = mg/\sigma$, ft./sec.
u_k	transport velocity of component k, ft./sec.
$\beta_k(T)$	a characteristic of species k and a function of temperature
σ	specific weight, lb./cu. ft.
σ_d	entropy production due to diffusion

σ_k* partial specific weight of component k, lb./cu. ft.

$\sum$ summation operator

ϕ function of

μ_k chemical potential of component k, ft.-lb./lb.

∂ partial differential operator

Subscripts

k, ℓ, m, n, 1, 2 components k, ℓ, m, n, 1, 2

*This quantity is not to be construed as a partial derivative of an extensive property as is the partial specific volume, for example. In the present discussion, the partial specific weight is the concentration of the component given by $\sigma_k = N_k \sigma$.

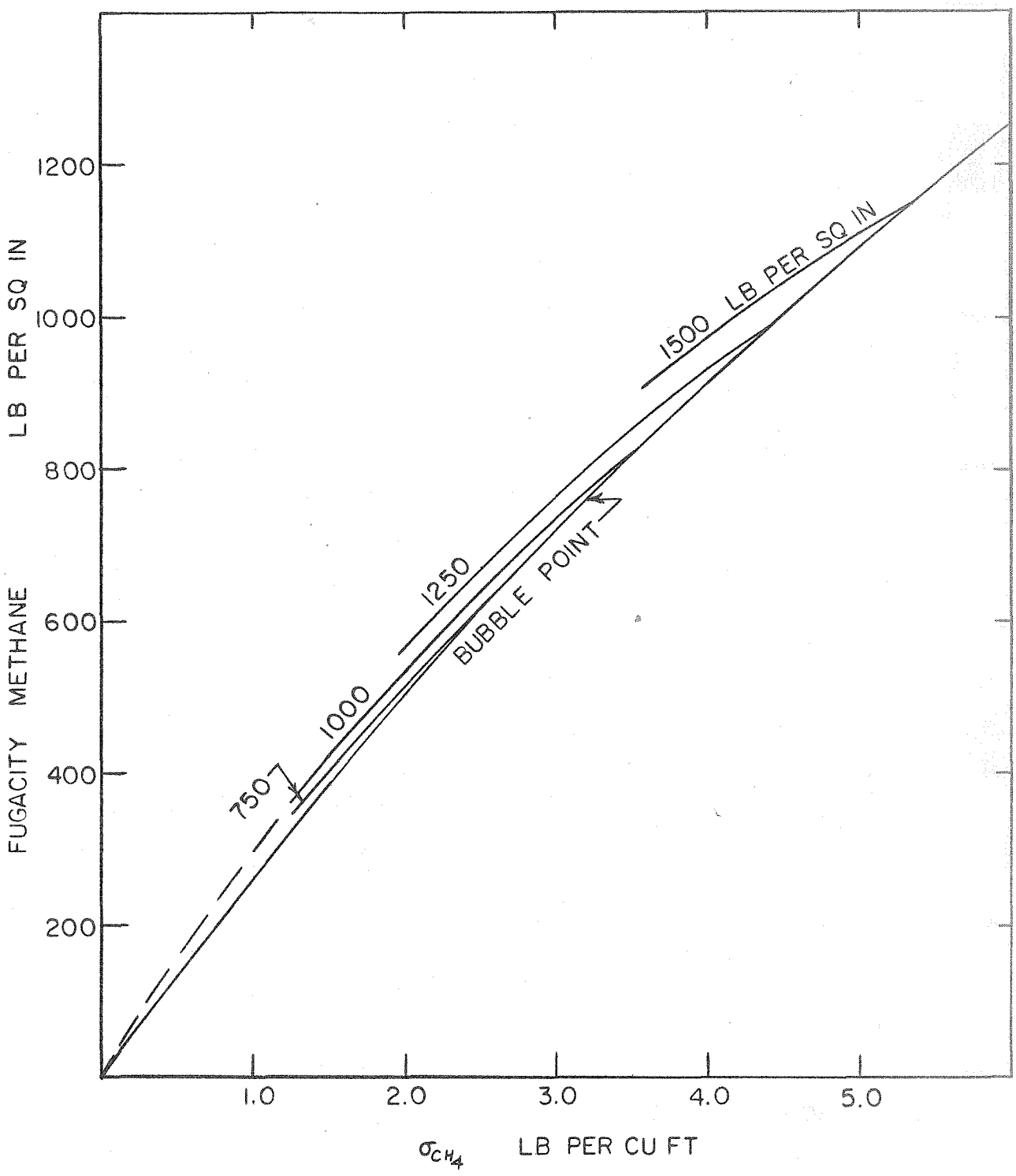

Figure 1. Fugacity of Methane Versus the Partial Specific Weight for Several Values of the Pressure Parameter at 100° F.

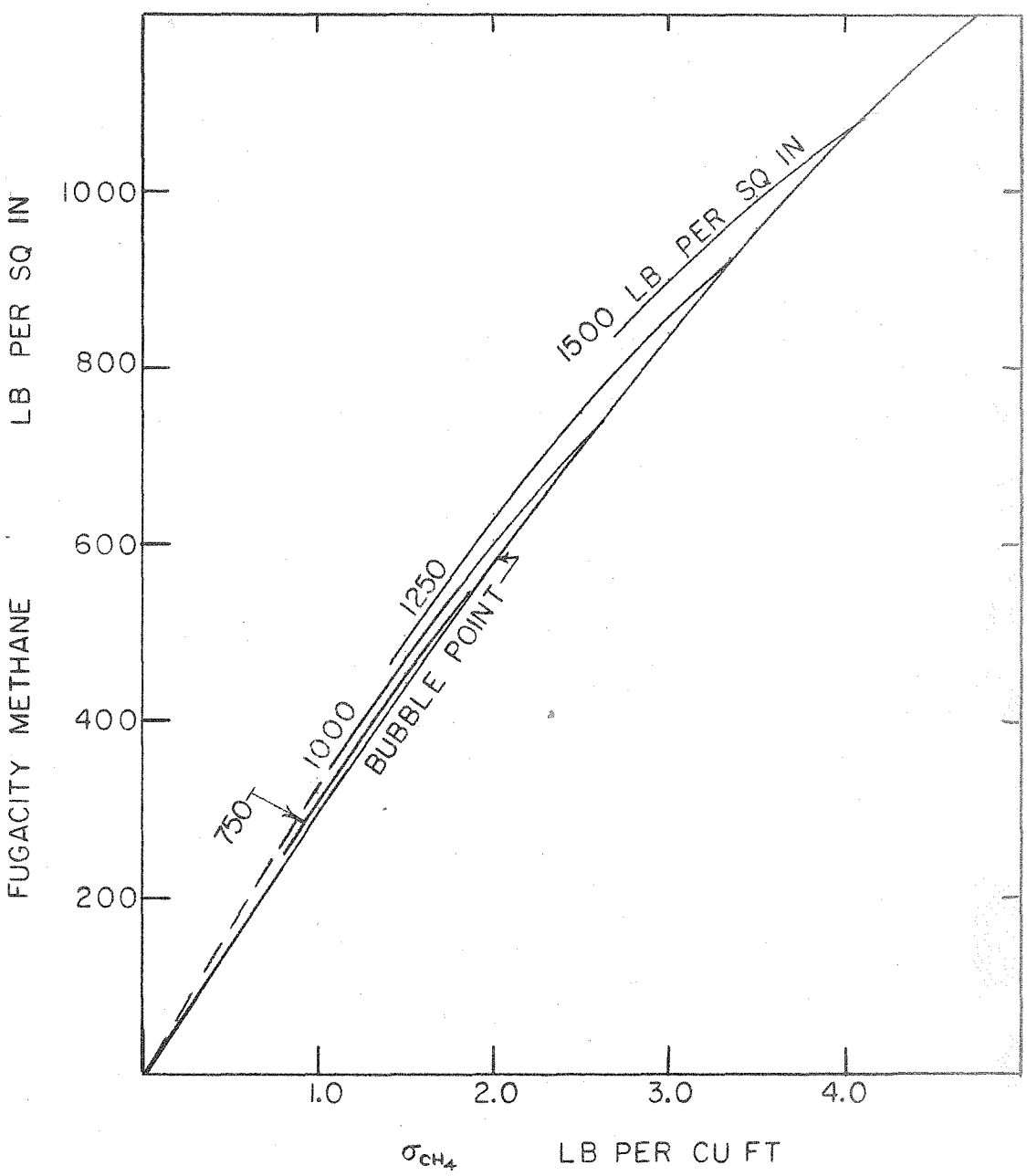

Figure 2. Fugacity of Methane Versus the Partial Specific Weight for Several Values of the Pressure Parameter at 160° F.

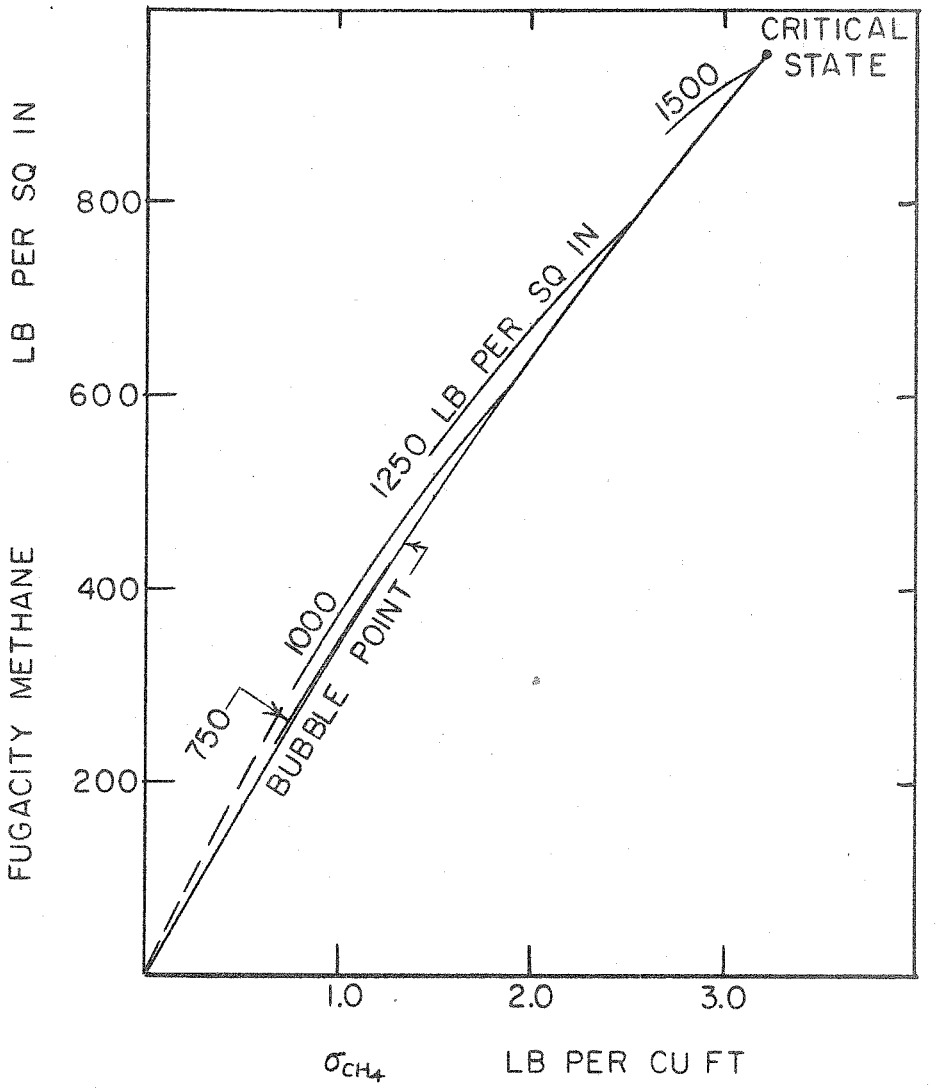

Figure 3. Fugacity of Methane Versus the Partial Specific Weight for Several Values of the Pressure Parameter at 220° F.

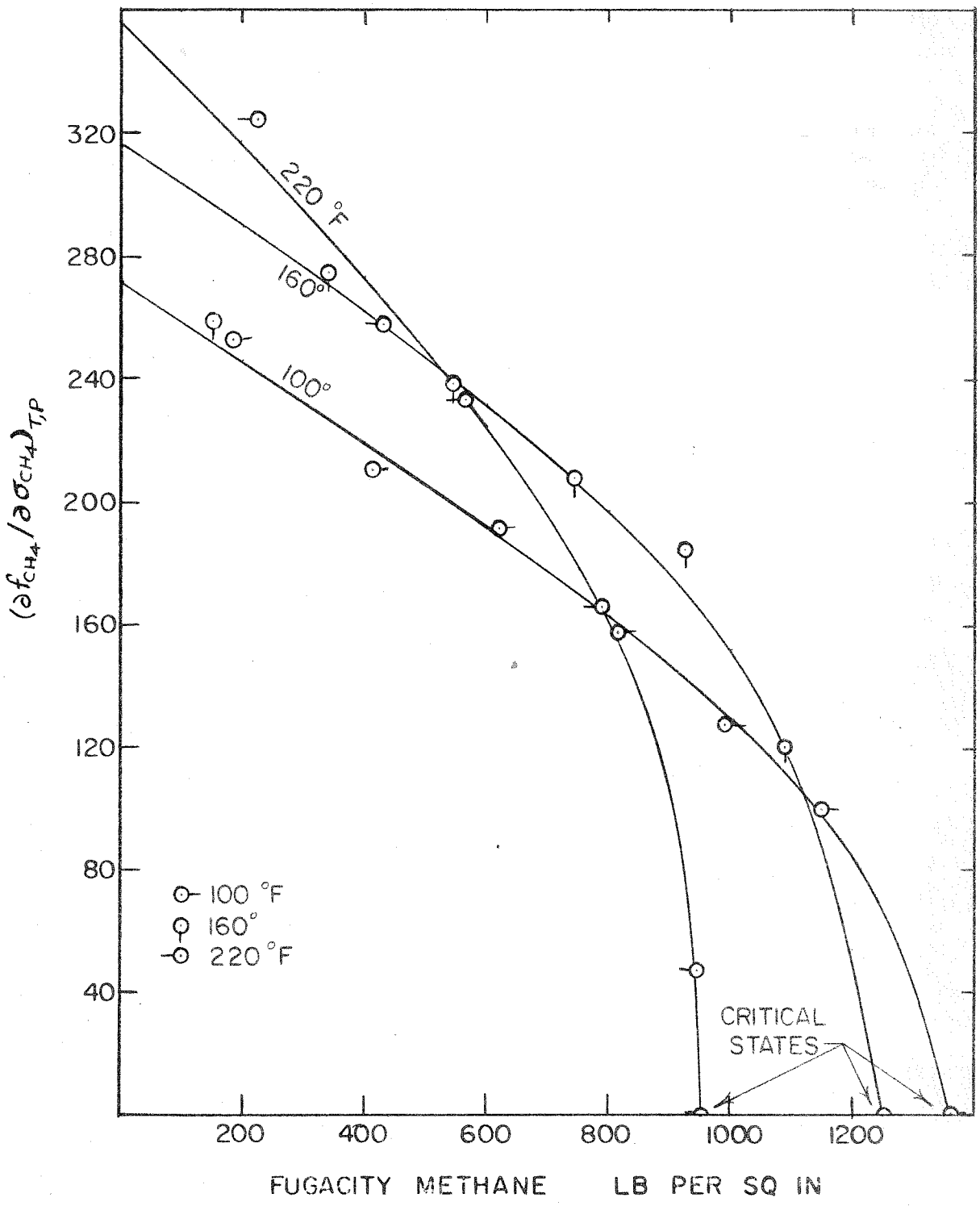

Figure 4. Plot of $(\partial f_{CH_4} / \partial \sigma_{CH_4})_{T,P}$ Versus the Fugacity of Methane for Three Temperature Parameter Values.

Table I

Fugacity Values for Methane in the Methane-n-Butane System

$100^{\circ}F.$

Pressure lb./sq. in.	Weight Fraction Methane X_{CH_4}	Partial Specific Weight Methane lb./sq. ft. σ_{CH_4}	Fugacity Methane lb./sq. in. f_{CH_4}
250	0.0049	0.172	47.23
	0.0100	0.348	94.85
	0.0152	0.524	141.3
*	0.020	0.684	186.4
500	0.0152	0.5231	148.0
	0.0257	0.880	241.6
	0.0368	1.239	330.2
	0.0484	1.601	413.4
750	0.0368	1.249	346.0
	0.0484	1.616	433.6
	0.0604	1.981	512.9
*	0.079	2.516	621.1
1000	0.0368	1.235	362.1
	0.0484	1.629	454.3
	0.0604	1.999	538.2
	0.0859	2.736	689.0
	0.1136	3.458	814.0
1250	0.0604	1.969	563.9
	0.0859	2.762	724.4
	0.1136	3.508	859.4
	0.1452	4.243	968.3
*	0.1540	4.420	990.6
1500	0.1136	3.547	905.0
	0.1452	4.323	1024.7
	0.1540	4.517	1050.3
	0.1821	5.051	1117.3
*	0.2030	5.345	1149

* bubble-point conditions

Table I (Continued)

160°F.

Pressure lb./sq. in.	Weight Fraction Methane X_{CH_4}	Partial Specific Weight Methane lb./sq. ft. σ_{CH_4}	Fugacity Methane lb./sq. in. f_{CH_4}
250	0	0	0
	0.0025	0.0811	26.50
	0.0068	0.219	71.32
*	0.012	0.376	115.3
500	0.0068	0.221	75.37
	0.0165	0.527	167.8
	0.0261	0.818	255.0
*	0.0363	1.112	337.1
750	0.0261	0.827	269.8
	0.0363	1.129	357.4
	0.0469	1.427	437.8
*	0.064	1.860	545
1000	0.0363	1.142	377.7
	0.0469	1.446	463.7
	0.0691	2.035	615.1
*	0.0943	2.628	742
1250	0.0469	1.463	489.6
	0.0691	2.067	652.3
	0.0943	2.683	792.3
	0.1210	3.228	903.2
*	0.1285	3.357	927
1500	0.0943	2.731	841.2
	0.1210	3.330	967.0
	0.1285	3.479	995.6
	0.1542	3.896	1060.6
*	0.1740	4.123	1089

*bubble-point conditions

Table I (Continued)

220° F.

Pressure lb./sq. in.	Weight Fraction Methane X_{CH_4}	Partial Specific Weight Methane lb./sq. ft. σ_{CH_4}	Fugacity Methane lb./sq. in. f_{CH_4}
500	0.0049	0.142	52.2
	0.0136	0.385	139.6
*	0.0229	0.6303	222.1
750	0.0136	0.393	150.1
	0.0229	0.645	239.9
	0.0328	0.899	323.1
*	0.0491	1.267	430.2
1000	0.0229	0.660	257.2
	0.0328	0.921	347.8
	0.0543	1.437	502.3
*	0.0784	1.904	616
1250	0.0543	1.481	541.9
	0.0784	1.995	674
	0.1063	2.430	772
*	0.1145	2.528	789
1500	0.1063	2.573	849
	0.1145	2.700	874
	0.1227	2.812	896
	0.1457	3.045	934
*	0.1768	3.181	944

*bubble-point conditions

Table II

Summary of Diffusion Coefficient Data

Temp. °F.	Pressure lb./sq. in.	Weight Fraction Methane	Partial Specific Weight Methane lb./cu. ft.	Methane Fugacity lb./sq. in.	$D_{F,\,CH_4}$ sq. ft./sec. ($\times 10^{-8}$)	$D_{\mu,\,CH_4}$ lb./sec. ft.^{2} ($\times 10^{-11}$)	$D_{f,\,CH_4}$ ft./sec. ($\times 10^{-12}$)	L_{11} lb./sec. ft.^{2} ($\times 10^{-11}$)
100	250	0.0200	0.699	186.4	17.5	0.239	4.79	0.234
	500	0.0484	1.601	413.4	17.4	0.631	5.71	0.601
	750	0.0790	2.529	621.1	17.2	1.031	6.22	0.950
	1000	0.1136	3.468	814.0	17.1	1.633	7.51	1.447
	1250	0.1540	4.418	990.6	17.0	2.436	9.21	2.061
	1500	0.2030	5.346	1149	16.9	3.580	11.68	2.853
160	250	0.0120	0.376	115.3	24.7	0.187	6.60	0.185
	500	0.0363	1.112	337.1	23.5	0.482	5.92	0.469
	750	0.0640	1.860	545	22.4	0.855	6.50	0.800
	1000	0.0943	2.628	742	21.2	1.265	7.06	1.146
	1250	0.1285	3.357	927	20.1	1.684	7.53	1.468
	1500	0.174	4.123	1089	19.0	2.868	10.92	2.369
220	500	0.0229	0.630	222.1	30.2	0.315	6.45	0.308
	750	0.0490	1.267	430.2	28.0	0.710	7.50	0.675
	1000	0.0784	1.904	616	26.1	1.048	7.74	0.966
	1250	0.1145	2.528	789	24.1	1.741	10.03	1.542
	1500	0.1768	3.181	944	22.3	6.528	31.44	5.577

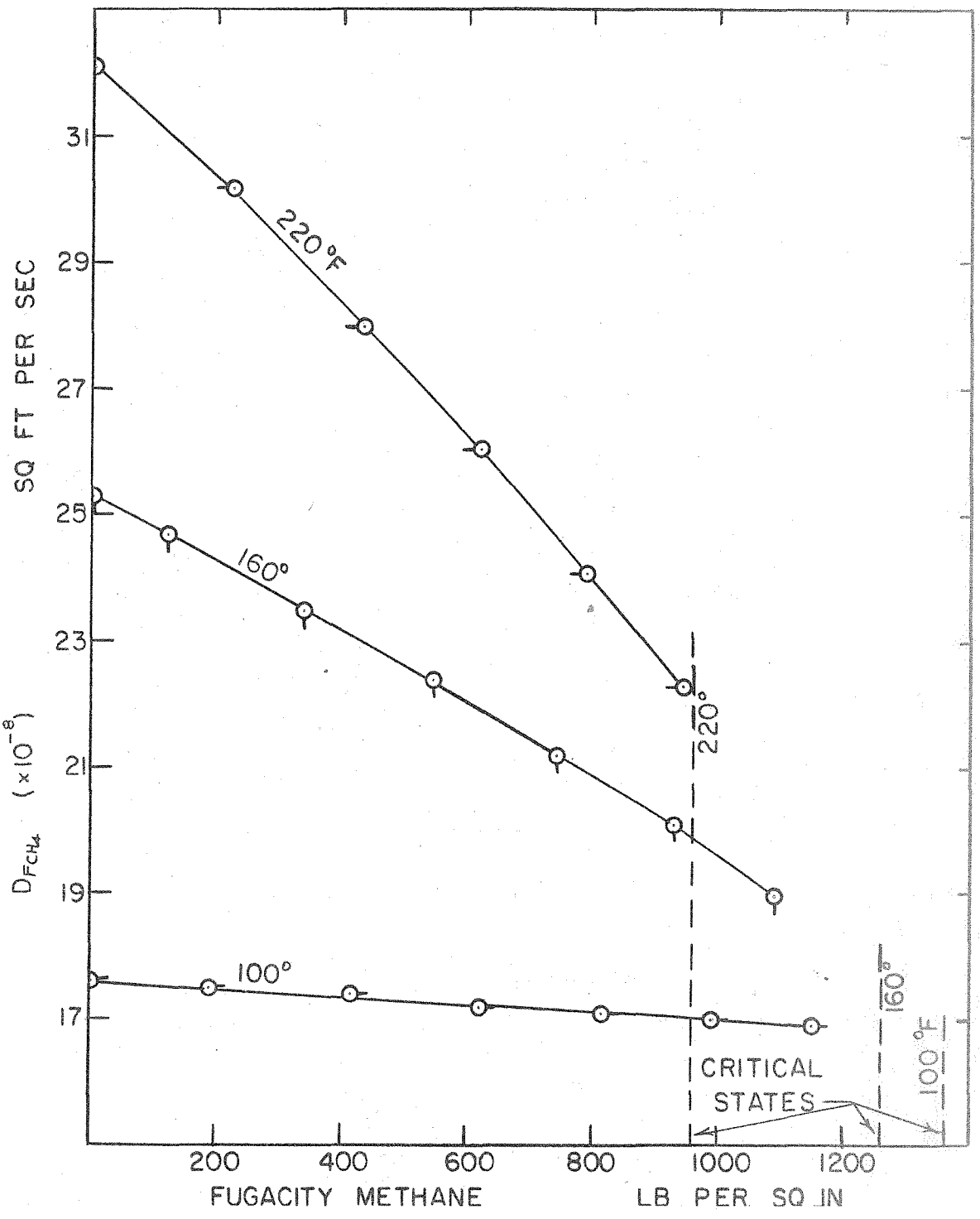

Figure 5. Fick Diffusion Coefficient for Methane as a Function of the Fugacity at Three Values of the Temperature Parameter.

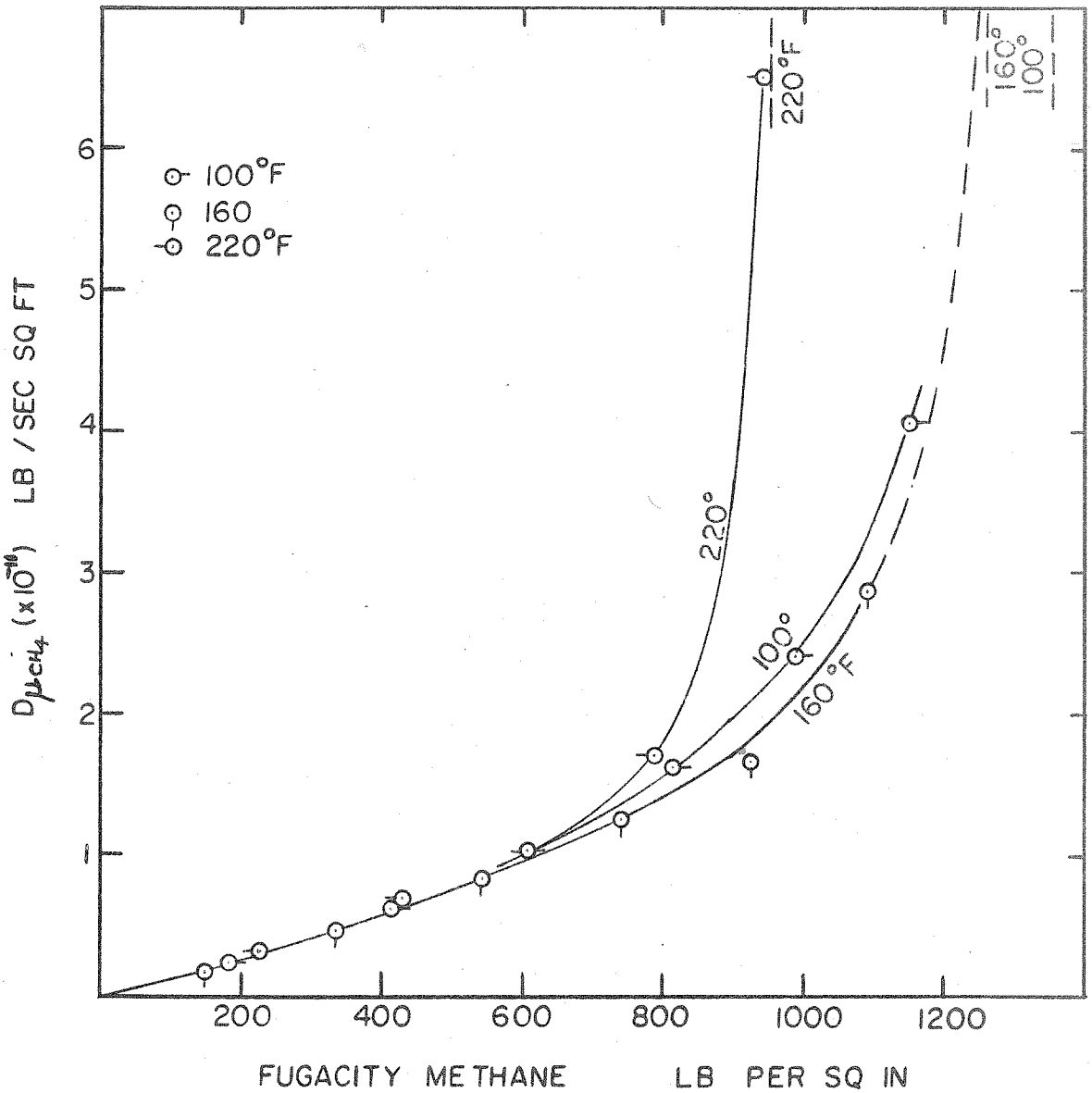

Figure 6. Chemical Potential Gradient Diffusion Coefficient for Methane as a Function of the Fugacity for Three Values of the Temperature Parameter.

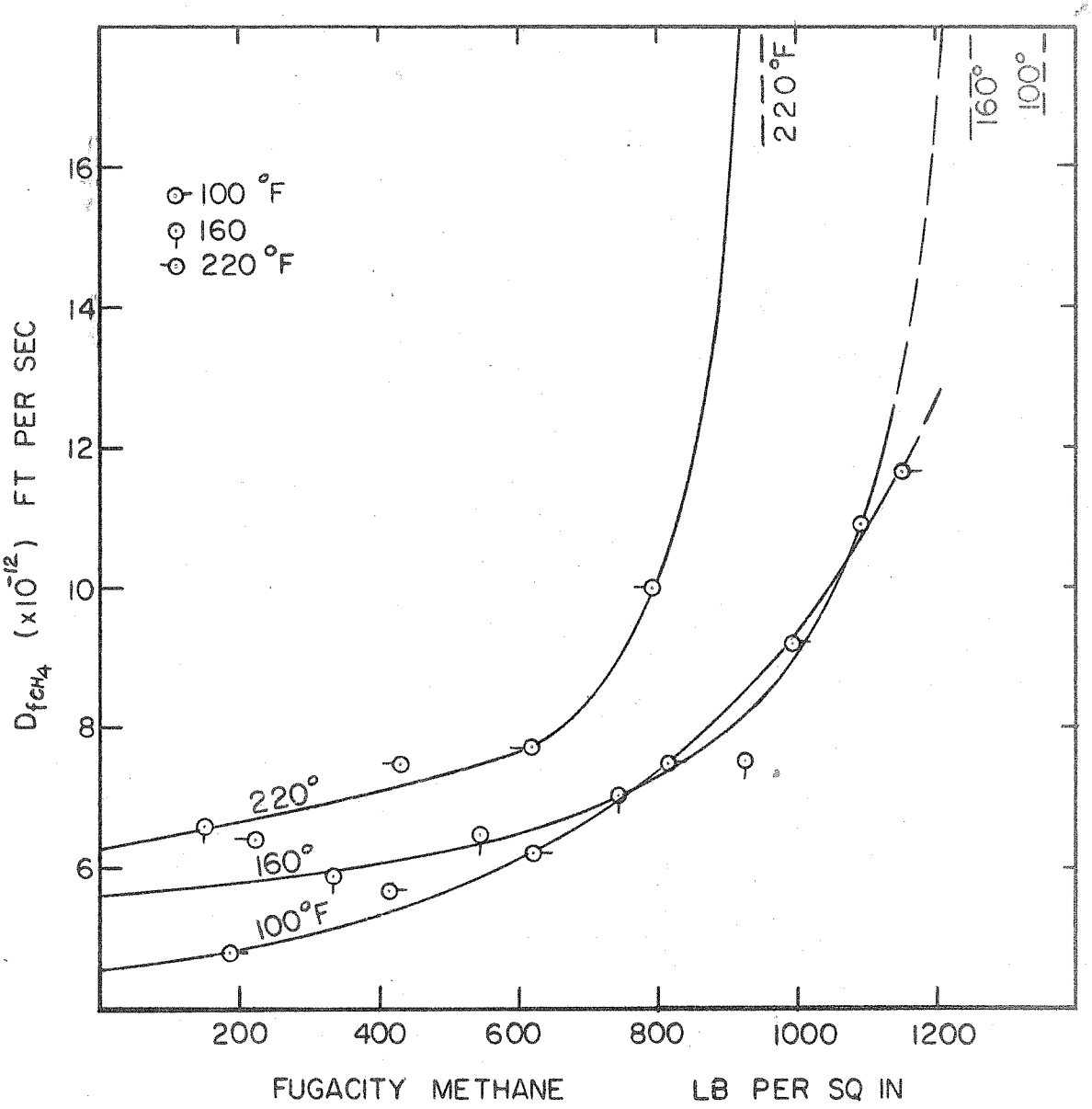

Figure 7. Fugacity Gradient Diffusion Coefficient for Methane as a Function of the Fugacity for Three Values of the Temperature Parameter.

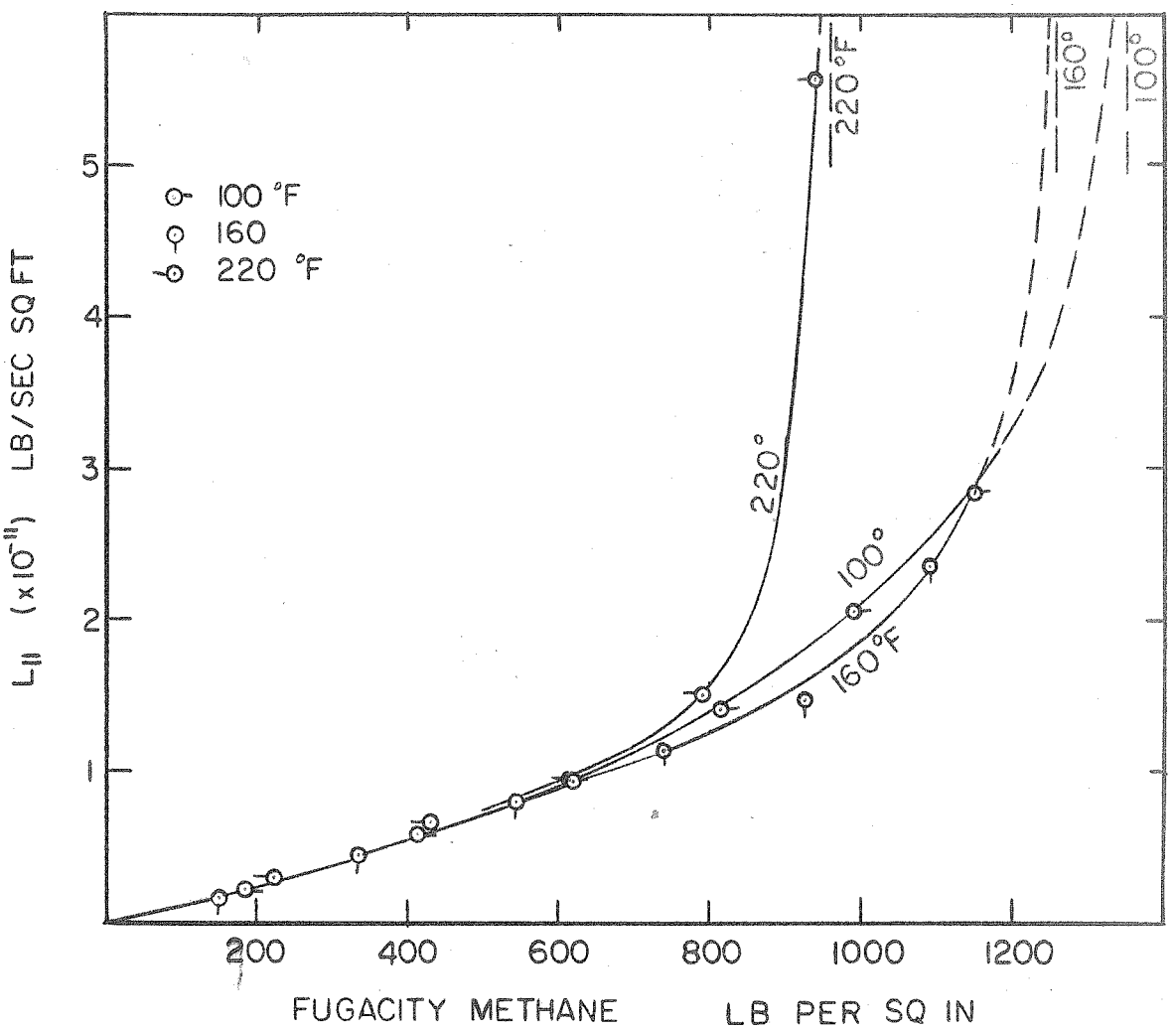

Figure 8. Phenomenological Diffusion Coefficient for Methane as a Function of the Fugacity for Three Values of the Temperature Parameter.

PROPOSITIONS

Proposition 1

A general relation, analogous to the Clapeyron equation (1) for pure substances, for the enthalpy change upon vaporization and another for the enthalpy change upon condensation is proposed for multi-component systems. These relations are, respectively, for vaporization

$$H_d - \sum_{k=1}^{n} N_{k,d} \bar{H}_{k,b} = T\left(\frac{dP}{dT}\right)''_b \left(V_d - \sum_{k=1}^{n} N_{k,d} \bar{V}_{k,b}\right), \quad (1)$$

and for condensation

$$\sum_{k=1}^{n} N_{k,b} \bar{H}_{k,d} - H_b = T\left(\frac{dP}{dT}\right)''_d \left(\sum_{k=1}^{n} N_{k,b} \bar{V}_{k,d} - V_b\right). \quad (2)$$

Derivation of Equation 1

For a multi-component system at equilibrium,

$$\mu_{k,d} = \mu_{k,b} \quad (k = 1, 2, \ldots, n) \quad (3)$$

and we can also write

$$d\mu_{k,d} = d\mu_{k,b} . \quad (4)$$

If the change in the equilibrium position of the system, along the two phase boundary, is at constant composition of the bubble-point liquid, then we may write

$$d\mu_{k,b} = -\bar{S}_{k,b}\,dT + \bar{V}_{k,b}\,dP \tag{5}$$

and

$$d\mu_{k,d} = -\bar{S}_{k,d}\,dT + \bar{V}_{k,d}\,dP + \sum_{\ell=1}^{n-1} \left(\frac{\partial \mu_{k,d}}{\partial N_{\ell,d}}\right)_{T,P,N_j} dN_{\ell,d} \,. \tag{6}$$

Equations 5 and 6 can be combined, with the help of the relationships

$$(d\mu_{k,d})_{T,P} = \sum_{\ell=1}^{n-1} \left(\frac{\partial \mu_{k,d}}{\partial N_{\ell,d}}\right)_{T,P,N_j} dN_{\ell,d} \tag{7}$$

and

$$\mu_k = \bar{H}_k - T\bar{S}_k \,, \tag{8}$$

to yield the following

$$\left(\frac{\bar{H}_{k,d} - \bar{H}_{k,b}}{T}\right) dT - (\bar{V}_{k,d} - \bar{V}_{k,b})dP = (d\mu_{k,d})_{T,P} \qquad (k = 1, 2, \ldots, n) \tag{9}$$

If both sides of equation 9 are multiplied by $N_{k,d}$ and a summation is made of the n relations resulting, recalling the Euler relations

$$V_d = \sum_{k=1}^{n} N_{k,d}\,\bar{V}_{k,d}$$

and (10)

$$H_d = \sum_{k=1}^{n} N_{k,d}\,\bar{H}_{k,d}$$

and also the Gibbs-Duhem relation

$$\sum_{k=1}^{n} N_{k,d}\, d\mu_{k,d} = 0 \quad (T, P \text{ constant}) , \tag{11}$$

we obtain the desired result, equation 1.

Equation 2 for the enthalpy change upon condensation can be obtained similarly. Equations similar to 1 and 2 can also be obtained for the fusion process.

Legend

d	differential operator
H	specific enthalpy
$\bar{H}$	partial specific enthalpy
k	component k
ℓ	dummy variable
n	nth component
N	weight fraction
P	pressure
$\bar{S}$	partial specific entropy
T	temperature
V	specific volume
$\bar{V}$	partial specific volume
μ	chemical potential

Subscript:

b	bubble-point
d	dew-point
j	represents all components but 2
k	component k

Superscript:

''	two-phase region

Proposition 2

Recalculated values of the equilibrium constant K for the dissociation reaction

$$N_2O_4 = 2NO_2$$

were presented by Giauque and Kemp (2). The purpose of this proposition is to point out the nature of the correction that is involved. The relations used by Giauque and Kemp in obtaining the corrected values are derived in the following analysis. It is shown that the difference between the corrected and uncorrected values can be attributed, simply, to the fact that Giauque and Kemp employed pseudo-empirical equations of state in the evaluation of the degree of dissociation of N_2O_4. This quantity was determined previously from the perfect gas relations. Both sets of values involve the ideal solution approximation.

Analysis

The following equations of state were employed by Giauque and Kemp:

For NO_2: $$PV = RT(1 + \frac{\beta}{2}P) \qquad (2)$$

For N_2O_4: $$PV = RT(1 + \beta P) \qquad (3)$$

The quantity β is a function only of the temperature.

The equilibrium constant for the above reaction is given by

$$K = \frac{a^2_{NO_2}}{a_{N_2O_4}} \quad , \tag{4}$$

which reduces to

$$K = \frac{P^2_{NO_2}}{P_{N_2O_4}} \tag{5}$$

with the assumption of an ideal solution, ideal gas behaviour and the choice of unit fugacity as the standard state.

Representing the degree of dissociation of N_2O_4 by α, it is easily shown that at equilibrium

$$N_{NO_2} = \frac{2\alpha}{1 + \alpha}$$

and (6)

$$N_{N_2O_4} = \frac{1 - \alpha}{1 + \alpha} \quad .$$

Recalling the definition of partial pressure, $P_{NO_2} = N_{NO_2} P$, equations 6 and 5 can be combined to yield

$$K = \frac{4P\alpha^2}{1 - \alpha^2} \tag{7}$$

Equation 7 permits the evaluation of the equilibrium constant from a knowledge of the degree of dissociation of N_2O_4 and the pressure of the system.

The fugacity of NO_2 can be obtained by means of the relation (3)

$$\ln \frac{f_{NO_2}}{N_{NO_2} P} = - \frac{1}{RT} \int_0^P \underset{\sim}{\bar{V}}_{NO_2} \, dP \quad , \tag{8}$$

assuming ideal solution behaviour and the equation of state for NO_2 given by equation 2. The expression obtained for the fugacity of NO_2 is

$$f_{NO_2} = N_{NO_2} P \, e^{(\beta/2)P} = P_{NO_2} \, e^{(\beta/2)P} \tag{9}$$

and similarly for $f_{N_2O_4}$,

$$f_{N_2O_4} = N_{N_2O_4} P \, e^{\beta P} = P_{N_2O_4} \, e^{\beta P} \tag{10}$$

Using these expressions, the equilibrium constant K in terms of fugacities becomes

$$K = \frac{f^2_{NO_2}}{f_{N_2O_4}} = \frac{P^2_{NO_2}}{P_{N_2O_4}} \quad , \tag{11}$$

which is the same as the partial pressure expression for K, equation 5. As a result, the equilibrium constant for this case can also be represented by equation 7.

It should be apparent from equation 7 that K is a function of the equation of state used in the determination of α. This is illustrated in the following.

Assuming an ideal solution and ideal gas behaviour, we can write

$$p\underline{V} = (1 + \alpha')\, RT \tag{12}$$

where α' is the degree of dissociation of N_2O_4 as computed by means of this equation. It is assumed that 1 mole of N_2O_4 is present initially.

For an ideal solution of gases whose equations of state are equations 2 and 3, respectively, we can write similarly

$$\underline{V} = \frac{2\alpha RT}{P}\left(1 + \frac{\beta}{2}P\right) + (1 - \alpha)\frac{RT}{P}(1 + \beta P) \tag{13}$$

Combination of equations 13 and 12 yields the following relationship between α, computed by means of equation 13, and α', computed with equation 12.

$$\alpha = \alpha' + \beta P \tag{14}$$

Substitution of this expression for α into equation 7 results in the same expression as presented by Giauque and Kemp (2),

$$K = \frac{4P(\alpha' + \beta P)^2}{1-(\alpha' + \beta P)^2} \quad . \tag{15}$$

It is seen that the correction to the equilibrium constant results from the use of equation 13 in place of equation 12 in the evaluation of the degree of dissociation of N_2O_4.

Legend

a	activity
d	differential operator
e	natural logarithm base
f	fugacity
K	equilibrium constant
ln	natural logarithm
N	nitrogen
N	mole fraction
O	oxygen
P	pressure
P	with subscript, partial pressure
R	universal gas constant
V	molar volume
$\bar{V}$	partial molar volume
$\underline{V}$	total molar volume
$\underset{\sim}{\bar{V}}$	residual partial molar volume, $\underset{\sim}{\bar{V}} = \frac{RT}{P} - \bar{V}_{NO_2}$

Greek:

α	degree of dissociation of N_2O_4
α'	degree of dissociation of N_2O_4 computed by eq. 12
β	a function of temperature

Proposition 3

A relation derived from thermodynamic considerations is presented which describes (4) the process of water sorption by cation exchange membranes of the styrene sulphonic acid type in atmospheres at low relative humidity. The relation is

$$\text{Per cent water in membrane} = \frac{-1.8\,\nu\phi\,(\text{capacity of membrane})}{\ln(\text{relative humidity})}$$

The osmotic coefficient ϕ is evaluated from osmotic coefficient data (5) for sulphuric acid solutions and the dissociation number ν is taken to be one for the cation exchange material.

Derivation of Relation

At equilibrium with respect to the process of water sorption, we can write

$$\mu_{w,g} = \mu_{w,m} \tag{1}$$

The chemical potential of the water vapor can be represented by

$$\begin{aligned} \mu_{w,g} &= \mu^{*} + RT \ln a_{w,g} \\ &= \mu^{*} + RT \ln \frac{P_{w,g}}{f^{*}} \end{aligned} \tag{2}$$

The second relation in equation 2 follows from the use of the Lewis Generalization and the assumption that the water vapor in the pure state behaves as an ideal gas.

The chemical potential of the water in the cation exchange membrane can be represented by (5)

$$\mu_{w,m,1\ atm} = \mu^{o}_{\ell,1\ atm} - \frac{\nu R T m \phi}{55.55} \qquad (3)$$

The following expression can be written for the chemical potential of pure water at the pressure of 1 atmosphere:

$$\mu^{o}_{\ell,1\ atm} = \mu^{*} + RT \ln \frac{P^{o}}{f^{*}} + \int_{P^{o}_{w,g}}^{1\ atm} V^{o}_{\ell}\, dP \qquad (4)$$

Combination of equations 3 and 4 yields

$$\mu_{w,m,1\ atm} = \mu^{*} + RT \ln \frac{P^{o}}{f^{*}} + \int_{P^{o}}^{1\ atm} V^{o}_{\ell}\, dP - \frac{\nu R T m \phi}{55.55} \qquad (5)$$

Combination of equations 1, 2 and 5 and rearrangement of the expression obtained, after also equating V^{o}_{ℓ} to zero, will yield

$$\ln \left(\frac{P_{w,g}}{P^{o}} \right) = - \frac{\nu\, m \phi}{55.55}$$

Replacing m, the internal concentration of the membrane by the capacity and the water content at equilibrium, according to the relation,

$$\frac{\text{per cent water}}{\text{capacity}} = \frac{100}{\text{molality}}$$

we end up with the final relation, after some rearrangement,

$$\frac{\text{per cent water}}{\text{capacity}} = \frac{-1.8\ \nu\ \phi}{\ln \frac{P_{w,g}}{P^{o}_{w,g}}} = \frac{-1.8\ \nu\ \phi}{\ln(\text{relative humidity})}$$

Definitions

The capacity of a cation exchange material is a measure of the number of exchange groups present. It is measured by direct titration and is determined as milliequivalents per gram of bone dry resin.

The per cent water in the exchange material is determined on a dry weight basis.

Legend

a	activity
atm.	atmosphere, pressure unit
f	fugacity
ln	natural logarithm
m	molality
P	pressure
P^o	vapor pressure of water
R	universal gas constant
T	temperature
V^o	molar volume of pure water

Greek:

μ	chemical potential
μ^o	chemical potential of pure water
ν	dissociation number of electrolyte
ϕ	osmotic activity coefficient

Subscripts:

g	gas phase
ℓ	liquid phase
m	membrane
w	water

Superscript:

*	standard state, not specified

Proposition 4

The information presented in Part II of the thesis indicates that the diffusion coefficients based on gradients in the chemical potential and fugacity are marked functions of the conditions describing the state of the system. It is proposed that evaluations be made of the diffusion coefficient based on the activity gradient to determine the variation of this coefficient with change in conditions. If the standard state selected in the evaluation of the activity is that of the pure liquid at the same temperature and pressure as the system, the relative positions of the coefficients will not be altered considerably from those of the Fick coefficients, as was the case in the evaluations based on the above gradients. The possibility exists that the alteration will bring the coefficients closer together.

Proposition 5

The ideal solution rule enables one to estimate the thermodynamic behaviour of multi-component systems from a knowledge of the behaviour of the pure substances. This principle can be extended so as to enable one to utilize thermodynamic data pertaining to multi-component systems in the prediction of the behaviour of higher multi-component systems.

REFERENCES

1. Lacey, W. N., Sage, B. H., "Thermodynamics of One-Component Systems," Academic Press, New York 3, N. Y. (1951).

2. Giauque, W. F., Kemp, J. D., J. Chem. Phys., 6, 40 (1938).

3. Sage, B. H., Lacey, W. N., Ind. Eng. Chem., 31, 1497 (1939).

4. Kozicki, W., M.A.Sc. Thesis, Dept. Chem. Eng., Univ. Toronto, Toronto, Canada (1957).

5. Harned, H. S., Owen, B. B., "Physical Chemistry of Electrolytic Solutions," Reinhold Publ. Corp., New York, N.Y. (1950).